Process defects and resulting structure of unidirectional CF/LM-PAEK after induction welding.

Master thesis

Monique E. G. Lamers
July 1, 2024

Chair of Production Technology,
Department of Mechanical Engineering,
Faculty of Engineering Technology,
University of Twente, Enschede

Exam committee:
prof.dr.ir. R. Akkerman (chairman)
dr.ir. W.J.B. Grouve (supervisor)
ir. I.J. Geschiere (daily supervisor)
dr. M.I. Abdul Rasheed (external member)
ir. G. Bieleman (internal member)

Summary

Thermoplastic composites (TPCs) answer the demand for high-performance and lightweight materials. Their main advantage is their ability to melt, which allows the assembly of complex structures using fusion bonding methods. One of these methods is induction welding. Induction welding is already applied on woven carbon-fibre fabric reinforced TPCs, but the application on unidirectional plies is still limited. The cause lies in the difficulty of defining a robust process window to ensure defect-free welds. This research maps the process-induced defects that can occur in a unidirectional, quasi-isotropic CF/LM-PAEK induction weld. The aim is to better understand the relation between process parameters and final material structure. Several assemblies are welded to characterise the temperature and pressure distributions. The welding temperatures are measured using thermocouples during welding. The pressure distribution is visualised using pressure-sensitive foils. Afterwards, non-destructive inspection is done, followed by microscopic inspection. The highest temperature is reached in the central location at the weld interface and gradually decreases towards all edges. Visual inspection reveals edge effects in the assemblies and indents at the bottom of the high-temperature welds. The in-plane temperature distribution explains the indents. The indent is most apparent where the temperature is the highest. The pressure distribution supports this finding because this appears to be uniform across its application area. Non-destructive inspection showed that the bonded area at the weld interface has a similar shape to the in-plane temperature distribution. Microscopic analysis of the cross-sections of the indents of the weld revealed material flow, especially in the bottom laminate. Some delamination is visible at the thick indent edges seen in the high-temperature welds. The plies in the bottom laminate lying parallel to the welding direction show the greatest thickness differences. On the other hand, plies oriented orthogonal to the welding directions are relatively unaffected. The discussed changes in the material structure are caused by the local heating pattern rather than an inhomogeneous pressure distribution. Applying a cooling system at the bottom of the welded assembly can be considered to avoid the resulting defects.

Contents

Chapter 1

Introduction

1.1 Background

Thermoplastic composites (TPCs) are a promising material class to answer the demand for high-performance lightweight materials [1–13]. One of the advantageous properties of the thermoplastic matrix in a TPC is its ability to melt [10]. This is an advantage in the processing and manufacturing of composite products [6, 11]. Therefore, the TPCs slowly replace their metallic and thermoset counterparts [2, 3, 6, 11, 14].

This increases the need for joining as more composite components are assembled. Several joining methods are used, but they all come with their own difficulties [1–3, 5, 15]. Mechanical fasteners puncture the material, which introduces stress concentrations and fibre disruptions in the material. This can cause damage [1–4, 10, 16], such as cracks due to the aforementioned increased stress concentrations. Alternatively, adhesives do not require punctures by drilling holes. However, these methods require extensive surface preparation and chemical compatibility [1–4, 10, 14].

Fusion bonding considers methods to join components by melting, pressurising and cooling them. Polymer chains diffuse across the welding interface [3] and create entanglements. This method avoids the use of undesired fasteners and adhesives, and it allows one to achieve bond properties close to the original matrix material properties [3, 10].

Induction welding is one of the fusion bonding methods. An induction welding machine is shown in Figure 1.1. The robot (Figure 1.1a) moves an induction coil to the workpiece. This induction coil (Figure 1.1b) is placed in the vicinity of an electrically conductive susceptor. An alternating current in the coil generates an alternating magnetic field, creating eddy currents in the susceptor. The susceptor may be an electrically conductive mesh [1–3, 10, 14, 17–20]. Alternatively, susceptorless heating can be achieved using the carbon-fibre reinforcement in a TPC. These reinforcing fibres are electrically conductive and create the circuit to form the required closed loops [1, 3, 5, 10, 14, 16, 17, 19–23]. The energy is lost in the form of volumetric heat, melting the thermoplastic matrix [1–3, 5, 16–22].

Fusion bonding of laminates can be achieved as pressure is applied to the melted zone. The pressure is applied at the weld area, creating intimate contact between the laminates. The surface irregularities of the weld interface are deformed while being pressurised [2, 6, 10, 24, 25]. The intimate contact allows the polymer chains in the matrix material to move across the interface, entangle and (re-) consolidate [1, 2, 5, 6, 15, 21, 22]. In this way, a bond is formed after the material is cooled down. This welding process is affected by process parameters which depend

on the material, the lay-up and the welding set-up. Major advantages of susceptorless welding are the rapid heating [1, 10, 13] without requiring direct contact [1]. It is a promising method, allowing fast [1, 14], clean [3] and automatised [10, 13, 14] production and manufacturing.

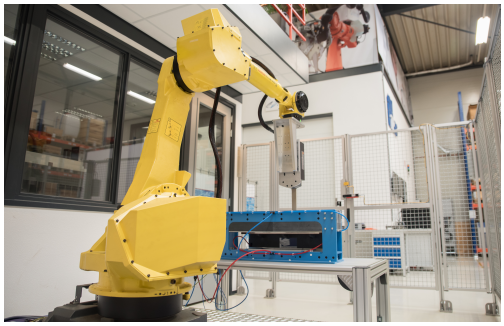

(a) *Induction welding robot.*

(b) *Induction welding coil.*

Figure 1.1: *Induction welding set-up (source: TPRC).*

1.2 Aim

The induction welding process of TPCs poses challenges that need to be overcome [1, 15]. For example, preserving the properties of the material is such a challenge [18]. The welds can show defects that significantly affect the mechanical integrity of the bond, such as thermal degradation, deconsolidation and kissing bonds. The parameters influencing the welding process have to be optimised to achieve a good weld. The temperature in the welding process has to lie in the range from the melting temperature to the degradation temperature to allow the polymer chains to diffuse [1, 3, 6, 10, 22] without degrading the material. The pressure prevents deconsolidation and should preserve the laminate's mechanical properties [1–3, 15, 17, 21]. A lack of pressure or temperature decreases the degree of intimate contact, thus molecular diffusion. This can cause a kissing bond [4, 26–28]. On the contrary, excessive pressure squeezes material out of the weld [1, 3, 25]. Therefore, this relationship has to be well understood to increase the robustness of the welding process and to be able to predict or prevent defects.

This research attempts to map the process-induced defects in induction welds for carbon fibre-reinforced low-melting polyaryletherketone (CF/LM-PAEK) unidirectional (UD), quasi-isotropic (QI) lay-up and investigate their cause. First, an overview is given of the process parameters affecting the induction welding process and the defects occurring in an induction weld of a TPC. The currently available relationship between the process parameters and defects is discussed. Secondly, the issues and challenges in the available research are indicated. From this, a method is presented to identify and investigate the process-induced defects. Laminates are prepared for the welding process, and several assemblies are welded in the induction welding set-up. The welded assemblies are subjected to non-destructive inspection: photographs and measurements are taken, followed by an ultrasonic scan. After this non-destructive inspection, samples are cut

from the assemblies to perform microscopic analysis. The results are presented, after which the discussion values these results.

Chapter 2

Literature review

Fusion bonding is also known as welding. The interfaces of the parts to be connected are brought into intimate contact, and heated [2, 3, 10, 14]. Susceptorless induction welding is a promising manufacturing method, because of its fast [1, 1, 10, 13, 14], clean [3] and automatable [10, 13, 14] application without needing direct contact [1] and foreign materials. The induction welder heats the material using the conductive properties of the carbon fibre reinforcement. The heated, mobile polymer chains can interdiffuse across this weld interface [3, 10, 14]. The resulting weld is a fusion of the components with properties similar to the components' original matrix properties [3, 10].

2.1 Heating process

The induction welding robot places the induction coil close to the workpiece. A schematic overview of the set-up is shown in Figure 2.1. This section describes how a current in the induction heater translates to heat generation in the workpiece.

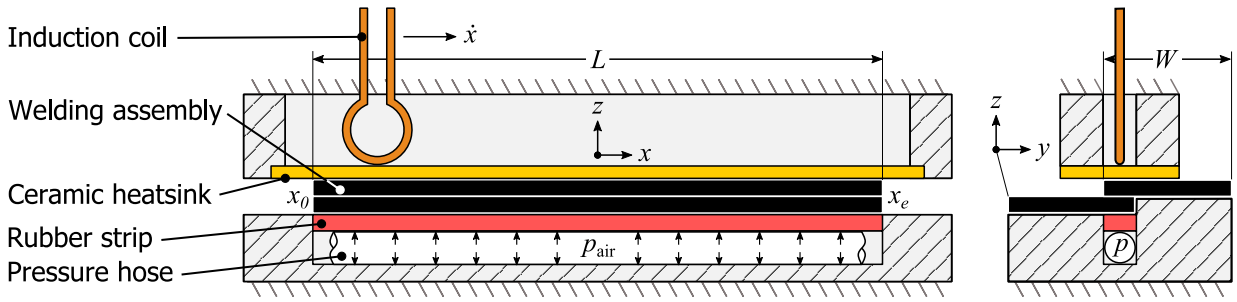

Figure 2.1: *A schematic overview of the induction welding coil against an electromagnetically transparent heatsink close to the workpiece (source: TPRC).*

An alternating current I runs through the induction coil, which creates an alternating magnetic field $\vec{B}$ [1–3, 10, 29]. This magnetic field reaches the workpiece, which can be described with the Biot-Savart law [5, 10, 15, 16, 22, 29]. Although the induction coil does not need to touch the workpiece [2], the magnetic field strength is inversely related to the distance from the induction coil to the workpiece. The magnetic field creates an electric field in the workpiece [5, 10, 16, 22, 29, 30]. The electric field causes a current density to run through the conductive loops, called eddy currents [1–3, 17, 19, 23, 30].

The material needs to be or have an electrically conductive susceptor to allow this current to flow. The susceptor can be applied to a TPC in the form of conductive particles, a conductive mesh [1–3, 14, 17–19] or touching carbon fibres [1, 3, 5, 14, 16, 17, 19, 21–23]. The eddy currents lose energy while propagating through the loops formed by the conductor, heating the material. Three heating mechanisms can be present in a TPC: Joule losses, contact resistance and dielectric hysteresis [1, 20, 30]. Joule losses are caused by the resistance along the fibres [1–3, 10, 17, 19–23]. Secondly, contact resistances are present at the fibre junctions [1, 2, 10, 17, 20, 22, 23]. This occurs where the warp and weft meet [23], at angled plies [1, 17] and within plies themselves due to randomness of the fibres. Fibre waviness and matrix squeeze-out increase the number of contact points, increasing the influence of the junction heating [1]. The third heating mechanism, dielectric hysteresis, occurs in the matrix material between fibres [1, 2, 10, 17, 20, 22, 23]. The highly frequent [3] alternating electric field causes charge to move and molecules to rotate, creating a capacitor effect [1, 10, 21, 30]. This effect is thought to be negligible for low-frequency induction welding. It appears that the dominant heating mechanism depends mainly on the fibres and lay-up [1–3, 19]. The eddy current generation is schematically visualised in Figure 2.2. The heat is conducted to the surrounding material [10, 31], allowing one to determine the temperature distribution in the workpiece [2, 6, 22].

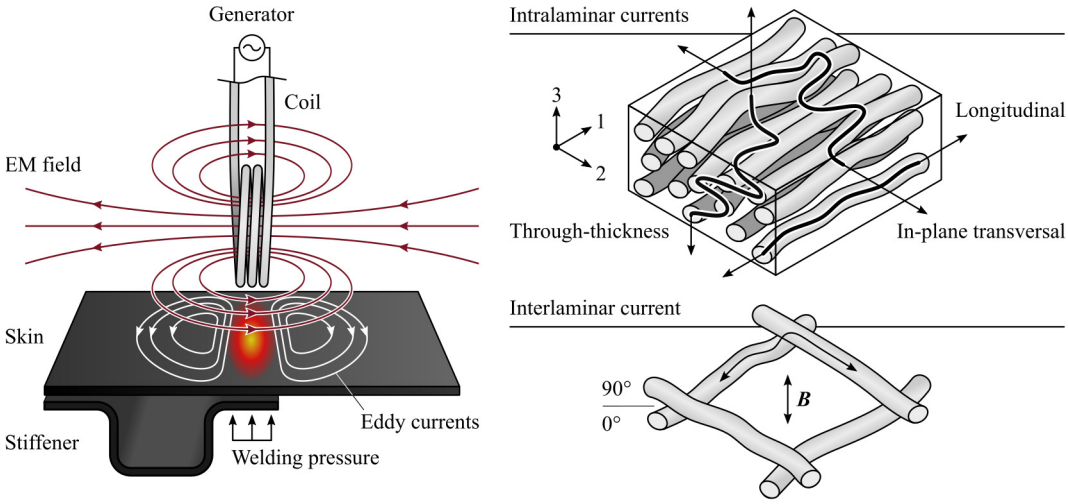

Figure 2.2: *An overview of eddy current generation during induction welding (source: TPRC).*

Ideally, only the weld interface is melted; the ideal temperature distribution is shown in Figure 2.3. However, the intensity of the magnetic field decreases with increasing distance to the source, as described by the Biot-Savart law. Since the intensity relates to the heat generation in the material, the coil's side of the workpiece reaches the highest temperature. This can lead to a thermally degraded surface, although the weld interface is still below T_m [15]. However, the interfacing surfaces should achieve the maximum temperatures. Additionally, other material properties are affected by the induction welding process. The crystallinity can be affected by the cooling rate [24] after welding, for

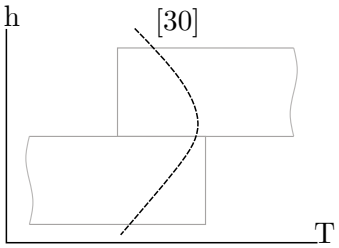

Figure 2.3: *A sketch of the ideal temperature distribution through the weld's thickness.*

example. A uniform temperature distribution in the in-plane directions is essential for successful bonding [3]. In other words, the temperature distribution through the laminates' thicknesses is of significant importance to understanding the welding process [3, 22, 24].

2.2 Welding parameters

The welding parameters are the factors affecting the product's final properties. The parameters affecting the welding process are shown in Figure 2.4. These are divided into three inter-connected categories: design, material and process. Although many parameters are displayed in one category, many can be assigned to multiple categories. Some of the parameters' relationships are displayed, connecting the groups. The design and material categories are briefly discussed. The process parameters are discussed in more detail, as the research focuses on their influence on an induction weld and its defects.

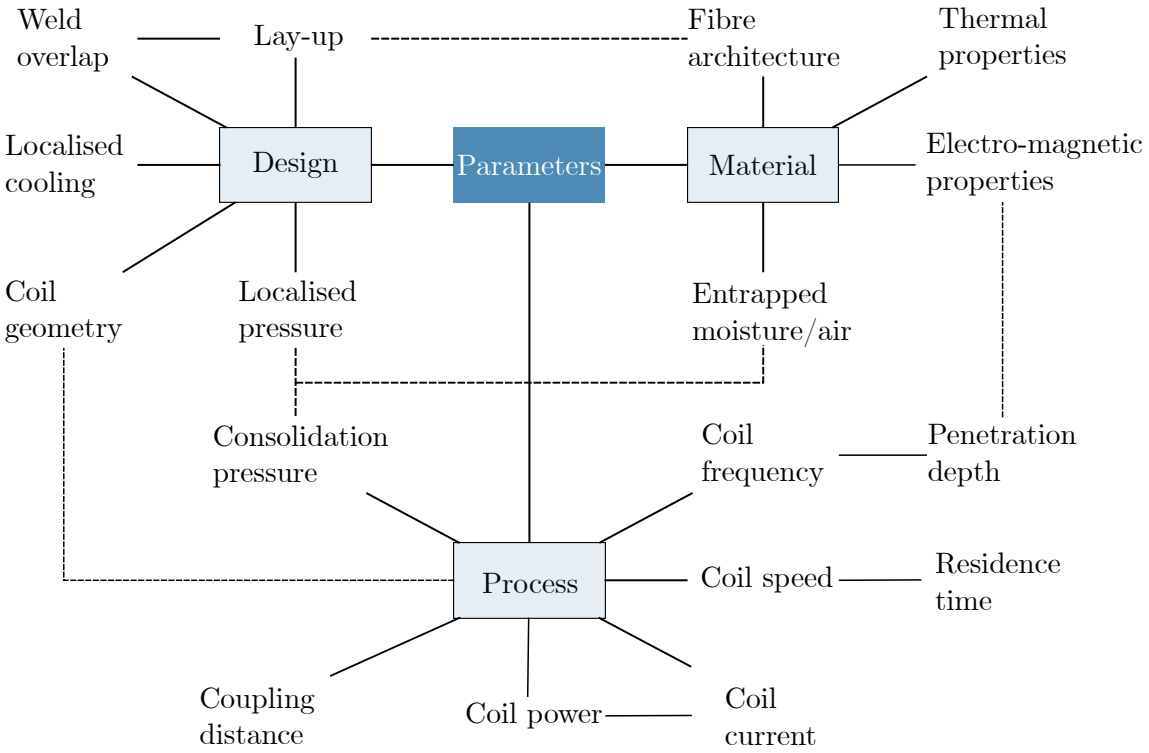

Figure 2.4: *Schematic overview of the welding parameters used during induction welding.*

2.2.1 Design and material parameters

Design

The design category covers choices related to the workpiece and its components and the set-up of the induction welder. The workpiece consists of laminates having some specific lay-up of UD plies. The lay-up plays a significant role in the heat generation during welding, contributing to the forming of conductive circuits.

An additional parameter is the weld width. The weld width is the overlapping width of the laminate components. This overlap has to correspond to the induction welding set-up.

The induction welding set-up and the equipment's properties also affect the final weld, such as the coil geometry and pressure application. The coil geometry is mirrored in the heating pattern in the workpiece [1, 3, 15, 19, 21]. The heating pattern is dictated by the eddy currents that flow through the material following the coil's geometry [17, 19, 22]. Additionally, the weld overlap has to be pressurised to prevent deconsolidation of the laminates. The pressurised area is fixed for the set-up, but the user can choose the pressure. Moreover, the top of the laminate has to be cooled to prevent thermal degradation. Also, the weld interface should be the hottest part of the weld overlap. Cooling is necessary to prevent degradation, but it still needs to allow the weld interface to melt. This affects the through-the-thickness temperature distribution.

Material

The general material properties of both the matrix and the fibres are important factors in the welding process [1, 3, 10, 24, 32]. The matrix material has to melt, so its thermal properties such as heat capacity influence the welding process [2]. Another material parameter is the penetration depth that relates to the depth δ at which the eddy current decreased to $1/e$ =37% [1, 10, 30], which is schematically shown in Figure 2.5. The penetration depth depends on the material's electromagnetic properties and the frequency chosen in the process. The penetration depth shows the degree of skin effect [10] and influences the through-the-thickness temperature distribution.

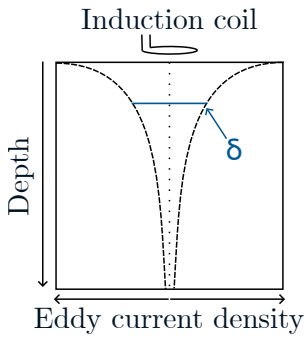

Figure 2.5: *Schematic overview of the penetration depth.*

The fibre lay-out determines the electrically leading paths [21]. The paths must form closed loops to support the eddy currents to propagate through the material [1–3, 15, 17–19, 21]. The fibre lay-out, therefore, directly relates to the heat generation mode and pattern in the laminates [17].

The workpiece in the welding set-up can deconsolidate if the temperature is too high and the pressure too low. Deconsolidation is caused by voids in the laminate [8]; fibre reinforcement decompaction [7, 33–35]; differences in thermal expansions of the fibre and matrix materials [9, 14]; and anisotropic laminate properties [14]. The moisture content in the laminates affects this defect [17] as well as the fibre architecture in the plies and general material properties.

2.2.2 Process parameters

The major process parameters are defined as coil frequency [2, 17, 29], current [17, 29], distance [1, 10, 15, 17, 21, 29], pressure [17] and time [1–3, 17] or speed.

Frequency

The frequency is a process parameter closely related to a material property: the penetration depth. A higher frequency provides more energy to be converted into heat generation. However, it causes the penetration depth to decrease [1, 17–19]. This skin effect influences the through-the-thickness temperature distribution [19] and maximum temperature in the weld [10, 21]. The excitation frequency depends on the coil's resonance frequency [1] and is therefore not operable for the user.

Current and power

The current [17, 29] and power [1, 17] are two process parameters approximately related as $P = UI$. The power represents the energy input rate into the material [2]. This contributes to the maximum temperature in the weld [10, 19]. The heating rate increases with increased power, quadratically decreasing the heating time [19]. The current is closely related to the power. Therefore, it also contributes to the maximum temperature in the workpiece [21]. These parameters can be directly chosen by the operator.

Coupling distance

The distance between the coil and the workpiece affects the magnetic field intensity and heat generation. Increasing the distance between the workpiece and the induction coil decreases the magnetic field intensity in the workpiece. This causes the material to require a quadratic amount of time to heat up [19]. It also affects the maximum achievable temperature [10, 19].

Consolidation pressure

The consolidation pressure provides intimate contact [1, 2, 6, 10, 11, 15, 24, 32] between the components. The intimate contact allows polymer molecules to diffuse across the weld interface. Pressurising the workpiece avoids void expansion, thus preventing deconsolidation [1, 2, 34, 35]. This parameter is operable by the welding set-up user, making this an operator parameter.

Residence time

The residence time strongly depends on the speed of the induction coil. The longer the material is subjected to the magnetic field, the more heat will be generated. The maximum temperature in the weld depends on this residence time [10, 19]. The material is heated and melted as the coil approaches. Then, this melted area cools down after the coil passes by. The cooling time and the cooling rate affect the final weld's mechanical properties [10, 17]. The speed of the induction coil influencing the residence time is an operable parameter. The coil's speed can be used to change the residence time in different zones in the weld region. A start- and ending zone can have different speeds to improve the weld's final properties.

2.3 Welding defects

An overview of the defects occurring in an induction weld is given in Figure 2.6. Three main categories are visible: design, material and process. The design category covers the defects concerning the induction welding set-up. The material's state, including issues such as contamination and irregularities, affect the final weld quality as well. The welding process itself may introduce several defects—these range from major to minor damages. The defects are displayed in, but are not limited to, these categories. Most defects arise due to multiple causes, often lying in various categories. The cause of the defects lies in one or multiple of the "fusion bonding conditions": temperature, pressure and time.

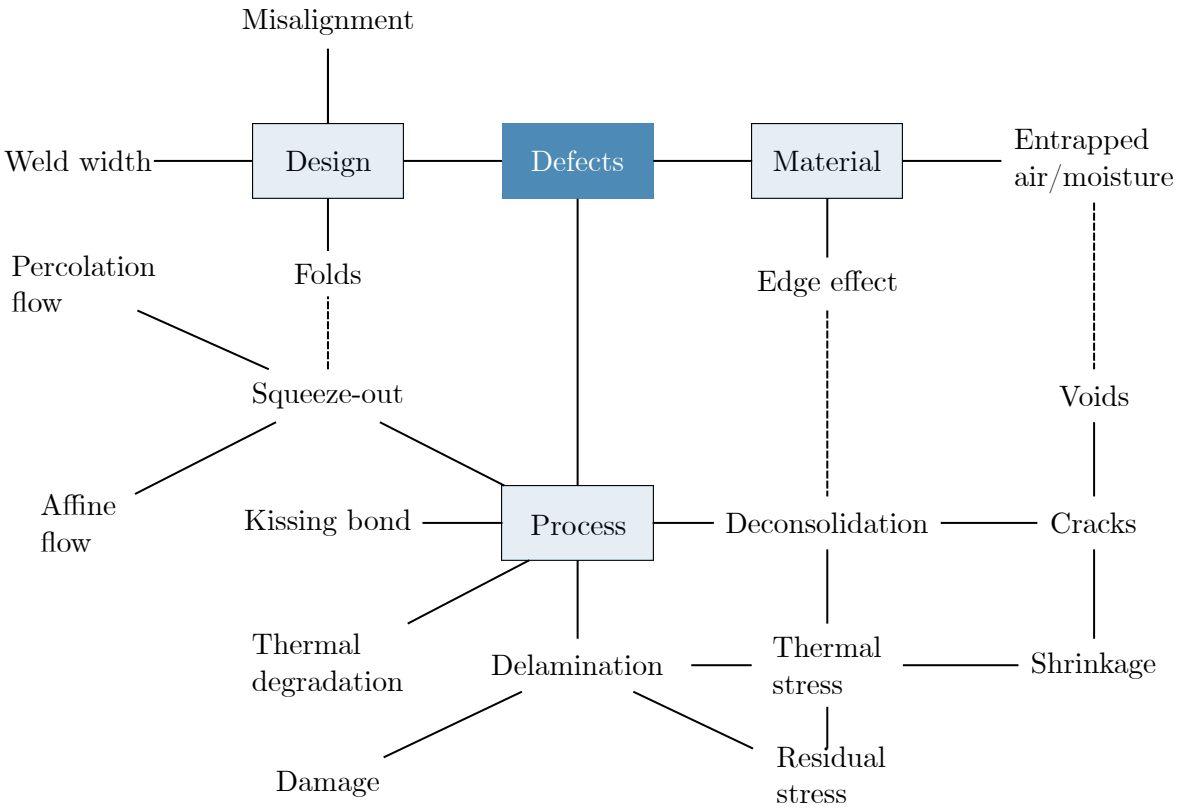

Figure 2.6: *Schematic overview of the defects in a weld using induction heating.*

The process defects are the focus of this research. This section serves as an overview of the defects commonly seen in TPCs and their induction welding processes. The process-related defects are discussed from major to minor defects.

2.3.1 Deconsolidation

Deconsolidation is described as void nucleation and growth [7, 8, 33, 34] leading to an increase in void content in a laminate [10, 34]. The laminate can contain entrapped air or moisture [1, 2, 8, 10, 36]. This heats and expands during processing, causing voids to nucleate [8, 9]. Meanwhile, the matrix softens at its melting temperature [10], allowing these voids to grow. Additionally, the soft matrix allows the stresses induced by consolidation to relax [1, 14, 33]. Decompaction of the fibre reinforcements seems to be the primary cause of void growth [7, 33–35].

Other causes are different thermal expansions of the fibre and matrix materials [9, 14] and anisotropic properties of the laminate [14]. The roots of the problems mentioned above may lie in the temperature gradient in the through-the-thickness direction of the weld zone [9]. Deconsolidation appears as a propagating front in the direction of the heat flux [34] and is parallel to the welding interface [35]. The plies can separate when these voids are sufficiently large and appear at the ply interfaces, which leads to delamination [8]. Although delamination can be induced by damage and excessive loading [37, 38], this shows that severe deconsolidation can result in ply-separation as well as is visible in Figure 2.7. The two fusion bonding conditions corresponding to deconsolidation are temperature and pressure.

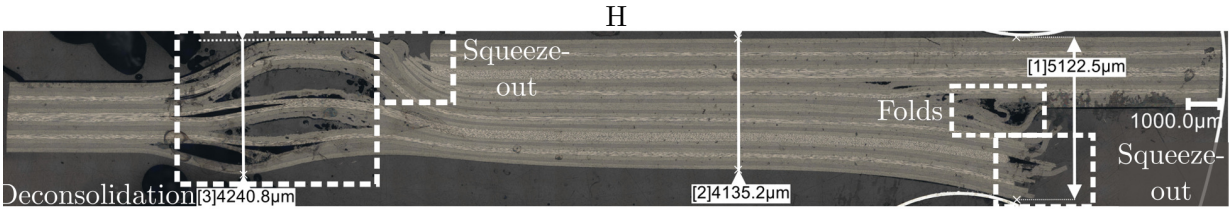

Figure 2.7: *Micrograph of a cross-section of an induction weld with visible deconsolidation (left), squeeze-out (left and right) and folds (right)[39].*

2.3.2 Squeeze-out

The induction welding set-up pressurises the laminates to (re-) consolidate the weld using the pressure tube shown in Figure 2.1. The pressure and elevated temperature allow the melted polymer matrix to flow [1, 3, 25]. This deforms the surface of the components [6, 10, 25] and possibly leads to squeeze-out [1, 3, 25] if the pressure is too high. Two types of squeeze-out flow can occur. Firstly, there is affine flow, also known as transverse fibre flow or squeeze flow. Both the matrix and fibre can be squeezed out of the pressure region, causing thinner plies. The squeezed-out plies are visible outside the pressure region. Some plies are squeezed outwards but are restricted by solid material outside the weld region. This can fold plies and cause fibre buckling [1]. The ply squeeze-out and ply folding can be seen in Figure 2.7. Secondly, percolation flow can be described as matrix bleeding: only the matrix material is squeezed out. The squeezed bulk matrix material appears outside the pressurised region.

The consolidation pressure provides intimate contact between the components in which the surface irregularities are deformed [6, 10, 25]. The welding set-up defines the pressure application area while the pressure can be set by the user. However, the weld overlap area of the workpiece changes if the user misaligns the components, affecting the actual applied pressure. Excessive squeeze-out changes the component's properties in the weld area. The fibre volume fraction of the weld region increases [1] as a result of matrix bleeding. This can cause flash to be visible at the components' edges [1, 40]. Additionally, the fibre lay-out compacts and changes due to the compression [41, 42]. Moreover, the weld thickness decreases [42]. Summarised, too much pressure can reduce the weld's mechanical performance. Note that a suitable pressure application strongly co-acts with the temperature because of the matrix's viscosity [10]. Therefore, the fusion bonding conditions related to squeeze-out are pressure and temperature.

2.3.3 Kissing bond

This interfacial defect is mainly seen in adhesive bonding [14, 43]. It describes a defective bond as it has little to no strength [4, 26–28]. The visible intimate contact makes the bond seemingly strong despite its weakness, which poses a risk [26]. Detecting the weak bond is difficult using non-destructive inspection methods [43]. A good bond is achieved when the components fully fuse. This is done in two phases. First, intimate contact is formed between the two components. The asperities of the surfaces are deformed while squeezing the components together [2, 6, 10, 24, 25]. Next, the polymer chains can diffuse across the interface surface, also called healing or autohesion [2, 3, 5, 6, 9, 15, 24, 25, 36]. Intimate contact development and healing happen simultaneously [6, 24, 25]. The temperature accounts for the low viscosity and the pressure allows intimate contact of the interfaces. Time is needed to allow the polymer chains to diffuse across the interface. Insufficient heat generation and time result in insufficient bonding [3, 30]. Therefore,

the requirements needed for this fusion bonding process are pressure for intimate contact and temperature and time to account for bonding [1, 3, 6, 10].

2.3.4 Edge effects

The heat generation is caused by energy losses of the eddy currents propagating through the carbon fibres. The eddy currents' loops become smaller at the edges of the weld or laminate, increasing the current density at this location. This causes an increased temperature at the material's edges [1, 17, 21]. This phenomenon occurs at the edge of a material and can result in delaminations, deconsolidation or even thermal degradation.

2.3.5 Thermal degradation

Thermal degradation is a decrease in material properties due to excessive heat [1, 10]. Elevated temperatures reduce the mechanical and physical properties of the material [44]. Eventually, chain scission, cross-linking, and oxidation decompose the polymer chains [45]. Degradation can occur when the material is overheated by adding excessive energy [30, 40]. The heating pattern is uneven due to the anisotropic material properties and, potentially, the coil shape, as the heating pattern mirrors this shape. Therefore, the pattern can have a region where a maximum temperature is reached, possibly exceeding the thermal degradation temperature of the material [10, 17]. Besides, an excessive duration, or welding time, can overheat the material as well [1–3, 17, 40]. Summarising, the main contributors to thermal degradation are temperature and time [40].

2.3.6 Suboptimal crystallisation

The mechanical properties of a semi-crystalline polymer are determined by the crystallinity of the polymer [6, 10, 12, 24, 40]. Therefore, suboptimal crystallisation causes suboptimal mechanical properties of the weld. A semi-crystalline polymer crystallises as it cools down after it has been processed above its melting temperature [10, 24]. The main stages of crystallisation are nucleation and crystal growth [40].

The degree of crystallinity directly relates to the properties of the final product [6, 10, 24, 40]. A semi-crystalline polymer having a high degree of crystallinity is stiff compared to a less crystalline polymer. The material is less elastic in melt too [40]. The crystals cause the material to shrink upon cooling, possibly causing cracks [1]. Applying pressure to the workpiece prevents this defect [1]. Crystallinity relates to both material properties and defects.

The fusion bonding conditions for optimal crystallinity cover two aspects: degree of crystallinity and shrinkage control. The final degree of crystallinity depends on temperature [24, 40], cooling rate [6, 10, 24] and time [6, 40]. Cracks caused by severe, uneven shrinkage are prevented by pressurising the workpiece [1]. Therefore, the temperature [32] and pressure need to be appropriately applied [1, 32] to achieve the desired and uniform crystallinity, and therefore material properties. The fusion bonding conditions are temperature, pressure and time.

2.4 Process window

The failure or success of the weld lies in the proper application of all parameters of the material, design and process. To achieve an induction weld, the material has to be melted, and pressure has to be applied to ensure fusion of the laminates. The three main process contributors to

a successful fusion are temperature, pressure and time, which form a set of ”conditions”. The process defects described below can be attributed to failing one or more of these conditions. An ideal process window appears where the material's state is suitable for welding without inducing defects.

A temperature contradiction appears. Insufficient heat generation does not allow the polymer chains to inter-diffuse across the welding interface, resulting in a kissing bond. A kissing bond can be prevented by using a higher temperature at the weld interface to reduce the matrix's viscosity and increase chain mobility. However, more material is squeezed out of the weld, and the degradation temperature nears. Moreover, diffusion and crystal growth are encouraged, which are necessary for proper bonding and (re-) consolidation. These factors all influence the overall development of the load-carrying capability of the resulting weld. The optimal temperature allows good diffusion and crystal growth while still staying sufficiently far away from the degradation temperature.

A similar contradiction arises for the pressure application. Insufficient pressure reduces intimate contact, preventing polymer chains from flowing across the reduced contact surface. This could result in a possible kissing bond. It also allows deconsolidation and leaves voids inside the weld area. However, excessive pressure causes severe squeeze-out. The weld area thickness reduces as material is squeezed out of this region. The laminate properties may even change if the fibre volume fraction increases. The optimal pressure consolidates the components and the weld while keeping as much material as possible in the weld area.

Chapter 3

Problem statement

The previous chapter discussed the welding parameters and defects related to induction welding. The induction welding process faces several challenges, especially for uni-directional plies. The literature identified various challenges and issues concerning the induction welding process, which is discussed in this chapter. The poorly defined process window is the main issue in creating a successful weld. The relationship between the defects and process parameters is discussed below but is not well-defined either. The discussed issues and the available relationship help define the goal of the presented research stated at the end of this chapter.

3.1 Issues indicated in other work

The induction welding process is a promising method for fusion bonding. However, it is a complex process [1, 2, 5, 10, 29] with many factors that affect the final product. Several authors indicate issues in different aspects of the welding process. First of all, it is difficult to determine the dominant heating mechanism [1, 2], which can even change during the process or due to processing parameters [1, 17]. Secondly, optimising the process parameters is essential [1, 3, 6, 10, 18] and requires a better understanding of the process and weld defects related to induction welding [1]. This can, for example, cover coil design [3, 5, 17, 29] for a uniform temperature distribution, which is key to a successful weld [3]. Surface cooling may be optimised as well to prevent the coil-side of the weld to suffer from thermal damage [2, 10, 14, 15, 17, 22]. Therefore, both the set-up and the process parameters have to be tailored to fit the workpiece's properties in order to achieve a high-quality fusion bond [1, 17]. Moreover, the relationship between the main process parameters - frequency, power/current, pressure and time [1–3, 17] – and the weld quality, properties and defects are still unclear [2, 33]. This shows the importance of an optimal process window, while chapter 2 shows the contradicting boundaries of this window to avoid or prevent defects in the weld.

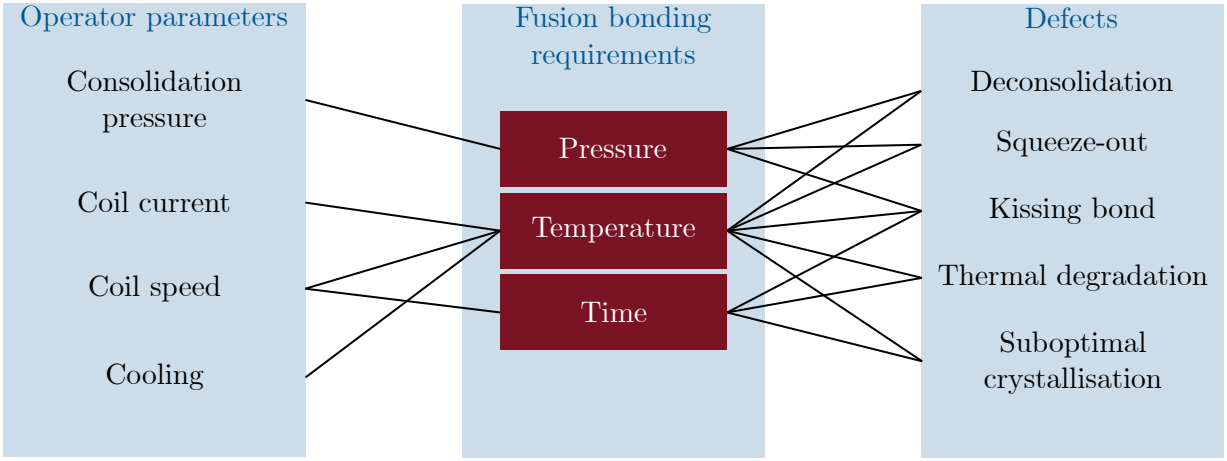

Figure 3.1: *The schematic relationships between operator process parameters and defects.*

3.2 Relationship operator parameters and defects

The process parameters control the fusion bonding conditions: pressure, temperature and time. Figure 3.1 shows the relationship of these requirements to both the parameters and the defects involved in induction welding. Although many more parameters were discussed in chapter 2, the shown process parameters in Figure 3.1 can be used for direct user control of the fusion bonding conditions. These process parameters are referred to as "operator parameters". Firstly, the pressure requirement can be satisfied using the consolidation pressure. Secondly, the temperature is controlled using the coil current and speed, and possibly cooling for the outer surfaces. The coil current and speed control the energy input in the material in a specified residence time frame. The cooling is used to correct the excessive surface temperatures and cools down the workpiece after welding. Lastly, the time is controlled by the coil speed. The slower the coil moves, the greater the residence time of the material in the magnetic field, which increases the temperature. The defects can be attributed to failing one or more of the fusion bonding conditions.

3.3 Goal

So far, the defects that can appear in an induction welded joint are known (chapter 2), but it is unclear when these defects occur. The relationship between the operator parameters and defects is visualised in Figure 3.1 but is not yet quantified to optimise the welding process of UD QI CF/LM-PAEK. The goal of this research is to identify the process defects as a function of the operator-controlled process parameters. This knowledge could be summarised in a map providing an overview of the occurring defects under specific process settings. The map can help the operator choose process parameter values that suit the workpiece and give the desired resulting weld.

Chapter 4

Method

This section shows the method used to map and investigate process-induced defects. First, the planned experiments are introduced for both mapping and investigation. The laminates' lay-up and consolidation process are discussed. The preparations for the assemblies and the induction welding set-up are described. The temperature during induction welding is monitored by thermocouples, whose placements are shown. The induction welding process requires a power curve to determine the relationship between the settings and the temperature in the workpiece. This is discussed before the induction welding process is described. Afterwards, a visual inspection is done to find surface defects. An ultrasonic scan shows internal defects using a non-destructive inspection method. The destructive inspection method is performed as microscopic inspection. Experiments using pressure-sensitive foil help support the investigation into the cause of the defects.

4.1 Planned experiments

The process-induced defects are identified to provide a map of the defects. The defects are expected to appear in welds that are welded outside the recommended conditions. Besides, some assemblies are welded to investigate the cause of the defects. The recommended conditions, for example, are used to investigate the in-plane and through-the-thickness temperature distribution. An overview of the planned experiments is shown in a test matrix visible in Figure 4.1.

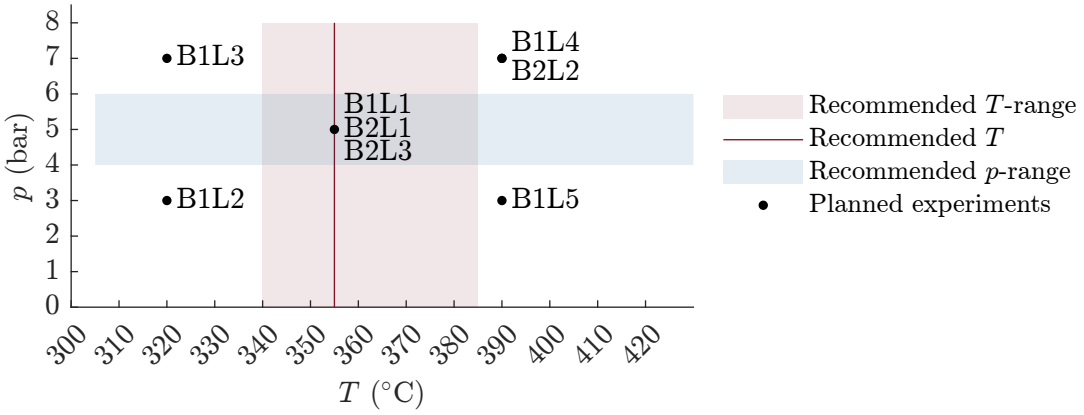

Figure 4.1: *Experiments to be executed.*

4.1.1 Identifying and mapping defects

Several process settings were chosen to map the different defects that are visible after induction welding. These induction welding experiments were performed in the first batch, B1. The mapping will be done using a reference weld using recommended conditions, and four welds outside these conditions. The assembly welded at the recommended settings serves as a reference weld: B1L1. The recommended process temperature and pressure for this situation are 355 °C and 5 bar, respectively. The process-induced defects are expected to occur at extreme conditions outside the recommended range. Therefore, the first assemblies (B1L2 to B1L5) are made at the outer corners of the test matrix. These are welded using several combinations aiming at low and high temperatures (320 °C and 390 °C) and low and high pressures (3 bar and 7 bar).

4.1.2 Investigating defect causes

The second batch (B2) of assemblies supports the investigation into the cause of the defects. The through-the-thickness and in-plane temperature distributions are measured using thermocouples. The thermocouple placement is discussed later, in subsection 4.3.2.

Through-the-thickness temperature distribution

The maximum temperature in the through-the-thickness T-distribution experiment (B2L1) is aimed at the recommended processing temperature (355 °C). The pressure is chosen in the middle of the recommended range, at 5 bar. The thermocouples track the temperature at the bottom, the interface and the top of the weld overlap at five locations along the welding direction.

In-plane temperature distribution

Two in-plane temperature distributions are measured: one on the bottom surface of the weld overlap and one at the weld interface. First, the temperature distribution at the bottom surface of the weld is measured in a high-temperature, high-pressure experiment (B2L2), aiming at 390 °C and 6.5 bar. This supports investigating the cause of the surface defects at the bottom of the weld. Secondly, an experiment is performed to measure the temperatures at the weld interface (B2L3) at the recommended conditions, which were discussed before. This experiment is intended to explain the processing conditions at the weld overlap.

Pressure distribution

The pressure is applied by a pressure tube which is covered by a rubber strip. The pressure at the contact area of the set-up with the workpiece is investigated as well. Two laminates (B1L6) are placed in the induction welding set-up and pressurised. In total, nine experiments are planned to both identify and investigate the process-induced defects. An overview of the experiments is shown in Table 4.1.

Weld	Conditions		Goal
	T (°C)	p (bar)	
B1L1	355	5	Reference assembly at recommended conditions.
B1L2	320	3	Identifying defects, mapping.
B1L3	320	7	Identifying defects, mapping.
B1L4	390	7	Identifying defects, mapping.
B1L5	390	3	Identifying defects, mapping.
B1L6	-	-	Investigating defects, p-distribution.
B2L1	355	5	Investigating defects, through-the-thickness T-distribution.
B2L2	390	6.5	Investigating defects, bottom in-plane T-distribution.
B2L3	355	5	Investigating defects, overlap in-plane T-distribution.

Table 4.1: *Overview of the test matrix's conditions, assemblies and their goals.*

4.1.3 Temperature to current conversion

The temperature is not a setting in an induction welding process but a target. The eventual welding temperature reached in the material highly depends on the equipment, material and operator parameters, as discussed in chapter 2. The induction welding process does, therefore, not guarantee that the chosen target temperature occurs in the weld.

The operator parameters that mainly influence the welding temperature are coil current and speed. To account for the dependability on the equipment and material, the test matrix axes can be expressed differently. The energy input can be expressed as $\frac{I}{v}$, referred to as power, because current relates to power and both the current and speed affect the temperature raise in an opposing manner. The y-axis shows the pressure applied to the material. The current that is used for the welding equipment settings has to be determined before the welding process can start. This is done using a power curve, which is discussed below as well.

4.2 Material

Nine laminates are made to facilitate the experiments, which are laid-up manually. The material used is Toray Cetex® TC 1225. This is a low-melting, carbon fibre-reinforced polyaryletherketone (LM CF-PAEK). The plies for the laminate are cut to size to fit a 12-inch, or 30.48 mm, picture frame. The lay-up sequence is $[45/0/\text{-}45/90]_{2s}$. Each ply is 0.14 mm thick [46], resulting in a 2.24 mm thick laminate consisting of sixteen layers. The lay-up is consolidated in a 200-tonne Pinette Emidecau Industries press. Consolidation takes place at 365 °C and 15 bar, after a controlled temperature increase and preheat phase. This process is schematically visualised in Figure 4.2.

The laminates' edges are trimmed using a diamond-coated water-cooled saw. From every laminate, two laminates are cut that are used for the induction welding process. The induction welding set-up supports laminates that are 4.25 inch wide to achieve a weld overlap width of 1.5 inch. The laminates are thus cut to be 300 mm by 108 mm. Before these laminates can be used for induction welding, they have to be dried in an oven for 16 hours and 15 minutes at 120 °C. The laminates cut from the consolidated laminate are shown in Figure 4.3 as light blue rectangles. The weld overlap area is highlighted in dark blue.

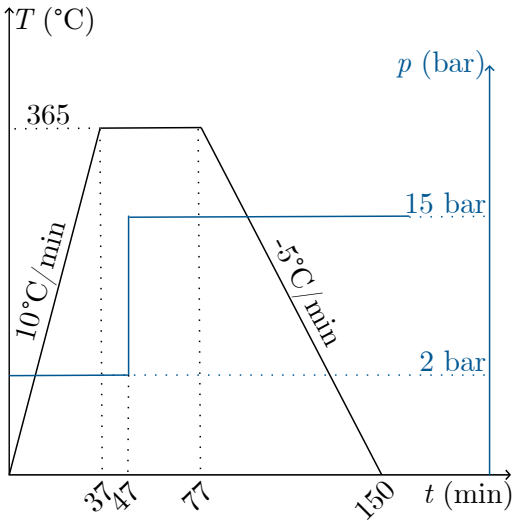

Figure 4.2: *A schematic visualisation of the consolidation process*

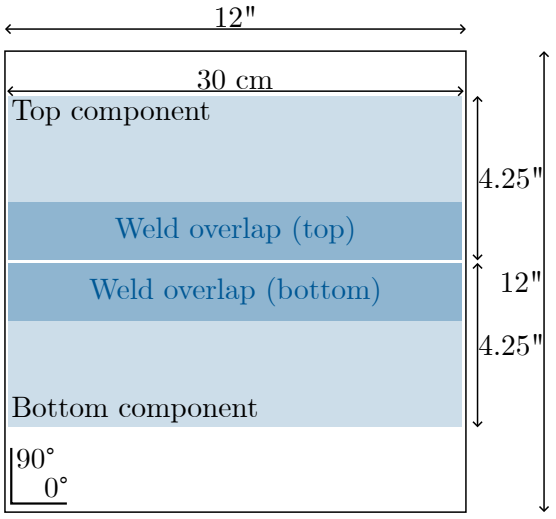

Figure 4.3: *The 12 inch picture frame with locations of where the two laminates are cut out.*

4.3 Induction welding

This section discusses the induction welding procedure. The induction welding tool and laminates have to be cleaned before use. The positioning of the laminates in the tool is shown as well as the placement of the thermocouples. Before welding, the relationship between operator parameters and welding temperature has to be determined. Therefore, a power curve is made for this purpose to assist the operator in choosing a welding current. Once the induction welder settings are chosen, the welding process is started.

4.3.1 Set-up preparation

The induction welding tool is cleaned with tissues and isopropyl alcohol (IPA) before use. The overlapping top laminate is supported by a riser in the consolidation tool. The laminates are aligned using a ruler in the tool to ensure a correct weld overlap width. Spacers left and right from the laminate ensure a good positioning of the laminates. The laminates are cleaned using new tissues and IPA as well. First, the bottom laminate is placed in the tool. Then, thermocouples are placed at the weld interface or on the outer surfaces of the weld overlap. The locations of the thermocouples are discussed below. Pieces of tape are used to keep the thermocouples, the supports and laminates in place. The assembly is shown as a schematic representation Figure 4.4. The tool is finally closed before starting induction welding.

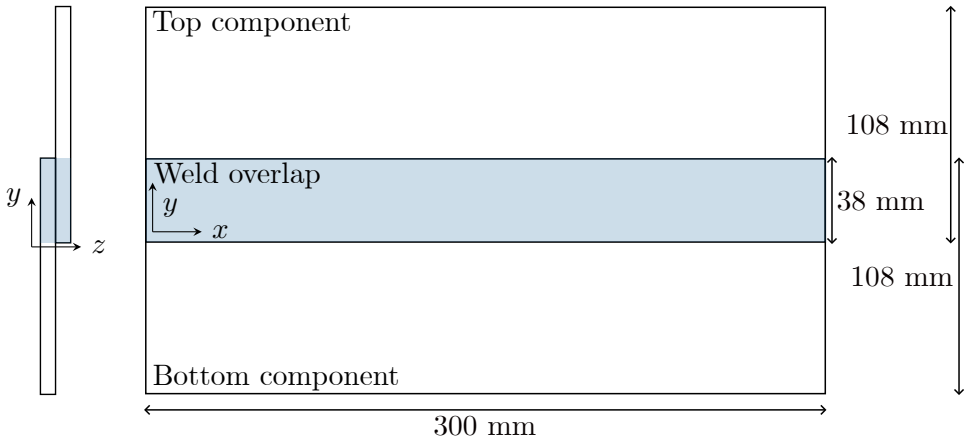

Figure 4.4: *Schematic overview of weld overlap.*

4.3.2 Thermocouples

The temperature can be logged using thermocouples. The thermocouples are Duplex Insulated CHROMEGA™-Constantan Type E wires. The small diameter, 0.25 mm, interferes the least with the electro-magnetic field. The wire is stripped from its insulator, which reveals the two wires that have to be connected. The connection is a small weld at the tips of the wires. The wires and the welded tip are taped in Airtech Kapton tape for protection. The placement of the thermocouples differs for various experiments. The different lay-outs are placed on different surfaces of the weld region, depending on the goal of the experiment. The top, interfacing and bottom surfaces are highlighted in Figure 4.5.

Placement for mapping weld defects

The reference assembly (B1L1) will be made with thermocouple placements as shown in Figure 4.6a. Five thermocouples are located in a line in the middle of the weld overlap along the welding, or x-, direction. Most other assemblies are made using placements as shown in Figure 4.6b (B1L2 to B1L5). For these assemblies, two thermocouples are located in the middle of the weld overlap along the welding direction.

Placement for through-the-thickness measurements

The reference assembly thermocouple lay-out (Figure 4.6a) is used again to find the through-the-thickness distribution (B2L1). Three rows of five in-line thermocouples are located on the bottom, interfacing and top surfaces of the weld overlap (Figure 4.5). In total, fifteen thermocouples are used to find an indication of the through-the-thickness T-distribution.

Placement for in-plane measurements

Figure 4.6c shows the fifteen thermocouple locations to measure the two in-plane temperature distributions. This scattered lay-out is used for logging the temperature distribution at the bottom surface of the weld (B2L2). The same lay-out is used for determining the temperature distribution at the weld interface (B2L3). The measured in-plane temperatures are used for a second-degree polynomial fit in x- and y-direction using `poly22` [47] to gain a better insight into the in-plane temperature distributions.

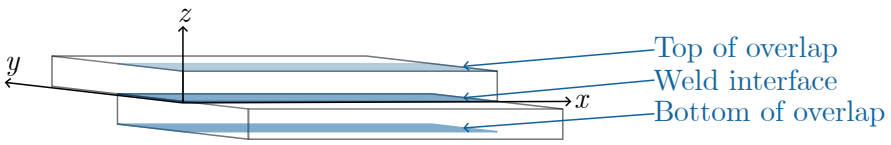

Figure 4.5: *Schematic overview of weld overlap for the locations of the thermocouples.*

4.3.3 Power curve

Before the actual welding can begin, the operator needs to determine the laminate-dependent relationship between coil current and welding temperature. This is done using a power curve, where several currents and measured temperatures are used to create a polynomial fit for this relationship. A quadratically fitted power curve is made for the first laminate for each batch. This means that the laminates B1L1 and B2L2 (recommended condition experiments) are used for determining both the power curve and welding experiments. The thermocouple lay-out used in these assemblies are the five in-line placements shown in Figure 4.6a. The average temperature of the three middle thermocouples is used for constructing the power curve. The resulting power curves are discussed in chapter 5.

4.3.4 Welding process

After determining the welding currents to achieve the target temperature, the welding process can start. All induction welding processes start at a laminate temperature of approximately 30 °C. The robot inserts the induction coil into the tool at the left end of the laminates. The coil moves with a speed of $v_{coil} = 2.5\,\mathrm{mm\,s^{-1}}$. The velocity of the coil is lower in a start- and end-zone of 50 mm to pre-heat the material: $0.833\,\mathrm{mm\,s^{-1}}$ and $1.667\,\mathrm{mm\,s^{-1}}$. The coil exits the tool at the right end of the laminates. The weld has to cool down to 20 °C below T_g before the tool can be opened to increase the cooling rate. The glass-transition temperature is $T_g = 147\,°\mathrm{C}$ for LM-PAEK [46], so the tool can be opened below 127 °C.

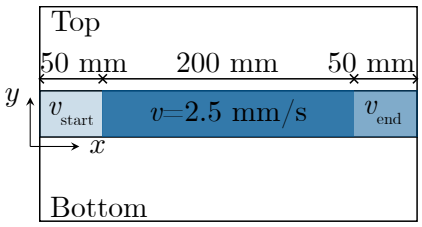

Figure 4.7: *Start- and end zone velocity of the induction coil.*

4.4 Visual inspection

The welded assemblies are placed in a photo booth after cleaning them with IPA. The welds are photographed from above and below, to capture the the top and the bottom sides. A ruler is placed next to the laminates for size reference. The surface defects on the back of the weld overlap are measured by hand. The thickness of the two laminates at the weld location is measured every cm in the middle line of the weld overlap in the x-direction using a thickness gauge.

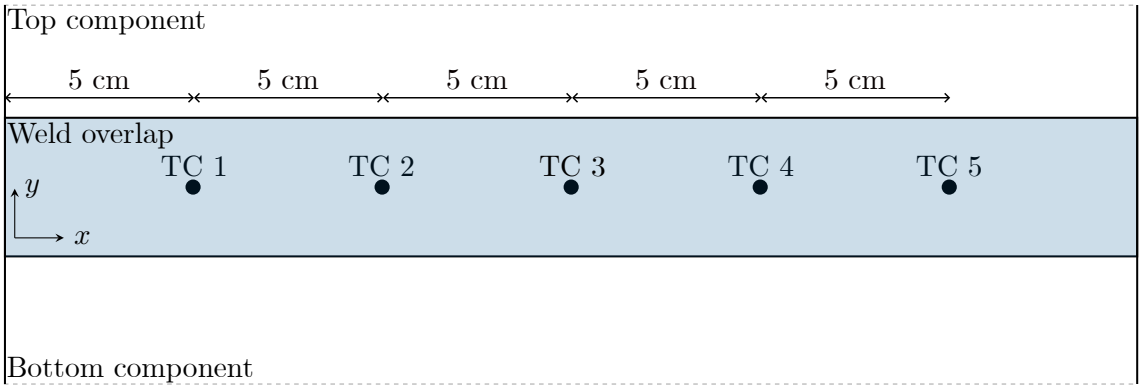

(a) *Locations in the reference assembly (B1L1) and the assembly to investigate the through-the-thickness T-distribution (B2L1).*

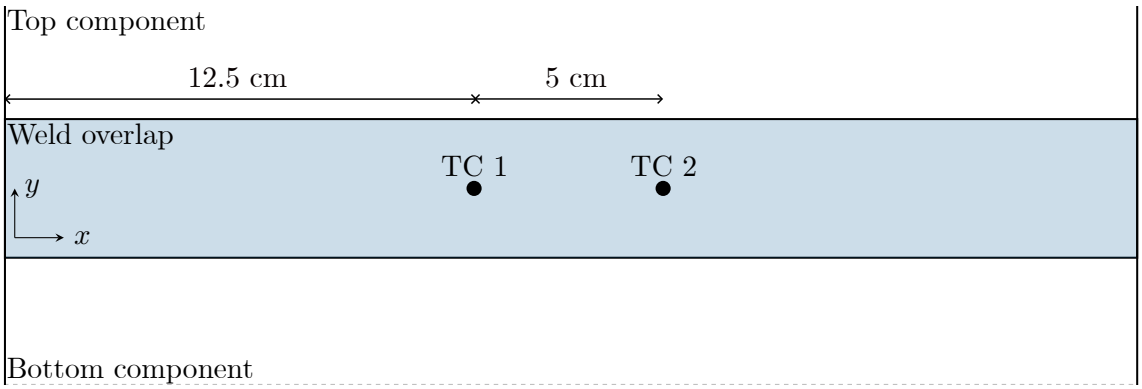

(b) *Locations in the assemblies at the extreme conditions (B1L2 to B1L5).*

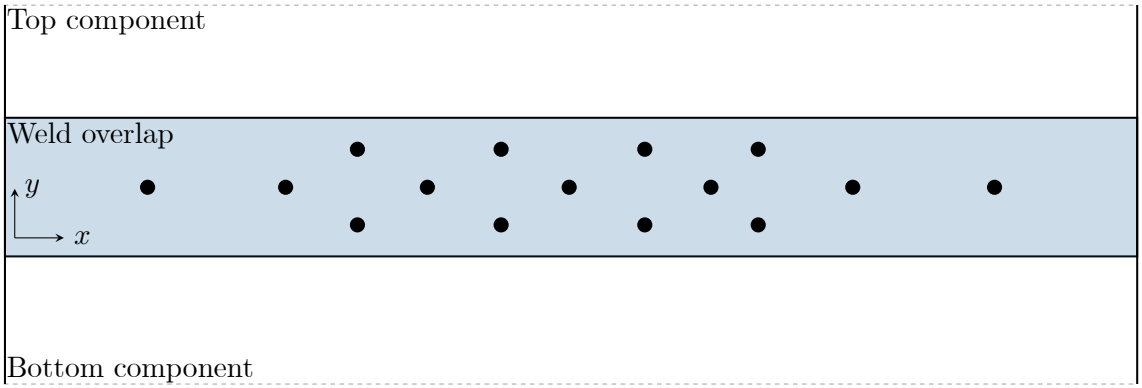

(c) *Locations in the assemblies investigated for their in-plane T-distribution (B2L2 and B2L3).*

Figure 4.6: *Schematic overview of thermocouple (TC) placements.*

4.5 Ultrasonic scan

After visual inspection, the laminates are inspected using an ultrasonic scan. For this inspection, a Sonatest NDTS RapidScan2 C-scan is used. An ultrasonic scan sends a signal through an object, which is returned by a back wall. The returned signal is used to locate defects and determine material thickness. The amount of contact at the weld interface can be determined using such a non-destructive inspection method.

First, the weld overlap is scanned. The bottom laminate is placed flat on the table, while the hovering top laminate is supported. The C-scan roller presses and rolls over the weld overlap (highlighted in blue in Figure 4.8).

Then, the C-scan is done at the long edges of the laminates, which is highlighted in red in Figure 4.8. This is done outside the weld overlap, where edge effects can occur. The assembly is placed flat on top of the C-scan table. The bottom laminate edge can be scanned similarly to the weld overlap scan, pressing and moving the roller on the bottom, long edge. This is repeated for the top laminate.

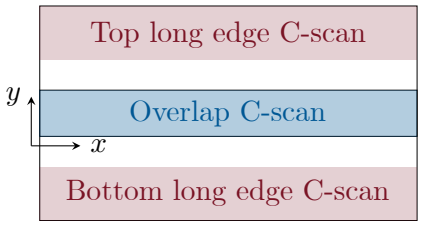

Figure 4.8: *Highlighted areas that are scanned using a C-scan for identifying (internal) defects.*

The weld area images are post-processed in order to find the area that is affected by the welding process. The weld overlap images can be converted to grayscale, after which they are converted to binary images (see Figure 4.9) using a threshold value (`adaptthresh` [47]). The threshold value is calculated locally, using a sensitivity of 0.7 in a neighbourhood size of 155. The black and white pixels can be counted to find the amount of affected pixels, thus affected area. The area affected by edge defects is found by masking the images before binarising.

It is important to note that the thermocouples are visible as non-welded areas on the C-scan. Unfortunately, the number of thermocouples used in the weld overlap varies for the different experiments. Therefore, the typical size of a few randomly chosen thermocouples will be subtracted from the investigated pixels to correct for the varying thermocouple areas as shown in Equation 4.1.

$$\%_{\text{affected}} = \frac{n_{\text{pixels, affected}} - n_{\text{TCs}} n_{\text{pixels, typical TC}}}{n_{\text{pixels, overlap}} - n_{\text{TCs}} n_{\text{pixels, typical TC}}} \tag{4.1}$$

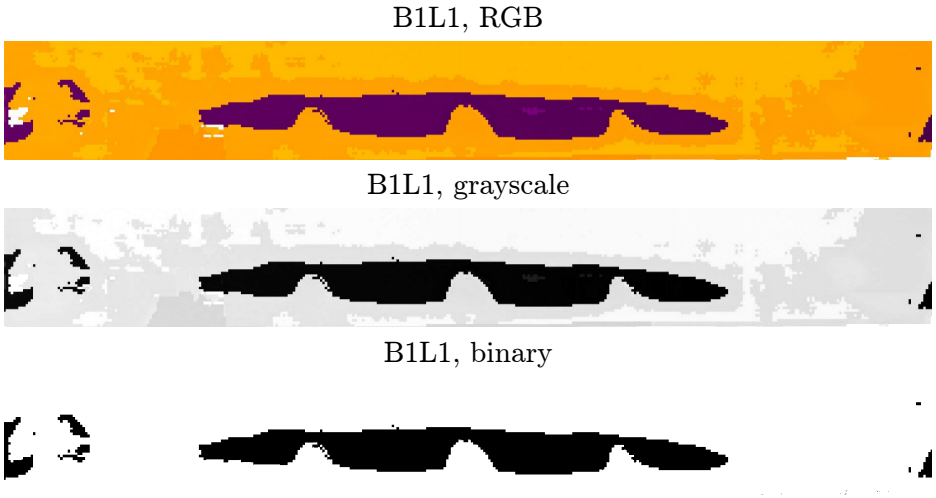

Figure 4.9: *Conversion from RGB image of the reference weld overlap (B1L1) C-scan to grayscale and binary.*

4.6 Pressure distribution

The induction welding set-up applies a pressure to the laminates to restrict the laminates from moving, provide intimate contact en assure re-consolidation of the weld overlap. The pressure is applied by a pneumatic tube, which is protected by a rubber strip (Figure 2.1). The rubber strip is in direct contact with the surface of the back of the weld overlap.

The pressure distribution of the tube on the weld overlap is determined by Fujifilm Prescale pressure-sensitive foil at room temperature. Pressures of 3 bar, 5 bar and 6.5 bar in the pneumatic tube are tested. This pressure range requires two types of pressure-sensitive foils. The Fujifilm Prescale LLLW foil is applicable on 2 bar to 6 bar applications. The Fujifilm Prescale LLW foil is applicable for higher pressure applications: 5 bar to 25 bar. The overlapping regions of the foils' specifications is around a pressure of 5 bar. This pressure distribution experiment is therefore done on both foils. The foils are two-sheet types, consisting of a colour-forming and colour-developing film. The colour-forming micro-capsules break according to their pressure range and react with the colour-developing film. This results in a coloured stain on the colour-developing film. Therefore, an intense, rich colour corresponds to a high pressure according to the specified pressure range. Afterwards, the foils are observed, scanned and saved for visual inspection.

4.7 Microscopic inspection

After the aforementioned non-destructive inspection, a microscopic inspection is performed. The cross-sections of the assemblies are cut from several locations in the weld overlap. Figure 4.10a shows the locations of the samples taken from the reference weld. Figure 4.10b depicts the locations of samples of the welds at extreme conditions. The bold lines in the schematic overviews show the inspected cross-sections. The samples are prepared by embedding in epoxy resin and polishing.

The embedded and polished samples are inspected using a digital Keyence VHX-7000 microscope. The microscope allows the user to measure distances in the images using a digital in-plane measurement tool. An overview of the inspected areas is shown in Figure 4.11. The in-plane

measurement tool is used for measuring several issues: the gaps between interfacing surfaces; the weld thickness at several locations; and the ply thickness at these and defective locations.

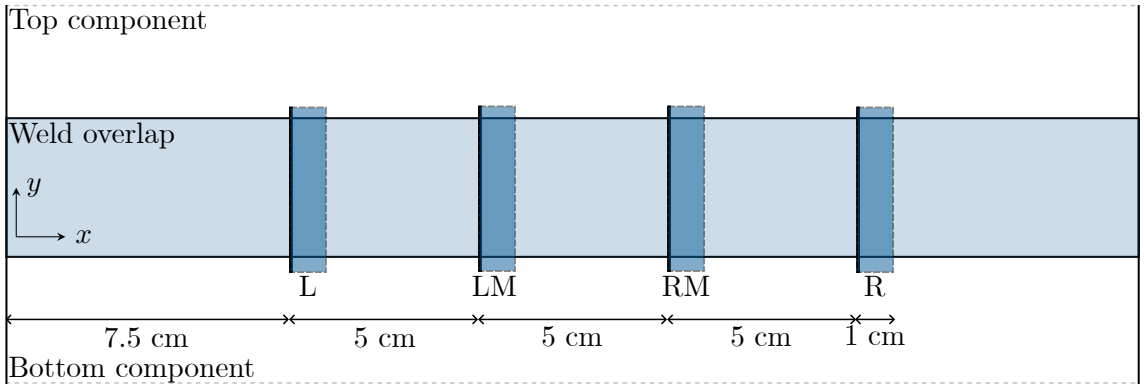

(a) *Sample locations in the reference assembly (B1L1).*

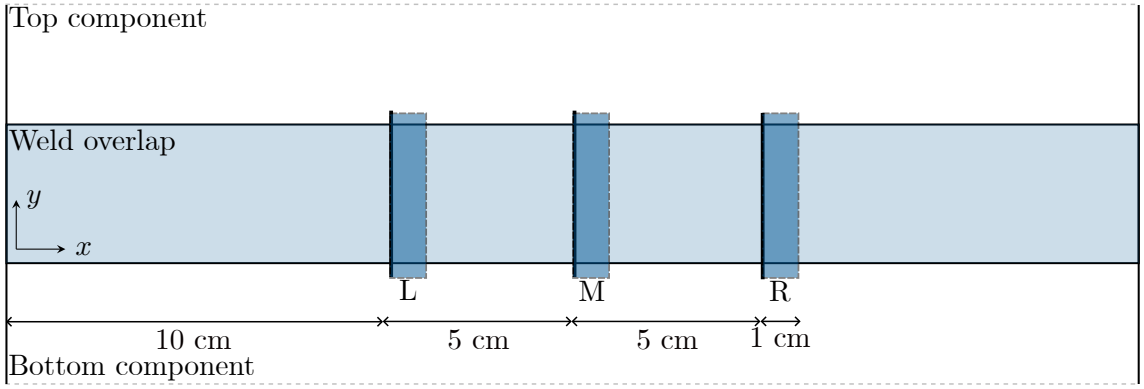

(b) *Sample locations in the assemblies at extreme locations (B1L2 to B1L5).*

Figure 4.10: *Schematic overview of microscopy sample locations.*

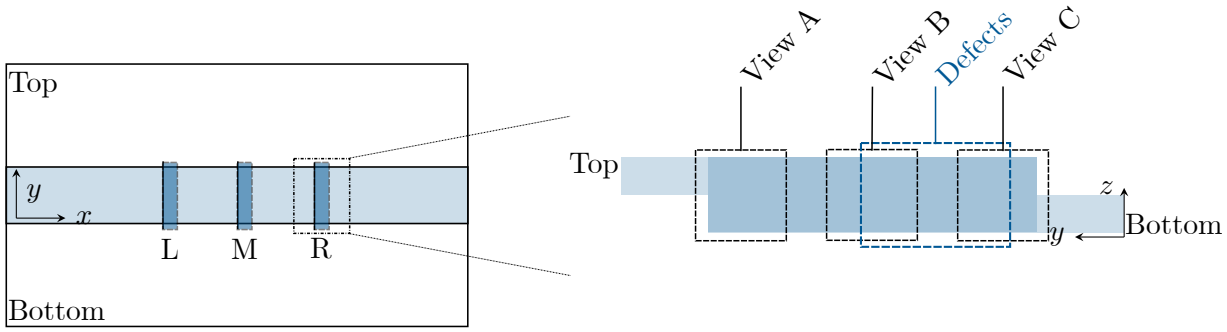

Figure 4.11: *Inspected areas of a sample during microscopy.*

Chapter 5

Results

This chapter presents the executed experiments and their results. The executed experiments are shown based on the presented power curve. The assemblies were welded while thermocouples tracked the temperature history. The temperature histories are presented for the mapping welds, as well as the temperature distribution in-plane and through-the-thickness. The in-plane temperature distribution measurements were used to create a quadratic fit to find the shape of the high-temperature areas. The assemblies' photographs for the visual inspection are shown. The visual inspection revealed edge effects and surface defects; the latter's measurements are given. An ultrasonic scan revealed the actual welded area in the weld overlap. Besides, some areas were affected by the edge effects, as the visual inspection showed before. These edge effects are captured in the ultrasonic scan along the long edges of the assemblies. The pressure distribution applied by the induction welding set-up is found using pressure-sensitive foil. Finally, microscopic analysis reveals the internal structure of several samples along the welding direction.

5.1 Executed experiments

The conditions of the executed experiments depend on the relationship between the current and the achieved temperature in the material. This relationship is determined using a power curve, which is discussed below. After this, the actually executed experiments are presented.

5.1.1 Determine current: power curve

The power curve is used to indicate the relationship between the coil current, or power, and the weld interface temperature during heating. Figure 5.1 shows a typical quadratic, mathematical fit used in this process. Three fits are shown in Figure 5.1: one used for the first estimate of the welding currents for the first batch (B1, using B1L1) and one to refine this curve. Additionally, a third fit is the power curve used for the second batch (B2, using B2L1).

A two-step approach is used to find the appropriate welding settings. The first step is to solely heat the assembly, without welding, to find a current-window to achieve the target temperatures. The second step refines this window by adding every data point obtained during welding ($T > T_m$).

The current to reach the target temperature in the first batch is estimated in the first step as $T = 0.0012I^2 + 0.0225I + 20.078$, which is based on the B1L1 assembly. The second fit shows how this first fit changes if other, higher temperatures are taken into account obtained during welding. This adjusted the fit to $T = 0.0007I^2 + 0.2969I - 18.503$ to become more accurate. The

second batch (B2) of assemblies was welded using a newly determined power curve expressed as $T = -0.005I^2 + 1.0247I - 118.45$, based on the B2L1 assembly.

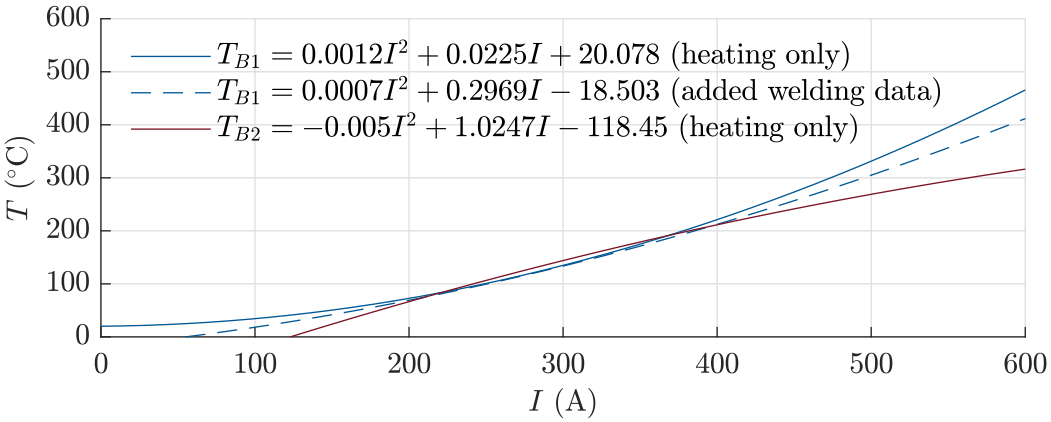

Figure 5.1: *Power curves.*

5.1.2 Resulting test matrix

The planned experiments (Figure 4.1) are based on the recommended temperature and pressure ranges. The desired pressure can be set directly using the induction welding set-up; the current has to be set indirectly using the power curve. The executed experiments are presented in Figure 5.2.

Sadly, the temperatures of the through-the-thickness T-distribution experiment (B2L1) were not recorded during welding. The through-the-thickness temperature distribution experiment (B2L1) was therefore recorded as a weld on an already welded assembly. Therefore, the results of the repeated weld on this assembly are presented.

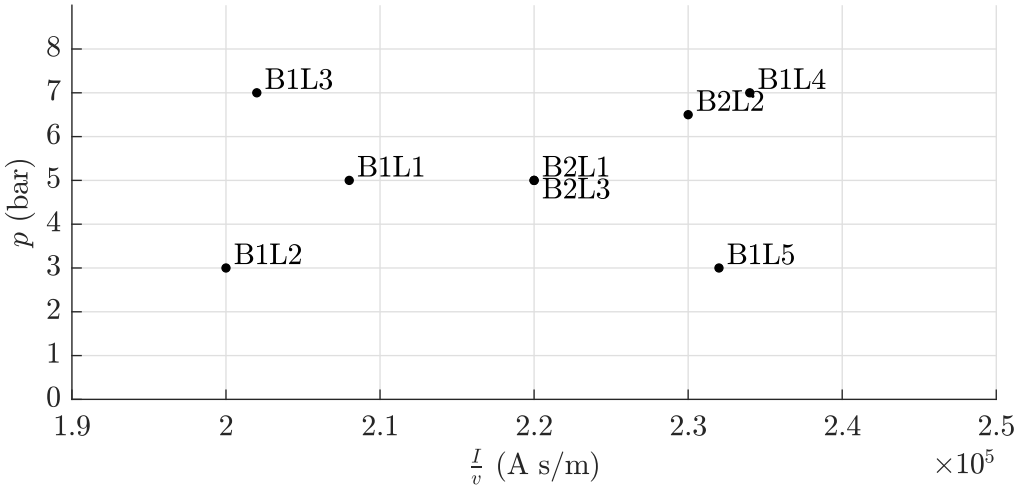

Figure 5.2: *The executed experiments following from the test matrix.*

5.2 Welding temperatures

Maximum reached temperatures

The thermocouples logged the temperatures during induction welding. The temperature history of the reference weld is shown in Figure 5.3. The first thermocouple in this assembly failed and is therefore not visible in the Figure 5.3. The fifth thermocouple failed as well. This can be seen as temperature fluctuations in the measurement, but it still shows a typical response and is therefore shown in the graph. However, the three middle thermocouples show the highest, most constant temperatures and are thus most important. The central thermocouple reaches the highest temperature of 336 °C.

This maximum temperature is lower than the target temperature, which holds for some other welds as well. The assemblies' maximum achieved temperatures are shown in Table 5.1. These results are, as mentioned before, closely connected to the current estimation of the power curve. The currents were adjusted after every obtained data point, which allowed the low-power, high-pressure (B1L3) and high-power, low-pressure (B1L5) experiments to be accurate estimates.

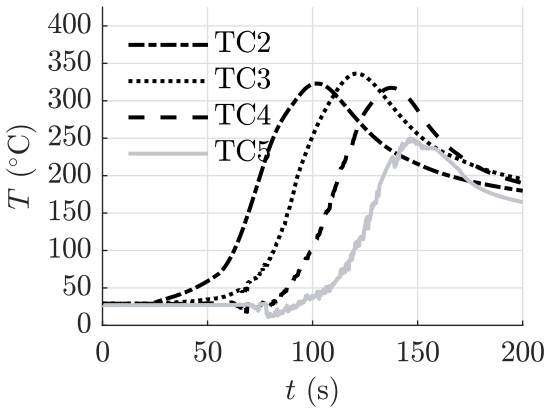

Figure 5.3: *The temperature measured in the reference weld using thermocouples at positions shown in Figure 4.10a.*

Weld	TC positions	T_{max} (°C)		T_{target} (°C)	Power curve
B1L1	5 at interface	336	✗	355	$T = 0.0012I^2 + 0.0225I + 20.078$
B1L2	2 at interface	313	✗	320	Adjusted from previous
B1L3	2 at interface	322	✓	320	Adjusted from previous
B1L4	2 at interface	413	✗	390	Adjusted from previous
B1L5	2 at interface	392	✓	390	$T = 0.0007I^2 + 0.2969I - 18.503$
B2L1	5 at top, interface, bottom	335	✗	355	$T = -0.005I^2 + 1.0247I - 118.45$
B2L2	15 scattered at bottom	349	-	-	$T = -0.005I^2 + 1.0247I - 118.45$
B2L3	15 scattered at interface	-	✗	355	$T = -0.005I^2 + 1.0247I - 118.45$

Table 5.1: *Maximum temperatures reached in the welds, at thermocouple locations shown in Figure 4.6a (5 in-line), Figure 4.6b (2 in-line) and Figure 4.6c (15 scattered).*

In-plane temperature distribution

Both the in-plane temperature distribution at the bottom and at the weld interface are measured. The measured maximum temperatures are used for a second-degree polynomial fit in x- and y-direction. The in-plane temperature distribution confirms that the highest temperature lies in the centre of the weld overlap.

The in-plane temperature distribution of the bottom of the weld overlap (B2L2) is shown in Figure 5.4. The maximum temperatures are shown in Figure 5.4a. The polynomial fit at the bottom of the weld is depicted in Figure 5.4b. The high power results in a measured and fitted temperature of almost 350 °C in the weld centre. This temperature lies in the recommended processing range of the material (chapter 4) [46].

The temperature distribution of the weld interface is presented in Figure 5.5. The polynomial fit is visible in Figure 5.5b at the x- and y-plane of the weld overlap. The thermocouples showed the lowest temperature to lie at the outer positions. The centre thermocouple of the B2L3 experiment failed during welding, so only the estimate from the fit is available. The estimated maximum temperature at the centre lies around 325 °C.

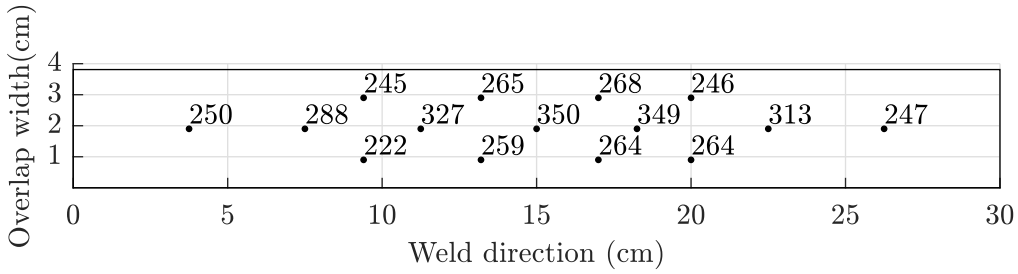

(a) *Maximum measured temperatures.*

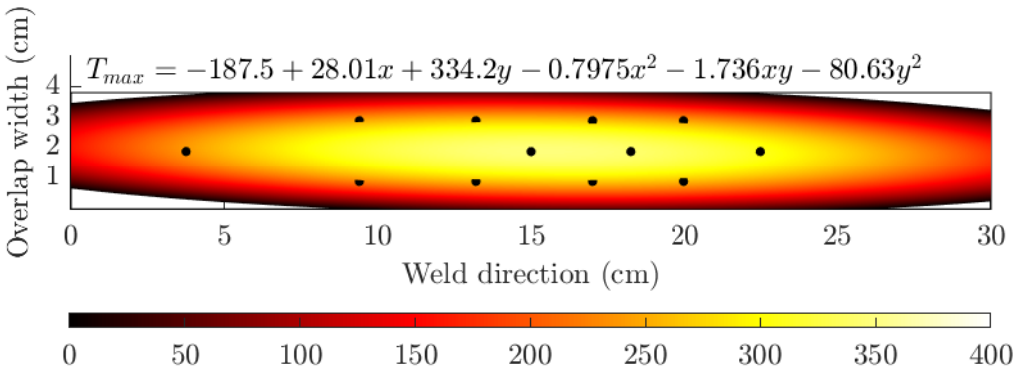

(b) *Temperature distribution fit.*

Figure 5.4: *In-plane temperature distributions at the bottom of the weld overlap (B2L2), using locations shown in Figure 4.6c.*

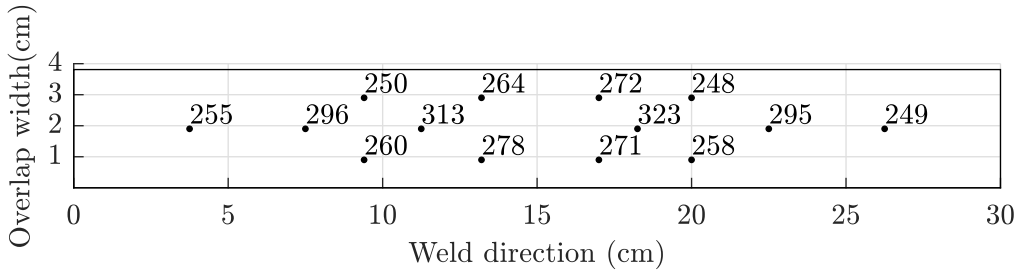

(a) *Maximum measured temperatures.*

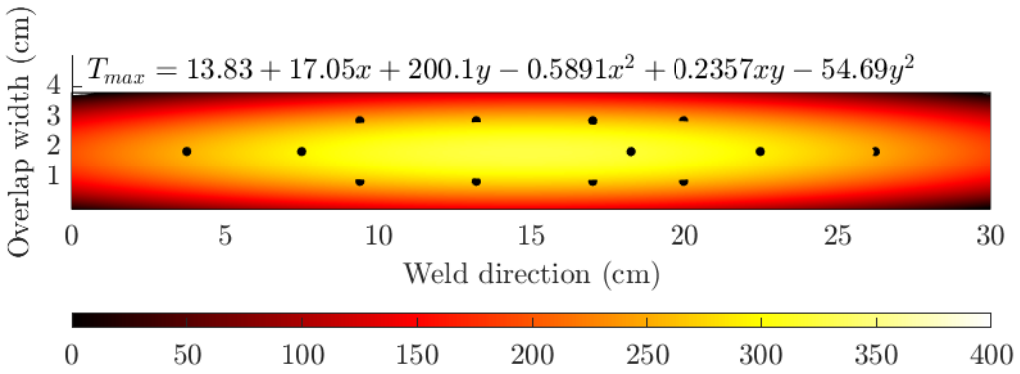

(b) *Temperature distribution fit.*

Figure 5.5: *In-plane temperature distributions at the weld interface (B2L3), using locations shown in Figure 4.6c.*

Through-the-thickness temperature distribution

An indication of the through-the-thickness temperature distribution is found using thermocouples at the top, interface and bottom of the weld overlap. The actual welding of this experiment is not recorded, so the presented measurements were obtained during re-welding the assembly. Figure 5.6 depicts the temperature history of these measurements. The central thermocouple measures a peak of approximately 335 °C, while lower temperatures are measured at the top and bottom of the weld overlap.

The temperature history curves of the top of the overlap look significantly flatter than those measured at the weld interface. The top of the overlap is cooled by the heat sink in the induction welding set-up. A maximum temperature of 221 °C is recorded by the middle thermocouple at the top of the weld overlap.

Lastly, the temperatures at the bottom of the weld overlap look similar to the temperatures at the weld interface. The maximum temperature measured at the bottom of the weld overlap is 311 °C. This lies slightly above the melting temperature.

The measured temperature distribution shows similarities to the desired temperature distribution as discussed in chapter 2 (Figure 2.3). The temperatures at the weld interface are the highest, and the top of the weld overlap is cooled. However, the temperature should be measured at more locations through the thickness in the laminates during welding to determine a

representative through-the-thickness temperature-distribution.

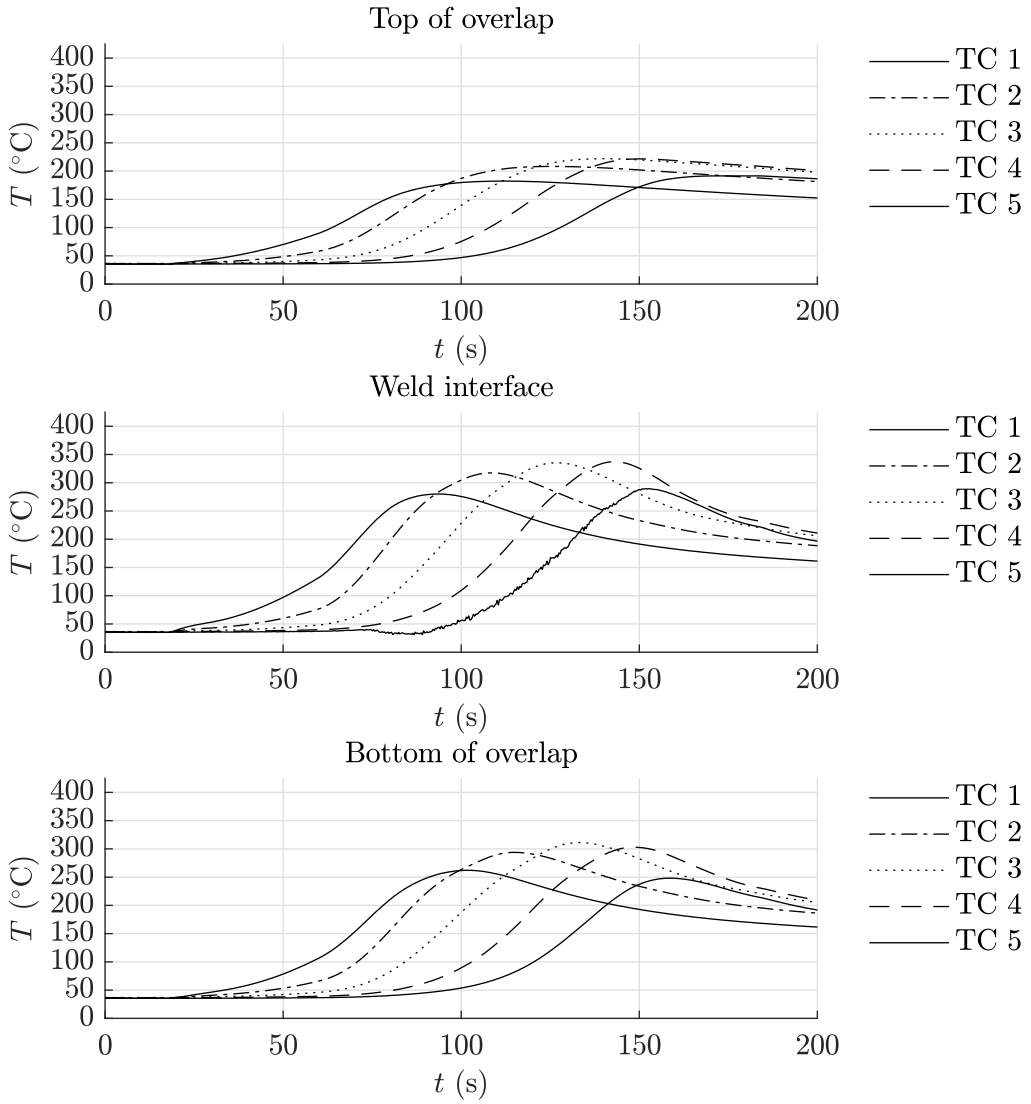

Figure 5.6: *In-line and through-the-thickness temperature distribution of the repeated weld (B2L1), measured at thermocouple locations as shown in Figure 4.6a at the top, interface and bottom of the weld overlap.*

5.3 Visual inspection

The assemblies undergo visual inspection after welding. The welding process caused edge effects to occur, which are highlighted. Also surface defects are visible at the bottom of the weld overlap. Both the surface defects and the weld overlap thickness are measured; these results are presented below.

Photographs

All welds are photographed for visual inspection. An example of the photographs is shown in Figure 5.7, taken of the reference assembly. The assemblies are photographed from the top (Figure 5.7a) and bottom (Figure 5.7b). The photographs of all assemblies are combined in Appendix B. All assemblies show some degree of edge effects at the start of the weld. Some welds show a surface defect at the bottom. Both types of defects are discussed below.

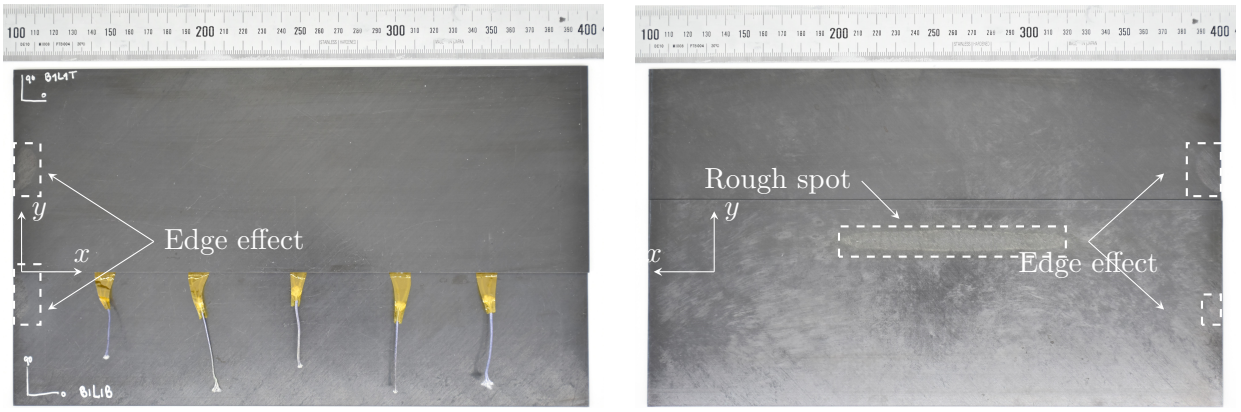

(a) *Top of the reference assembly (B1L1).* **(b)** *Bottom of the reference weld (B1L1).*

Figure 5.7: *Photographs of the reference weld (B1L1) taken for visual inspection. The other assemblies are shown in Appendix B.*

Edge effects

The defects are right outside the weld overlap at the start of the weld for low power-settings. However, the high-power assemblies (B1L4 and B1L5) show more extreme defects, which is shown in Figure 5.8. A close-up of such edge effects is shown in Figure 5.8b, which is welded at a high-power and high-pressure setting. The defects are clearly visible around both the start and the ending zones of the weld overlap. Besides, the long edges of the top laminates are affected as indicated in Figure 5.8a. The second weld, B1L2 shows the least amount of visible edge effects. The edge effect defect is only visible at the bottom laminate, which is not cooled by the heatsink, allowing a higher temperature in the material at the edges.

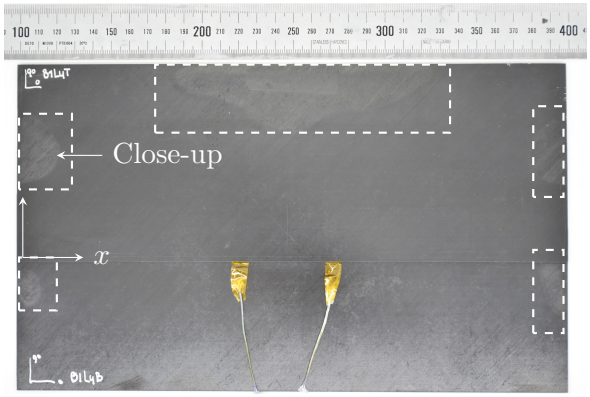

(a) *Edge effects, highlighted.*

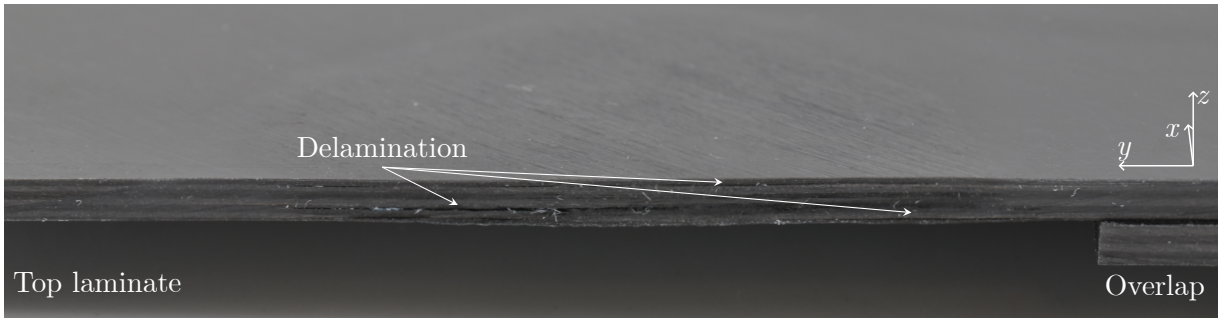

(b) *Close-up of an edge effect outside the start, imaged from the top.*

Figure 5.8: *Photographs of a high-power, high-pressure weld (B1L4) taken for visual inspection.*

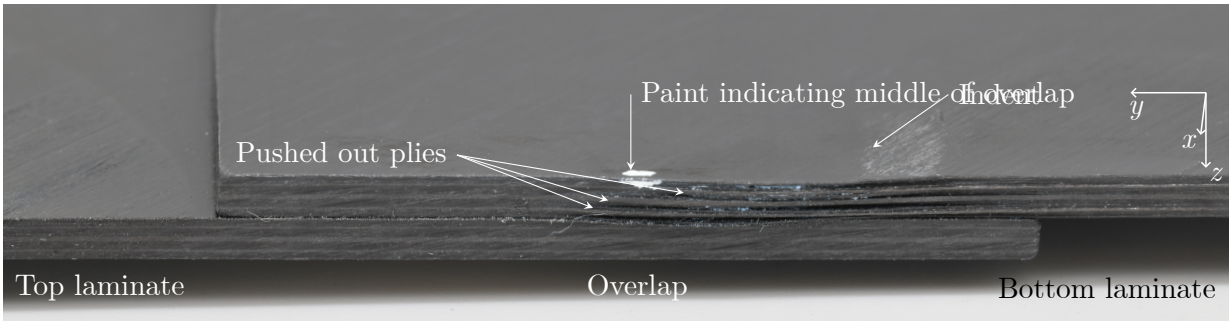

Figure 5.9: *Close-up of an edge effect at the end of the weld overlap of a high-power, high-pressure weld (B2L2), imaged from the bottom.*

Surface defects at bottom of overlap

The bottom of the weld overlaps is affected by the welding process as well. An example of the resulting surface defects is shown in Figure 5.10. The shape of these surface defects appears to be elliptical. Rough spots, visible in Figure 5.10a, show in the middle of the weld overlaps, especially in the low-power welds. This defect seems to result in dry fibres, which would be visible in the micrographs. However, the high-power settings result in an indent in this region, as is shown in Figure 5.10b. The bottom of the weld overlap is in direct contact with the pressure tube in the induction welding set-up (see Figure 2.1). The cause of these defects can be attributed to the

pressure or temperature distribution at this location. The size of the elliptical rough spots and indents are expressed in major and minor axes, provided in Table 5.2.

(a) *Bottom surface of the reference assembly weld overlap (B1L1) showing a rough spot.*

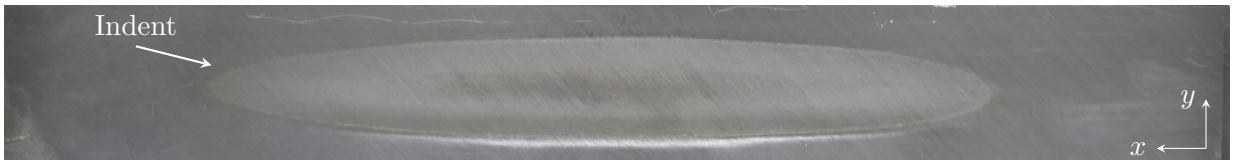

(b) *Bottom surface of the high-power, high-pressure assembly weld overlap (B1L4) showing an indent.*

Figure 5.10: *Bottom surfaces of the weld overlap showing defects.*

Weld	Major axis (mm)	Minor axis (mm)
B1L1	123	12
B1L2	29	4
B1L3	95	9
B1L4	191	25
B1L5	184	22
B2L1	158	18
B2L2	171	26
B2L3	131	12

Table 5.2: *Visible defect size in the origin of the bottom of the weld overlap.*

Manually measured weld thickness

Additionally, the thickness of the two laminates in the weld overlap is measured. The weld thicknesses are measured by hand using a thickness gauge (Figure 5.11a. Figure 5.11 shows a minimum weld overlap thickness at 20 cm from the start. This increases in the end zone of the welding process at 25 cm to 30 cm. This shows that the depth of the indent is not uniform nor is it in the centre of the bottom of the overlap. Instead, the indent is most apparent slightly right after the midpoint of the welding process.

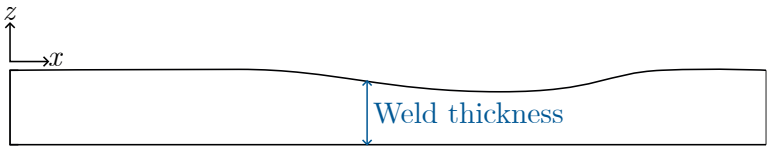

(a) *Schematic overview of weld thickness measurement.*

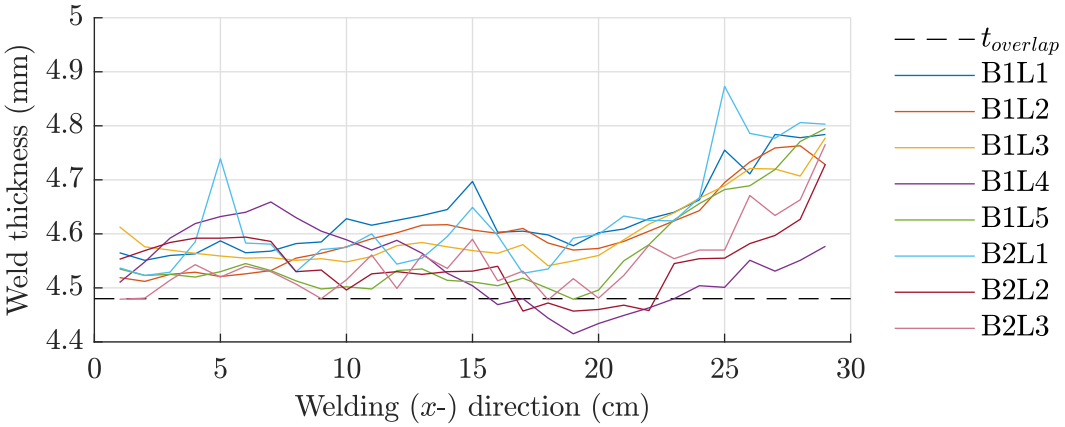

(b) *Weld thickness measurements.*

Figure 5.11: *Manually measured weld thicknesses in the middle of the weld overlap.*

5.4 Ultrasonic scans

The ultrasonic scan is used to locate defects and inconsistencies, and material thickness. The thickness is determined based on the time of flight of the ultrasonic signal. The signal is returned by the set-up's back wall or returned sooner due to inconsistencies or defects. The defects are displayed as smaller laminate thicknesses. The C-scan images are converted to grayscale and binary to quantify the defects (Figure 4.9).

5.4.1 Weld overlap

All weld overlaps were investigated using a C-scan. The C-scan converts the time of flight of the signal to a material thickness in mm. The scans show the areas where the material has a thickness of one laminate in yellow (approximately 2.24 mm). The purple colour corresponds to a thickness of two laminates (approximately 4.48 mm). The purple areas have an elliptical shape for the recommended and low power-setting welds. This shape is similar to the surface defects at the bottom of the weld. The high power-setting weld overlaps, however, show a more rectangular purple area where the materials are in continuous, intimate contact.

The welded or affected area is determined by counting the number of black pixels in the binary image. The percentage of affected (welded) pixels is presented in Table 5.3. The high-power weld overlaps (B1L4, B1L5 and B2L2) show the largest purple areas with approximately 40% of the pixels indicating a two-laminate thickness. The low-power and recommended welding settings result in a welded area of approximately 25%.

The last assembly, used for determining the in-plane temperature distribution at the weld overlap (B2L3), barely shows the purple-coloured contact points in the weld overlap. The weld

overlap was covered by fifteen thermocouples, interfering with the ultrasonic signal. However, the thermocouples were accounted for by compensating for the thermocouple areas interfering with the signal.

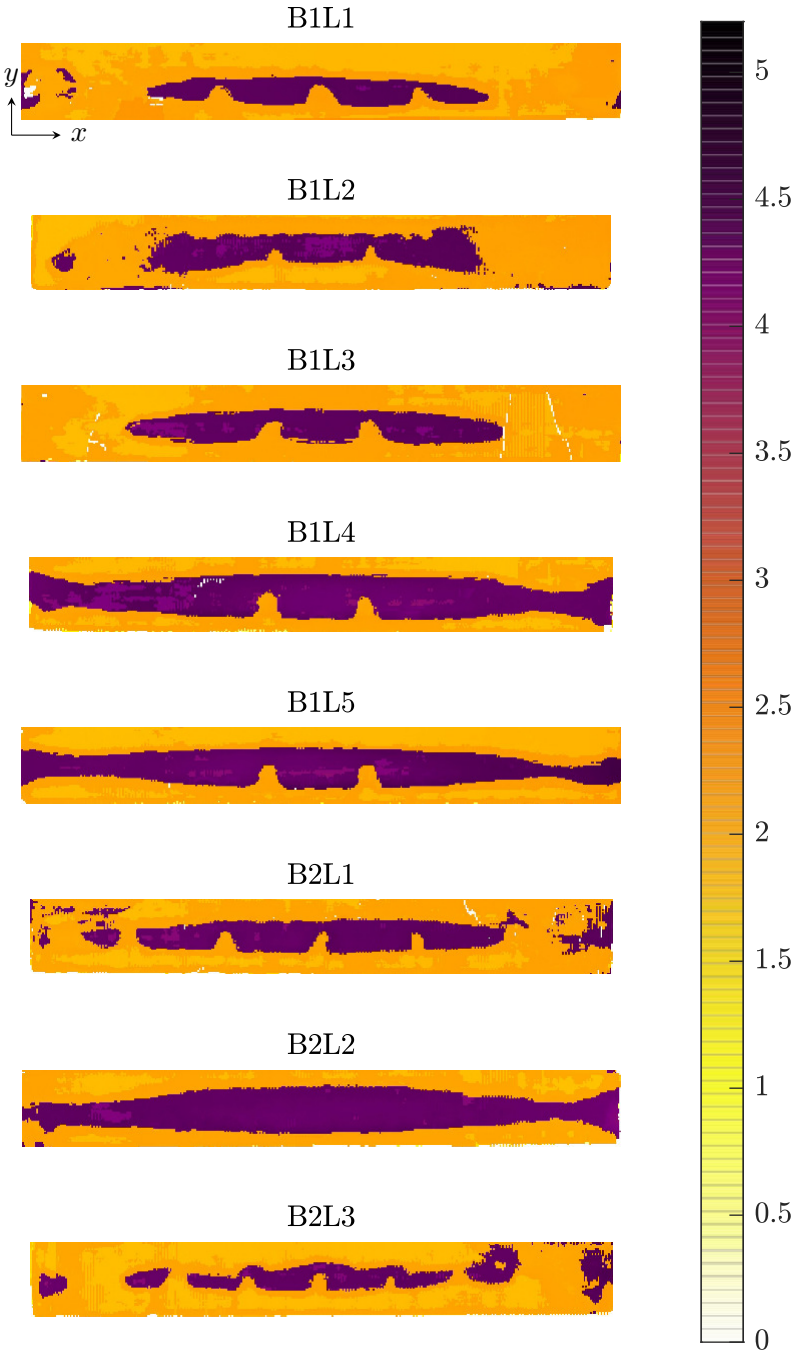

Figure 5.12: *The weld thickness (in* mm*) according to the C-scan. Theoretical thickness:* 4.48 mm.

5.4.2 Edge defects

Similarly, the edge effects are investigated using the C-scan by scanning the outer, long edges in the assemblies (highlighted areas in Figure 4.8). The resulting images are shown in Figure 5.13. The scanner did not capture the complete scanned area, which is visible as white pixels in the coloured images. The purple area depicts the unaffected, 2.24 mm thick laminate, whereas the yellow colour indicates a smaller thickness. The defects displayed in yellow at the top long edges and at the start- and end-zones are visible for the high-power settings (assemblies B1L4, B1L5 and B2L2). The shape of the defects are similar to the edge effects seen at the surface of the assemblies in the visual inspection.

The method used for finding the welded area, based on the number of affected pixels, is applied to these images as well. The percentages of affected pixels are given in Table 5.3. The edge effects cover up to 30% of the area that was scanned on the top laminate subjected to high-power settings. Some edge effects are visible at the bottom laminates at the start- and end-zone as well, but these are smaller than the effects seen in the top laminate. Summarised, the edge effects are most noticeable in the start-zone and long edge of the top laminate.

It should be noted that some pixels appear as white in the C-scans, which are included in the affected area. This increases the percentages shown in Table 5.3. Therefore, these percentages are rounded to the nearest multiple of five while still giving an indication of the degree of edge effects.

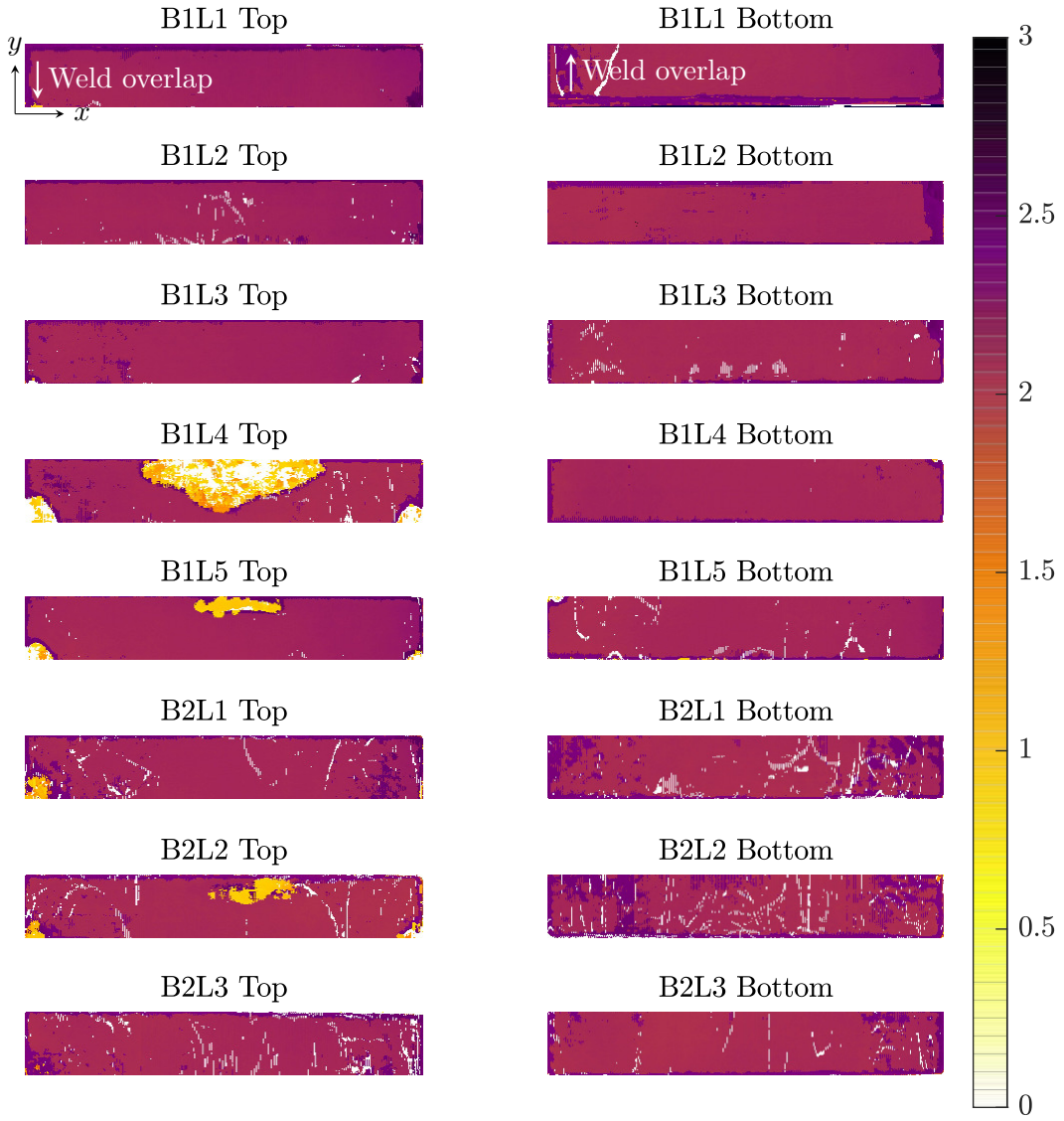

Figure 5.13: *Thickness of the top and bottom laminates (in* mm*) at the long edges (Figure 4.8) according to the C-scan to identify edge effects. Theoretical thickness:* 2.24 mm.

5.5 Pressure distribution

The (re-) consolidation pressure is applied by a pressure tube pressurised by air (see Figure 2.1). The pressure distribution was measured using pressure-sensitive foil and is shown in Figure 5.14. The colour-developing film shows an evenly (red) distributed colour density, indicating a homogeneously distributed pressure application. This uniform pressure distribution holds for all tested pressures, whose images are shown in Appendix D.

	Settings		T_{max}	Weld overlap	Edge effects	
Weld	I	pressure	°C	**Welded area (%)**	**Top (%)**	**Bottom (%)**
B1L1	520	5	336	15	0	0
B1L2	500	3	313	25	0	0
B1L3	505	7	322	20	0	0
B1L4	585	7	413	45	30	0
B1L5	580	3	392	35	5	5
B2L1	555	5	335*	30	5	5
B2L2	575	6.5	349**	45	10	5
B2L3	555	5	350***	25	5	0

Table 5.3: *Welded area in the weld overlap (corrected for the thermocouples) and affected area due to edge effects, according to the C-scan. * re-welded assembly; ** bottom of weld overlap; *** estimated using polynomial fit.*

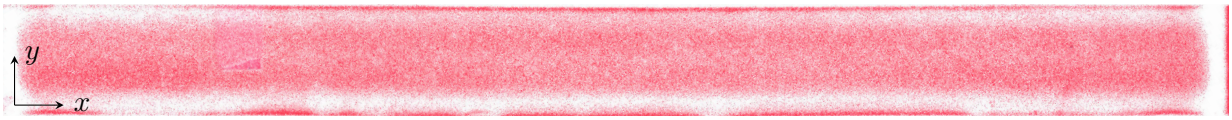

Figure 5.14: *The pressure distribution on the weld overlap using* 5 bar *on a Fujifilm Prescale LLLW pressure-sensitive foil.*

5.6 Microscopic inspection

The assemblies are cut after the non-destructive inspection in several samples (Figure 4.10a and Figure 4.10b). These samples are used for microscopic inspection. Both an overview and close-ups are imaged to observe the samples. Two samples are shown below because of their defects. This section is closed by providing a summary of the observed defects.

5.6.1 Microscopic observations

The microscopic inspection revealed several defects. Firstly, the weld overlap did not connect over its complete width; the gaps' measurements are presented. The internal structure showed thin regions and thick regions. The ply thicknesses in these regions are presented and reveal a material flow. Lastly, dry fibres are located at the bottom of the weld overlap, where the rough spots were seen during visual inspection.

Gap between laminates

The C-scan showed that the weld does not extend to the entire weld overlap length and width. This appears in the micrographs as well. All samples show gaps at the outskirts of the weld overlap. The reference assembly's (B1L1) outer samples (left, right) show an extremely poor connection. The outer left sample is not connected at all, as is visible in Figure 5.15. This sample lies outside the welded area shown in the C-scan images.

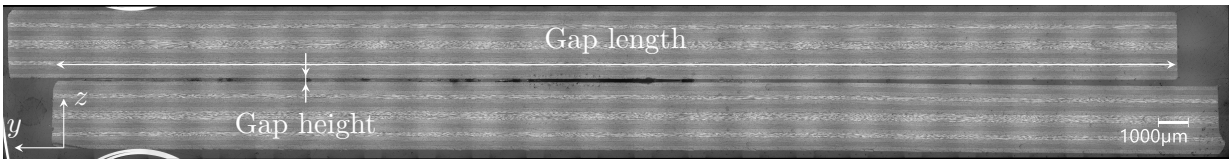

Figure 5.15: *Overview, enlarged 100x, of sample L of the assembly welded at recommended conditions (B1L1).*

The micrographs of the other assemblies resemble the example given below in Figure 5.16. The low-power, low-pressure assembly shows gaps at the edges of the weld overlap. The complete weld overlap is shown in Figure 5.16a. This image indicates the gaps, which are shown as close-ups in Figure 5.16b and Figure 5.16c.

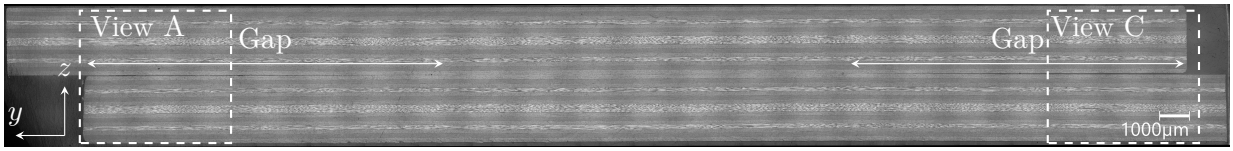

(a) *Overview, enlarged 100x, of sample L of the assembly welded at low power and low pressure (B1L2).*

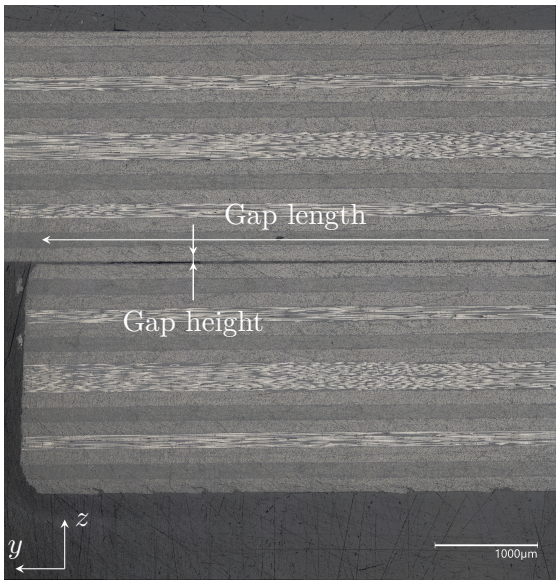

(b) *Close-up, enlarged 200x, view A.*

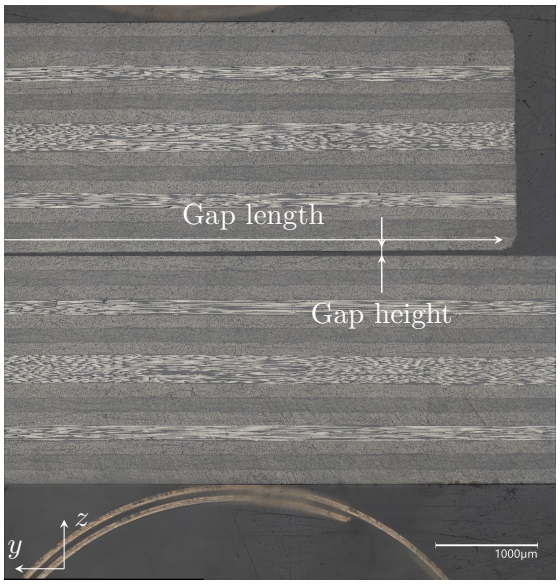

(c) *Close-up, enlarged 200x, of view C.*

Figure 5.16: *Micrographs depicting the cross-sections of the weld overlap and gaps seen at the outskirts of the weld overlaps of the low-power, low-pressure assembly (B1L2).*

These gaps' lengths and heights are measured using the microscope's measurement tool and are presented in Table 5.4. The table's last column shows how much of the weld overlap width shows intimate contact. As expected, the gap between the laminates in the left sample from the reference assembly (B1L1) reaches across the entire overlap width. The middle samples of B1L1 do show welded regions, but are connected for less than 50% of the overlap width. Conversely, the welded area in the high-power assemblies reaches further towards the outskirts of the overlap. The welded width at high-power settings covers approximately 70% of the weld overlap width.

Weld	Sample	Gap size				Contact
		View A		View C		
		Length (µm)	Height (µm)	Length (µm)	Height (µm)	(%)
B1L1	**L**	37360	94	-	316	0
	LM	11866	20	9377	107	44
	RM	10600	22	9289	116	48
	R	17065	20	12290	88	23
B1L2	**L**	12387	22	11283	54	34
	M	10026	17	11227	85	44
	R	16031	28	11714	63	27
B1L3	**L**	12403	25	8238	39	46
	M	10313	18	7147	41	54
	R	11548	19	8207	52	48
B1L4	**L**	8207	15	5281	101	65
	M	6077	58	3944	157	74
	R	6551	28	4579	132	71
B1L2	**L**	8097	7	6806	92	39
	M	7340	65	5356	108	67
	R	9701	36	7476	115	55

Table 5.4: *Gap size at the outskirts of the weld overlap where the laminates do not make intimate contact.*

Internal structure

Besides, the high power welds showed indents at the bottom of the weld overlap. These indents are visible in the cross-sections of B1L4 and B1L5 as well; an example is given in Figure 5.17a. The weld thickness varies between the locations of view B and C, which are positioned in the middle and right sides of the weld overlap (Figure 4.11).

A thin region is seen close to the middle (view B) of the sample; the thick region corresponds to the indent edge and is located closer to the weld overlap edge (view C). The thin region is shown in Figure 5.17b and does not show defects. Conversely, the indent's edge is visible as a thick region, depicted in Figure 5.17c, where some plies have separated. Interestingly, this assembly showed delamination in the thick regions in all its samples (L, M and R, as indicated in Figure 4.10b). The most extreme delamination is visible in the middle sample of the high-power, low-pressure assembly (B1L5), depicted in Figure 5.17c. The high-power, high-pressure weld (B1L4) shows the onset of delamination as well in the middle sample (M as indicated in Figure 4.10b), but not in the left (L and R, respectively).

The bottom plies of the samples in all assemblies show some randomly distributed cracks. In some cases, even small pieces seem to be torn from the bottom ply. These defects can be attributed to splintering from the saw blade during cutting.

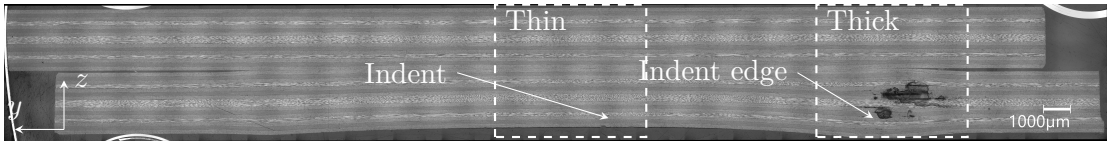

(a) *Overview, enlarged 100x, of the complete sample.*

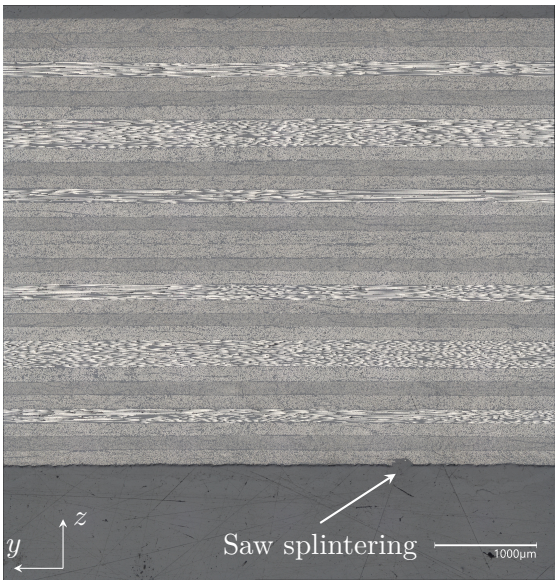

(b) *Close-up, enlarged 200x, of the thin region.*

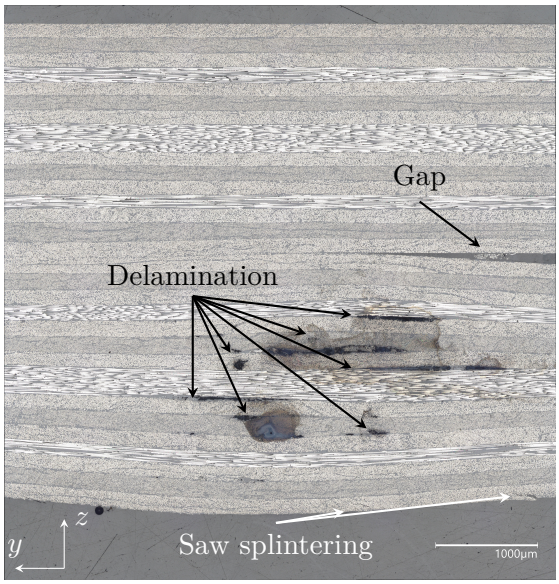

(c) *Close-up, enlarged 200x, of the thick region.*

Figure 5.17: *Micrographs of sample M in the high-power, low-pressure assembly (B1L5).*

Dry fibres

The visual inspection shows rough spots at the bottom of the weld overlaps. The weld overlap of the reference (B1L1, Figure 5.10a) and low-power, high-pressure assembly (B1L3) shows this surface imperfection the most clearly. The surface defect is located in the middle of the bottom of the weld overlap. The image shown in Figure 5.18 shows a part of the bottom ply of the middle sample of the low-power, high-pressure assembly where this surface defect is located. The bottom ply shows some fibres lying at the laminate's bottom surface, which are highlighted in the figure.

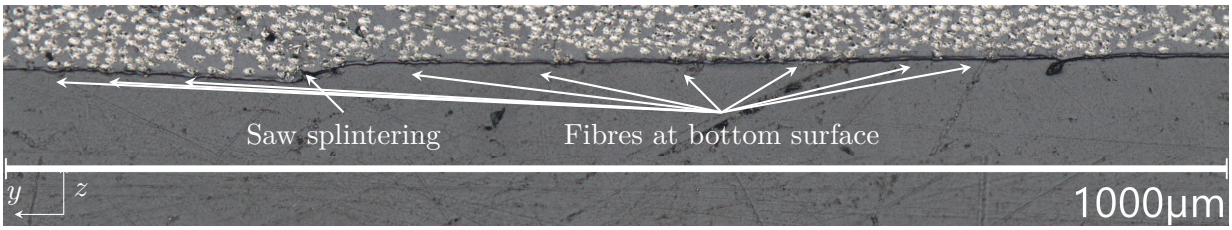

Figure 5.18: *Close-up, enlarged 400x, of middle region of the bottom ply in sample M of the low-power, high-pressure assembly (B1L3).*

Material flow

The ply thicknesses in the micrographs taken from views A, B and C are measured during microscopic inspection. Additionally, the ply thicknesses in the thin (indent centre) and thick (indent edge) regions are measured. The measurements are visualised in box charts shown in Appendix C, which all taken measurements. The ply thicknesses of the thin and thick areas of the high-power, high-pressure assembly (B1L4) are discussed below, using Figure 5.19.

The average ply thicknesses of the top laminate measured in the thin region are close to the usual consolidated ply thickness of 140 µm [46]. However, the thickness decreases slightly towards the bottom of the weld overlap, often being less than the usual consolidated ply thickness. The bottom laminate experiences higher temperatures than the top laminate, as the top is cooled using the heatsink. Besides, the pressure tube pushes on the bottom laminate, which causes the bottom laminate to deform.

Conversely, the ply thickness in the thick region increases towards the bottom of the weld overlap. The bottom laminate has a few thick layers in the 0° orientation, parallel to the welding direction, or x-direction as shown in Figure 2.1. The plies oriented in 90° (y-direction), however, are the least affected and their thicknesses still lie close to the consolidated ply thickness. The greatest difference between average ply thicknesses of the thick and thin regions is seen in the 0° orientation or x-direction, followed by the ±45° orientations. This increase indicates a material flow from the thin region to the thick region.

The squeezed plies mostly have a fibre orientation of 0°, lying parallel to the welding direction, x. The pressure tube pressurises the weld overlap in the welding direction as well. The plies are strong in their fibres' orientation but not in their transverse direction, where the movement of the fibres is solely restricted by the matrix material. However, the matrix is melted during welding, which allows the matrix to flow and the fibres to move. In the case of the squeezed plies, this allows the material to flow outwards, where less pressure is applied. This appears as the indent's edge at the bottom of the weld overlap. In other words, the material of the bottom of the weld overlap was pushed towards the side of the overlap, resulting in the edge of the indent.

5.6.2 Structural defects

The microscopic analysis is closed by summarising the defects found in the structure seen in the samples. All samples showed gaps at the outskirts of the weld. The gaps cover a larger distance at the outer samples (left, L, and right, R) than the samples located in the weld overlaps' centres. The high-temperature assemblies show the largest amount of contact over the weld overlap width. These findings correspond to the welded areas seen after the C-scan.

Internal defects were found in the high-temperature assemblies (B1L4 and B1L5). The assemblies all showed an indent (as visible in the visual inspection), which is also visible in the cross-sections of the weld overlap. Around the central region (view B), a thin part of the laminate is seen. The edge of the indent is seen next to view C, where the laminates' thicknesses increased. The thick area of the high-temperature, high-pressure assembly shows the onset of delamination. However, the high-temperature, low-pressure assembly showed delamination and voids in the thick region. The ply thicknesses show that the plies with a 0° fibre orientation, parallel to the welding direction, in the bottom laminate move to the thick region. The ±45° plies in the bottom laminate are squeezed as well, but less.

The low-temperature welds showed rough spots in the visual inspection. These regions were observed during the microscopic inspection as well, revealing some fibres at the bottom side of the weld overlap. The ply thicknesses of the thick and thin regions of the bottom ply do not show

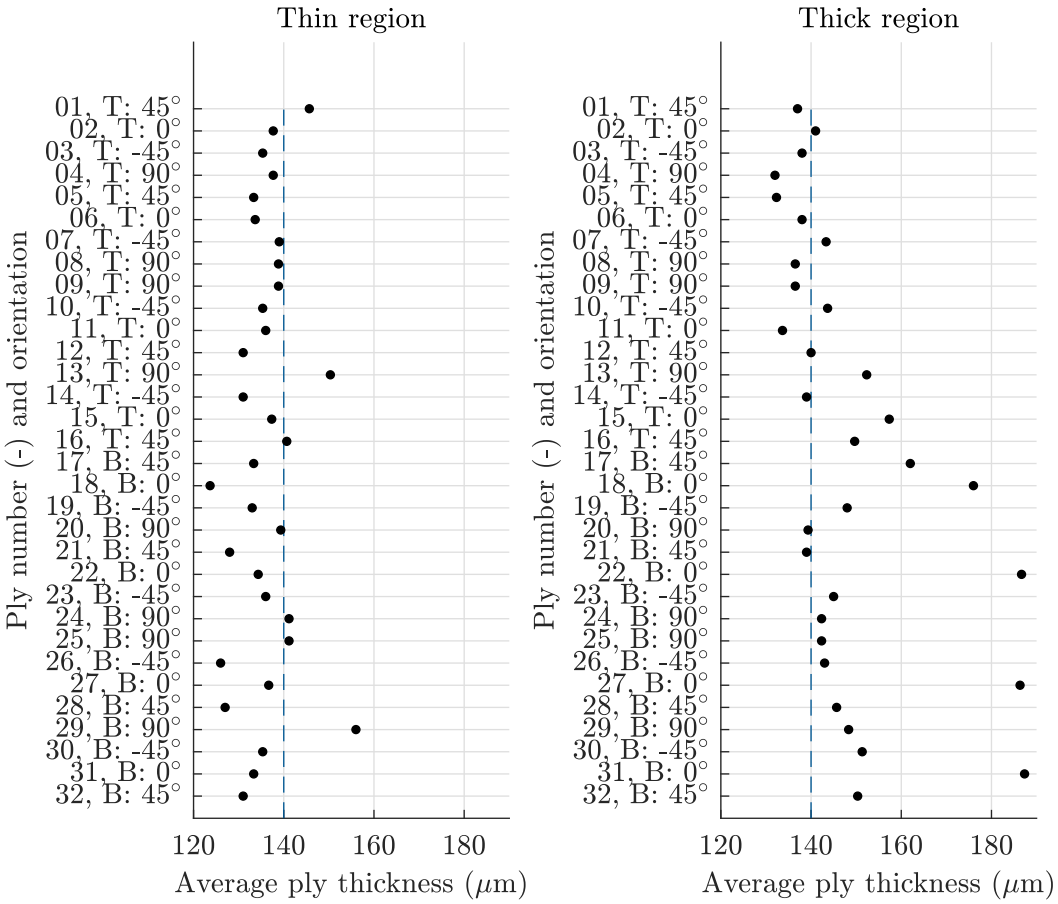

Figure 5.19: *Average ply thickness of the thin and thick regions in the high-power, high-pressure weld (B1L4).*

a great difference, indicating only a minor material flow. The dry fibres could have been exposed by a matrix material redistribution.

Chapter 6

Discussion

This chapter interprets the results presented in chapter 5. The issues encountered during the experiments and processing of the results are discussed. The discussion is followed by the identification of the seen defects, visualised in a ”defect map”. Afterwards, the investigation into the cause of the defects is discussed.

6.1 Experiment remarks

The limitations of the experiments are presented in this section. The section starts at the welding temperature. The target temperature was not achieved in many experiments, whose causes are discussed. The results from the C-scan are discussed as well to indicate the issues encountered. Finally, the pressure distribution experiment's possible improvement is presented.

6.1.1 Welding temperature

The experiment cases were chosen such that the most extreme conditions could be compared to a reference. The reference assembly, however, was welded at a lower temperature of 336 °C than desired (355 °C). The same holds for the second assembly: the welding temperature barely passed the melting temperature. This shows that the quadratic power curve could not provide an accurate prediction to achieve the desired process conditions.

Power curve

The power curve was determined for one, the first laminate of the experiment goals: B1L1 for mapping and B2L1 for investigating the defects. The power curve was fitted based on the current and temperatures while heating, before welding, these assemblies. The currents that are used for the first power curve are below the melting temperature. This is done to keep the assembly unwelded before the actual welding experiment. The data points of the welding experiments are used to improve the accuracy of the power curves by adding these points to the current-temperature relationship that was obtained during welding. The quadratic fit caused the welding temperature to be consistently lower than the target temperature. A linear fit could give more accurate results, as shown in Figure 6.1.

The shown suggestion for the linear fit is based on the temperatures above the glass-transition temperature, to account for crystallisation effects. The improvement of the suggested fit is demonstrated using an example of the high-power, high-pressure and low-pressure experiments (B1L4

and B1L5, respectively). The high-power, high-pressure experiment (B1L4) aimed at a temperature of 390 °C, whereas the actual welding temperature measured in the weld was 413 °C. The current in the following high-power, low-pressure experiment (B1L5) was lowered to reach the same target temperature of 390 °C. The new, actually measured temperature was 392 °C. As is visible in Figure 6.1, this adjusted temperature of 392 °C lies on the improved linear fit. Conversely, the temperature that overshot the target lies on the quadratic fit, including all data points. Therefore, linear fit based on temperatures below T_g seems to improve the estimation for the current settings.

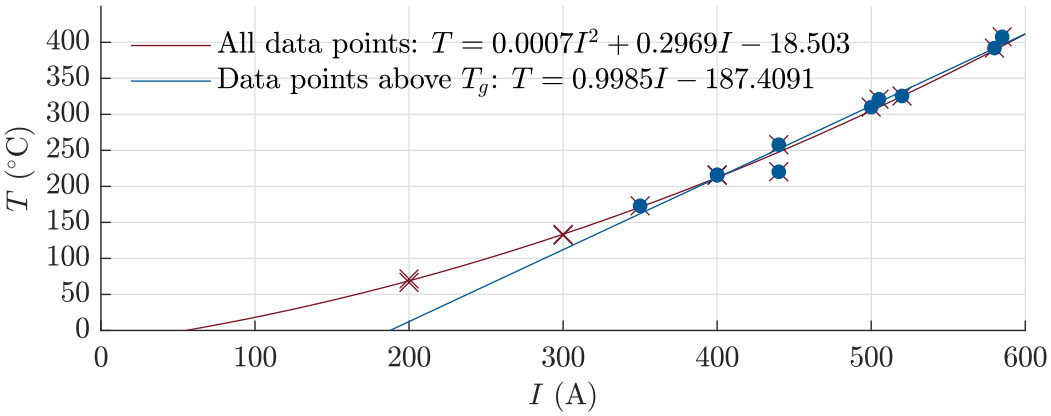

Figure 6.1: *Comparison of the linear power curve based on the measured temperatures above $T_g = 147$ °C and the original power curve using all data points.*

In-plane temperature distribution

Also, the in-plane temperature distribution experiment at the weld interface (B2L3) showed lower temperatures then desired. There were fifteen thermocouples tightly wrapped in Kapton tape located in the weld overlap to record the process. This prevented intimate contact of the laminates at the thermocouples' locations. This means that the fibre contact points are compromised, possibly reducing the heat generation in this region.

The in-plane temperature distribution was measured and fitted based on the measurements. The presented fit was created using the thermocouple data only. This data did not include the laminate's edge temperatures, so the fit is not representative for quantitative conclusions. However, it does show the shape of the temperature gradient, giving an indication of the heating pattern in the welding process. The in-plane temperature distribution fit can be improved by choosing additional thermocouple locations to measure the temperature.

Through-the-thickness temperature distribution

The through-the-thickness temperature distribution was measured using five in-line thermocouples at the bottom, weld interface and top of the weld overlap. Two main issues appeared: the temperature measurements failed to be recorded and the lack of placed thermocouples.

The temperature measurements during welding were not available. The presented results are therefore based on a re-welded assembly. To find the actual through-the-thickness temperature distribution, the welding process has to be redone on a new assembly.

Besides, the laminate consolidation process did not allow several thermocouples to be consolidated in the laminate. Only three through-the-thickness locations could be measured: at the top

and bottom of the weld overlap and at the weld interface. The number of through-the-thickness measurement locations does not suffice to find an actual distribution; it rather gives an indication.

6.1.2 C-scan

Performing an ultrasonic C-scan was part of the non-destructive inspection. The C-scan outputs images that show the measured thickness of the material, which are affected by three issues. The first issue is the inaccuracy due to unscanned, white pixels that are counted as defects. Secondly, the thermocouples located at the interface interfere with the ultrasonic signal, appearing as defects. The last issue is the inability of the C-scan roller to reach the complete laminate to find the edge effects. The issues are discussed below.

Scan inaccuracy

Firstly, the images still show some unobserved pixels. These regions are visible in the image as white pixels, especially in the C-scans performed on the edge effects of the laminates. The pixels are used for post-processing to find the affectedd areas. The white pixels are interpreted as unwelded or defective by the post-processing method, similar to the yellow pixels. The results are, therefore, affected by these inaccurate scans. The percentage of white pixels in the images ranges from one to five per cent. The presented percentages are rounded to the closest multiple of five to account for these inaccuracies. A different approach could consider subtracting the white pixels from the C-scan, similar to the method used to account for the thermocouples discussed below.

Thermocouple area

Secondly, the unwelded regions of the thermocouples are compensated for. The typical size of the thermocouple tips is estimated as half ellipses. These areas are subtracted from both the welded and total scanned areas in the weld overlap. A more accurate estimation can be made if the actual thermocouple tip areas are subtracted, rather than a typical estimate. The difficulty in subtracting the actual thermocouple size lies in the production of the thermocouples themselves. The thermocouples' shapes and Kapton tape reinforcements vary, as these were manually prepared for the experiments.

Incomplete scan

Finally, the edge effects close to the weld overlap are not captured in their entirety. The roller of the C-scan did not reach the weld overlap edge, capturing approximately 50 mm of the laminate edge instead of the complete laminate outside the weld (69.5 mm, see the schematic overview in Figure 4.8). The affected area in the reference assembly, for example, shows edge effects in the top and bottom laminate (Figure 5.7). However, the roller of the C-scan was not able to pass over this area in the reference assembly. The edge effects in a high-power assembly, for example Figure 5.7, are larger and lie in the area that the C-scan can scan. Therefore, the C-scan images do not show the entire laminate, thus not all edge effects.

6.1.3 Pressure distribution

The pressure distribution at the bottom of the weld overlap is investigated by inserting a pressure-sensitive foil in the induction welding set-up. The flexible pressure tube is covered by a flexible

rubber strip that is in direct contact with the bottom of the weld overlap (Figure 2.1). The laminates were at room temperature during the pressure distribution experiment, as the pressure-sensitive foil's manual requires to do so. This means that the laminates were rigid. However, the laminates are melted during welding, making them soft. The pressure distribution on the laminates in melt may differ from the distribution at room temperature. Repeating the experiment is necessary to give more representative results. This can be done by either using a soft stand-in assembly to mimic the melted laminate or change measurements methods allowing the high temperature.

6.2 Phenomena

The goal of the research was to map the process-induced defects after induction welding of CF/LM-PAEK in a UD, QI lay-up. The defects are caused by changing the coil power, operated by the input current, and are investigated for their causes. The two possible causes are the temperature distribution and the pressure distribution during the welding process. The identification of the defects is done by gathering and combining the results of the previous chapter. The results are summarised in a defect map, revealing a relationship between process parameters and process-induced defects. The cause of the defects is investigated by performing experiments to find the temperature and pressure distributions, as well as ply thickness measurements.

6.2.1 Identification and mapping defects

The visual inspection showed two main defects. Edge effects are visible in all assemblies. Additionally, the bottom of the weld overlap shows indents in the high-power settings. These two main defects are discussed separately.

Edge effects

First, the edge effects are a commonly seen phenomenon, appearing mostly at the start of the welds. The eddy current density is higher at the edge, leading to more heat generation in these regions, as was discussed in chapter 2. However, also the long edges of the top laminates in the assemblies welded at high power showed edge effects. The size of the workpiece's laminates could be the cause of these defects. The eddy current density is lower if the currents can flow along greater paths found in larger laminates. Using larger laminates may, therefore, reduce the degree of these defects.

The defects along the long edges are shown in the top laminate only. The magnetic field is stronger close to the coil than far away from the coil, as described by the Biot-Savart law (chapter 2). The top laminate of the assembly is closest to the coil and would thus experience the most heat generation. However, the weld overlap is locally cooled to prevent thermal degradation. The heat sink is limited to this overlap area, which leaves the remaining area of the laminates unprotected. These two reasons may be the cause of the edge effects at the long edges of the top laminates.

Indents at bottom of weld overlap

Secondly, the bottom of the high-power welded assemblies show indents (Figure 5.10b). The weld thickness decreases along the weld direction, after which it increases again (Figure 5.11). The increase is a redistribution of material, as no material seemed to have flowed out of the weld.

The indent is elliptically shaped and shows a thick edge, similar to a crater. The temperature and pressure distribution are suspected to contribute to the forming of this indent. The pressure distribution, however, is almost uniform across the rigid weld overlap which is tested at room temperature. The in-plane temperature distribution at the bottom of a high-power assembly (B2L2) is found to have an elliptical pattern with temperatures at recommended processing temperatures (around 350 °C). Both the measurements and the fit based on the data show a temperature peak in the centre of the weld overlap. The temperature decreases towards the long edges, start- and end-zones. Therefore, the indent's shape at the bottom of the weld overlap is caused due to an inhomogeneous temperature distribution rather than a non-uniform pressure application. The material flowed from the weld's thinnest region and caused the thick edges of the bottom's indents.

A similar temperature distribution is visible for the temperatures at the weld interface. Again, an elliptical heating pattern can be recognised, where the centre reaches a higher temperature than the edges. The shape of this pattern, measured in the B2L3 assembly, resembles the results of the C-scan. The C-scans of the reference and low-power welds show the elliptical contact area as well. The non-contacting areas are outside the high-temperature zone that lies in the centre of the weld. Although the non-destructive inspection can neither rule out or identify a kissing bond, this may be considered as a possible defect.

It is unlikely that the pressure distribution is the main responsible factor for process-induced defects. This is strengthened by the findings in Figure 6.2 and Figure 6.3, where the relationships between the power and pressure, respectively, with the welded area are shown. An increased input power results in a greater welded area, demonstrated by a positive trend. However, the relationship between the welded area and the pressure does not show a correlation. The temperature distribution allowed the material at the back of the weld to re-distribute and the welded area at the interface to form an elliptical shape. Meanwhile, the flexible pressure tube provides the driving force and causes the material to actually flow.

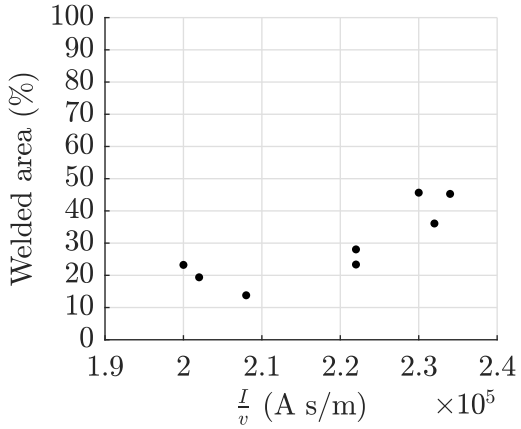

Figure 6.2: *Relationship between input power and welded area.*

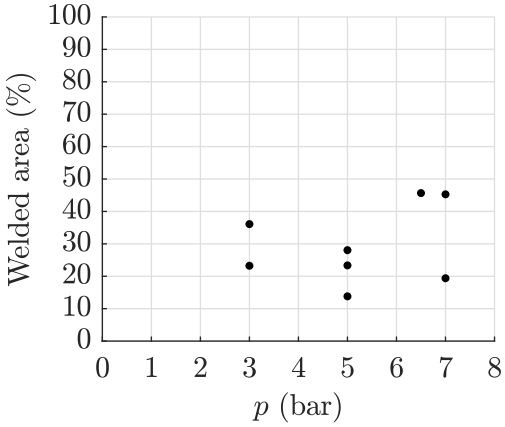

Figure 6.3: *Relationship between pressure and welded area.*

6.2.2 Investigation into mechanisms

The lack of intimate contact is also visible in the microscopic analysis as gaps between the laminates. The gaps cover roughly 60% of the weld overlap width in the low-power welds. The high-power welds show gaps across roughly 30% of this overlap.

The indent that appeared in the visual inspection is also visible in the micrographs. The high-power assemblies' cross-sections show a region where the plies seem to be thinned out. A region with thick plies appears as the indent's edge seen in the visual inspection. This indicates that material flowed from the thin to the thick regions. The squeezed plies are oriented in the welding direction (0°) because of the low viscosity of the heated matrix material. Although the type of squeeze is not investigated, no clear matrix bleeding is observed. Finally, the indent edges show some delamination (Figure 5.17c). Whereas this is just beginning in the high-power, high-p weld (B1L4), this is especially present in the lower pressure experiment B1L5. The combination of the presence of heat and the occurrence of delamination when the pressure reduces, points towards deconsolidation. A schematic overview of the defects seen in the cross-sections is shown in Figure 6.4.

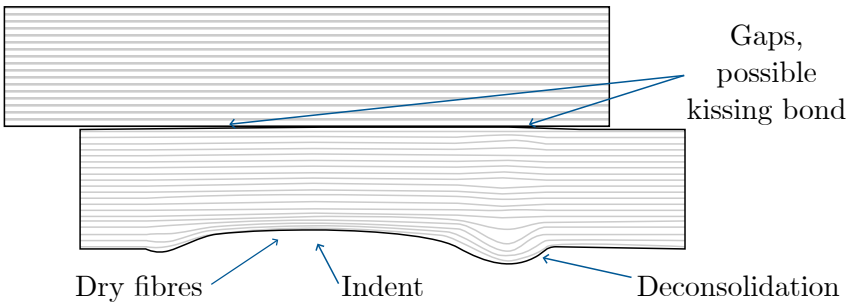

Figure 6.4: *Schematic overview of the defects found during microscopy.*

6.3 Defect map

An overview of the defects are given in a defect map, shown in Figure 6.5. The map depicts the general occurrence of defects for the several experiments which were shown in Figure 5.2). The dark regions indicate that many defects have been seen. Conversely, the light regions show only a few defects. The size of the defect description corresponds with the severity of the defects.

The dark region in the high-power settings shows that a high temperature causes several issues. The low-power settings result in fewer defects. However, the weld is at high risk of being a kissing bond due to the low welding temperature resulting from the low power input. Therefore, the ideal process window lies approximately at the recommended settings, as was expected.

The recommended settings led to a weld showing dry fibres, some edge effects and a possible kissing bond, but all in moderate severity. The map can be more detailed by adding data points, to define the boundaries of the ideal process window. Semi-extreme experiments would add to the now-empty spaces. The empty spaces lie mostly in the recommended temperature (or power) range, where different pressures can be chosen. Summarised, the map gives a general overview of the occurrence and severity of the defects, but it would benefit from additional experiments to define the process window more accurately.

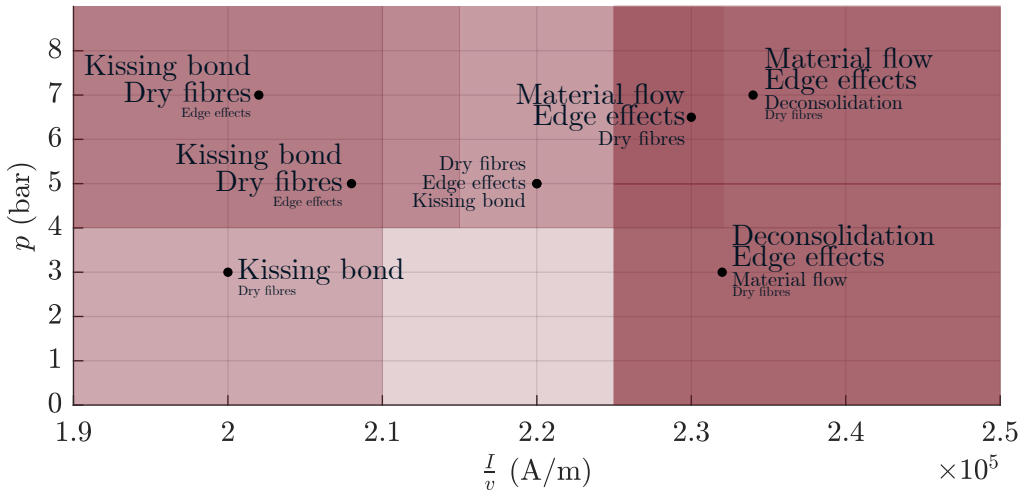

Figure 6.5: *Defect map.*

Chapter 7

Conclusions and recommendations

7.1 Conclusion

Induction welding of TPCs seems to be a promising method to join components. However, this process still poses challenges, especially for carbon-fibre-reinforced UD lay-ups. The ideal process window is hard to define, partly due to the nature of a UD, QI lay-up. Moreover, it is unclear what relationship the process parameters have with the process-induced defects. The process-induced defects occurring in an induction welded carbon-fibre reinforced TPC need to be identified and mapped. Additionally, these mapped defects have to be understood to help define a suitable window for the process parameters. This research presents the defects seen in assemblies that were induction welded using several operator parameters. The assemblies were welded at recommended conditions and extreme conditions outside the recommendations.

Almost all assemblies showed edge effects to some degree, especially when the high-temperature settings were used. The low-temperature settings may have caused kissing bonds. All surfaces on the bottom of the weld overlap had some defects. The low-temperature assemblies showed rough spots, whereas the high-temperature assemblies also had indents. The indents experienced material flow from their thinnest region towards the weld overlap edge. The indent edge was revealed to suffer from deconsolidation, especially in low-pressure settings. The defects that were found are discussed below.

- Edge effects appeared close to the start- and end-zone of the weld overlap. Moreover, the assemblies welded at high temperatures showed edge effects on the free, long edges of the top laminates. The increased eddy currents at the edges increase the temperature. The used laminates were too small to prevent the higher eddy current density. Besides, the local cooling did not extend to these areas to decrease the heat generation.

- The weld overlap of the low-temperature assemblies was not well-bonded. A successful fusion bond can be solely recognised in the centre of the weld overlap. The in-plane temperature distribution showed that the temperature reached in the weld overlap did not suffice to fuse the remaining overlapping area. Although the used non-destructive inspection is not capable of confirming a kissing bond, these welds may be at risk of this weakness.

- All assemblies showed elliptical surface defects at the back of the weld overlap. The weld overlap of the low-temperature assemblies showed rough spots, likely to be dry fibres. The high-temperature assemblies were indented in the weld overlap, especially at high pressures.

Material was redistributed from the thin region in the indent to the indent edge. The indents' causes and their mechanisms were further investigated.

- The in-plane temperature measurements of the bottom of the weld overlap showed that the temperature distribution shared the elliptical shape of the overlap. The temperature of the bottom of the weld overlap reached processing conditions using the high-power settings.
- The through-the-thickness temperature measurement showed a temperature distribution where the highest temperature was reached at the weld interface, as desired. However, the temperature of the bottom laminate is capable of being in melt during welding at recommended conditions.
- The pressure distribution is uniform in the welding direction. This distribution is unlikely to cause the shape of the indent. However, the pressure applied by the pressure tube is the driving force in the creation of the indent. The elliptically-shaped, inhomogeneous temperature distribution allows the flexible pressure tube to create the indent's elliptical shape.
- The indent edge showed the onset of deconsolidation in the centre of the weld overlap in the high-temperature, high-pressure assembly. Conversely, the high-temperature, low-pressure assembly showed deconsolidation in all its samples. The lower pressure setting allowed the plies to separate and expand, resulting in the indent's thick edge.
- The ply thicknesses measured during microscopic analysis showed that material had flowed from the thin region of the indent towards the indent's edge. The plies that were most affected had a fibre direction orienting in the welding direction (0°). The plies having an orientation perpendicular to that direction (90°) were the least affected. The flexible pressure tube pushed the plies to the edges of the weld overlap, which was allowed by the melted matrix material.

7.2 Future work

Several issues and unanswered questions appeared in this research. The research demonstrated the need for a well-defined process window to successfully fuse laminates using induction welding. The induction welding process can be improved using a better understanding, for which several suggestions are done. Some process-related recommendations are presented, such as the improvement of the power curve. Besides, some recommendations are discussed for the set-up.

7.2.1 Research recommendations

The temperature in the weld overlap is mainly determined by the operator parameters current and coil speed. The coil speed was not varied in this research and may influence the process defects as well. The test matrix and defect map are already prepared by allowing the coil speed to be implemented in the input power.

The through-the-thickness temperature distribution was measured using thermocouples at the top, weld interface and bottom of the overlap. This does not suffice to create a well-defined temperature distribution; it rather gives an indication. The laminate consolidation process did not allow several thermocouples to be consolidated in the laminate to increase the number of thermocouples through-the-thickness. Considering this difficulty, the use of modelling may offer insights.

The microscopy showed a material flow of the plies oriented in the welding direction. The type of flow was not determined and requires attention. This also holds for the cause of the dry fibres, which has to be identified.

7.2.2 Process recommendations

The welding temperature is a goal during induction welding rather than a process parameter. The current is the process parameter that mainly influences the welding temperature. A well-defined relationship is still to be determined and is usually estimated using a power curve. The power curve constructed in this research did not suffice to accurately obtain the desired welding temperatures. The used power curve had a quadratic fit which gave inaccurate estimations. This may be improved by using a linear fit based on temperatures above the glass transition temperature.

Additionally, the edge effects are a recurring defect, regardless of the extreme settings. The induction welding set-up currently uses a start- and end-zone with a lower coil speed to heat up the laminate. This is done using a commonly used rule of thumb. The edge effects may be reduced by optimising the coil speed in the start- and end-zones.

7.2.3 Set-up recommendations

The edge effects in the weld overlap can also be reduced by cooling the areas close to the start-end end-zones. However, many edge effects appeared outside these regions and require attention. Whereas additional (active) cooling systems may help avoid these defects, cooling may add to the challenges in defining a process window.

Additional cooling may conflict with the ideal through-the-thickness temperature distribution, by shifting the maximum reached temperature outside the weld interface. This would result in an unsuccessful or defective weld. Therefore, an alternative may be required.

Since the edge effects appear in regions where the current density is high, reducing this density may prevent these defects. The use of larger laminates may reduce the edge effects seen at the long edges of the laminates by allowing the eddy currents to follow greater paths. However, this may not be feasible for industry-defined parts. The eddy currents need to follow a greater path, so an alternative solution can lie in using a temporary extension of the material [48].

The deformation at the bottom of the weld overlap showed that the induction welding set-up can be greatly improved. The bottom laminate had a temperature above melt, allowing this deformation. Cooling the bottom laminate as well may avoid this indent defect. However, the desired through-the-thickness temperature distribution should be taken into account while applying an additional heatsink.

Bibliography

[1] T. Ahmed, D. Stavrov, H. Bersee, and A. Beukers, "Induction welding of thermoplastic composites—an overview," *Composites Part A: Applied Science and Manufacturing*, vol. 37, no. 10, pp. 1638–1651, oct 2006. (Page 1, 2, 5, 6, 8, 9, 10, 11, 12, 15)

[2] J. P. Reis, M. F. de Moura, and S. Samborski, "Thermoplastic Composites and Their Promising Applications in Joining and Repair Composites Structures: A Review," *Materials*, vol. 13, 2020. [Online]. Available: https://api.semanticscholar.org/CorpusID:229684021 (Page 1, 5, 6, 8, 9, 10, 11, 15)

[3] A. Yousefpour, M. Hojjati, and J.-P. Immarigeon, "Fusion Bonding/Welding of Thermoplastic Composites," *Journal of Thermoplastic Composite Materials*, vol. 17, no. 4, pp. 303–341, 2004. [Online]. Available: https://doi.org/10.1177/0892705704045187 (Page 1, 2, 5, 6, 7, 8, 11, 12, 15)

[4] K. Fernholz, *Bonding of polymer matrix composites.* Woodhead Publishing, 12 2010, pp. 265–291. (Page 1, 2, 11)

[5] D. Barazanchy, J. Pandher, and M. Van tooren, Eds., *The edge-effect in thermoplastic induction welding*, 01 2021. (Page 1, 5, 6, 11, 15)

[6] J. Schell, J. Guilleminot, C. Binetruy, and P. Krawczak, "Computational and experimental analysis of fusion bonding in thermoplastic composites: Influence of process parameters," *Journal of Materials Processing Technology*, vol. 209, no. 11, pp. 5211–5219, 2009. [Online]. Available: https://www.sciencedirect.com/science/article/pii/S0924013609000983 (Page 1, 2, 6, 9, 11, 12, 15)

[7] M. Brzeski and P. Mitschang, "Deconsolidation and Its Interdependent Mechanisms of Fibre Reinforced Polypropylene," *Polymers and Polymer Composites*, vol. 23, no. 8, pp. 515–524, 2015. [Online]. Available: https://doi.org/10.1177/096739111502300801 (Page 8, 10)

[8] T. Slange, L. Warnet, W. Grouve, and R. Akkerman, "Deconsolidation of C/PEEK blanks: on the role of prepreg, blank manufacturing method and conditioning," *Composites Part A: Applied Science and Manufacturing*, vol. 113, pp. 189–199, 2018. [Online]. Available: https://www.sciencedirect.com/science/article/pii/S1359835X18302628 (Page 8, 10)

[9] F. Cogswell, *Thermoplastic Aromatic Polymer Composites.* Butterworth Heinemann, 1992. (Page 8, 10, 11)

[10] L. Moser, "Experimental Analysis and Modeling of Susceptorless Induction Welding of High Performance Thermoplastic Polymer Composites," doctoralthesis, Technische

Universität Kaiserslautern, 2017. [Online]. Available: https://nbn-resolving.de/urn:nbn:de:hbz:386-kluedo-47404 (Page 1, 2, 5, 6, 8, 9, 10, 11, 12, 15)

[11] M. A. Valverde, J. P.-H. Belnoue, R. Kupfer, L. F. Kawashita, M. Gude, and S. R. Hallett, "Compaction behaviour of continuous fibre-reinforced thermoplastic composites under rapid processing conditions," *Composites Part A: Applied Science and Manufacturing*, vol. 149, p. 106549, 2021. [Online]. Available: https://www.sciencedirect.com/science/article/pii/S1359835X21002712 (Page 1, 9)

[12] X. long Ma, L. hua Wen, S. yu Wang, J. you Xiao, W. hao Li, and X. Hou, "Inherent relationship between process parameters, crystallization and mechanical properties of continuous carbon fiber reinforced peek composites," *Defence Technology*, vol. 24, pp. 269–284, 2023. [Online]. Available: https://www.sciencedirect.com/science/article/pii/S2214914722000848 (Page 12)

[13] P. Mitschang, R. Velthuis, and M. Didi, "Induction spot welding of metal/cfrpc hybrid joints," *Advanced Engineering Materials*, vol. 15, no. 9, pp. 804–813, 2013. [Online]. Available: https://onlinelibrary-wiley-com.ezproxy2.utwente.nl/doi/abs/10.1002/adem.201200273 (Page 1, 2, 5)

[14] M. Flanagan, A. Doyle, K. Doyle, M. Ward, M. Bizeul, R. Canavan, B. Weafer, C. M. Ó. Brádaigh, N. M. Harrison, and J. Goggins, "Comparative manufacture and testing of induction- welded and adhesively bonded carbon fibre PEEK stiffened panels," *Journal of Thermoplastic Composite Materials*, vol. 32, pp. 1622 – 1649, 2018. [Online]. Available: https://api.semanticscholar.org/CorpusID:139488146 (Page 1, 2, 5, 6, 8, 10, 11, 15)

[15] S. Becker and P. Mitschang, "Process Improvement of Continuous Induction Welding of Carbon Fiber-Reinforced Polymer Composites," *Journal of Materials Engineering and Performance*, vol. 31, 04 2022. (Page 1, 2, 5, 6, 8, 9, 11, 15)

[16] F.-J. van Zanten, H. Mohan, D. Barazanchy, and M. Van tooren, Eds., *The Effect of Temperature on the Electric Conductivity for Composite Induction Welding*, 01 2022. (Page 1, 5, 6)

[17] T. Bayerl, M. Duhovic, P. Mitschang, and D. Bhattacharyya, "The heating of polymer composites by electromagnetic induction – A review," *Composites Part A: Applied Science and Manufacturing*, vol. 57, pp. 27–40, 2014. [Online]. Available: https://www.sciencedirect.com/science/article/pii/S1359835X13002996 (Page 1, 2, 5, 6, 8, 9, 12, 15)

[18] T. Bayerl, R. Schledjewski, and P. Mitschang, "Induction Heating of Thermoplastic Materials by Particulate Heating Promoters," *Polymers and Polymer Composites*, vol. 20, no. 4, pp. 333–342, 2012. [Online]. Available: https://doi.org/10.1177/096739111202000401 (Page 2, 15)

[19] R. Rudolf, P. Mitschang, and M. Neitzel, "Induction heating of continuous carbon-fibre-reinforced thermoplastics," *Composites Part A: Applied Science and Manufacturing*, vol. 31, no. 11, pp. 1191–1202, 2000. [Online]. Available: https://www.sciencedirect.com/science/article/pii/S1359835X00000944 (Page 1, 5, 6, 8, 9)

[20] S. Yarlagadda, H. J. Kim, J. John W. Gillespie, N. B. Shevchenko, and B. K. Fink, "A study on the induction heating of conductive fiber reinforced composites," *Journal of Composite Materials*, vol. 36, no. 4, pp. 401–421, 2002. [Online]. Available: https://doi.org/10.1177/0021998302036004171 (Page 1, 6)

[21] P. Mitschang, R. Rudolf, and M. Neitzel, "Continuous Induction Welding Process, Modelling and Realisation," *Journal of Thermoplastic Composite Materials*, vol. 15, no. 2, pp. 127–153, 2002. [Online]. Available: https://doi.org/10.1177/0892705702015002451 (Page 1, 2, 6, 8, 9, 12)

[22] M. Holland, M. J. van Tooren, D. Barazanchy, and J. Pandher, "Modeling of induction heating of thermoplastic composites," *Journal of Thermoplastic Composite Materials*, vol. 35, no. 10, pp. 1772–1789, 2022. [Online]. Available: https://doi.org/10.1177/0892705720911979 (Page 1, 2, 5, 6, 7, 8, 15)

[23] S. van den Berg, M. Luckabauer, S. Wijskamp, and R. Akkerman, "Thermal response of an induction-heated fabric reinforced thermoplastic composite with anisotropic electrical conductivity: An experimental study," *Journal of Thermoplastic Composite Materials*, vol. 0, no. 0, p. 08927057231201353, 2023. [Online]. Available: https://doi.org/10.1177/08927057231201353 (Page 1, 5, 6)

[24] W. I. Lee and G. S. Springer, "A Model of the Manufacturing Process of Thermoplastic Matrix Composites," *Journal of Composite Materials*, vol. 21, pp. 1017 – 1055, 1987. [Online]. Available: https://api.semanticscholar.org/CorpusID:136948774 (Page 1, 6, 7, 8, 9, 11, 12)

[25] D. Grewell and A. Benatar, "Semi-empirical, squeeze flow and intermolecular diffusion model. I. Determination of model parameters," *Polymer Engineering & Science*, vol. 48, pp. 860 – 867, 05 2008. (Page 1, 2, 11)

[26] M. Wood, P. Charlton, and D. Yan, "Ultrasonic Evaluation of Artificial Kissing Bonds in CFRP Composites," *e-Journal of NOndestructive Testing*, vol. 19, 12 2014. (Page 2, 11)

[27] P. Marty, N. Desaï, and J. Andersson, Eds., *NDT OF KISSING BOND IN AERONAUTICal structures*, 01 2004.

[28] P. B. Nagy, "Ultrasonic detection of kissing bonds at adhesive interfaces," *Journal of Adhesion Science and Technology*, vol. 5, no. 8, pp. 619–630, 1991. [Online]. Available: https://doi.org/10.1163/156856191X00521 (Page 2, 11)

[29] D. Barazanchy, J. Pandher, and M. Van tooren, Eds., *The effect of induction welding coil shape on heat generation*, 01 2022. (Page 5, 8, 9, 15)

[30] O. Schieler, U. Beier, and P. Mitschang, "Control of the through-thickness temperature distribution in carbon composite aerospace parts during induction welding," *Journal of Thermoplastic Composite Materials*, vol. 31, no. 12, pp. 1587–1608, 2018. [Online]. Available: https://doi.org/10.1177/0892705717738390 (Page 5, 6, 8, 11, 12)

[31] V. Stokes, "Experiments on the Induction Welding of Thermoplastics," *Polymer Engineering & Science*, vol. 43, pp. 1523 – 1541, 09 2003. (Page 6)

[32] S. C. Mantell and G. S. Springer, "Manufacturing process models for thermoplastic composites," *Journal of Composite Materials*, vol. 26, no. 16, pp. 2348–2377, 1992. [Online]. Available: https://doi.org/10.1177/002199839202601602 (Page 8, 9, 12)

[33] L. Ye, M. Lu, and Y.-W. Mai, "Thermal de-consolidation of thermoplastic matrix composites—I. Growth of voids," *Composites Science and Technology*, vol. 62, no. 16, pp. 2121–2130, 2002. [Online]. Available: https://www.sciencedirect.com/science/article/pii/S0266353802001446 (Page 8, 10, 15)

[34] L. Ye, M. Lu, and H.-Y. Liu, *Deconsolidation and Reconsolidation of Thermoplastic Composites During Processing*. Boston, MA: Springer US, 2005, pp. 233–254. [Online]. Available: https://doi.org/10.1007/0-387-26213-X_13 (Page 9, 10)

[35] C. Ageorges and L. Ye, "Resistance welding of metal/thermoplastic composite joints," *Journal of Thermoplastic Composite Materials*, vol. 14, no. 6, pp. 449–475, 2001. [Online]. Available: https://doi.org/10.1106/PN74-QXKH-7XBE-XKF5 (Page 8, 9, 10)

[36] A. Smiley, M. Chao, and J. Gillespie, "Influence and control of bondline thickness in fusion bonded joints of thermoplastic composites," *Composites Manufacturing*, vol. 2, no. 3, pp. 223–232, 1991, flow Processes in Composite Materials '91. [Online]. Available: https://www.sciencedirect.com/science/article/pii/0956714391901446 (Page 10, 11)

[37] T. Jollivet, C. Peyrac, and F. Lefebvre, "Damage of composite materials," *Procedia Engineering*, vol. 66, pp. 746–758, 2013, fatigue Design 2013, International Conference Proceedings. [Online]. Available: https://www.sciencedirect.com/science/article/pii/S1877705813019619 (Page 10)

[38] M. Wisnom, "The role of delamination in failure of fibre-reinforced composites," *Philosophical transactions. Series A, Mathematical, physical, and engineering sciences*, vol. 370, pp. 1850–70, 04 2012. (Page 10)

[39] L. van der Hoeven and M. Lamers, "Defects in induction welding of thermoplastic composites," July 2023, part of the Composites Forming course at University of Twente. (Page 11)

[40] A. van der Vegt, *Polymeren*. Delft University Press, 1999. (Page 11, 12)

[41] V. C. Jamora, V. Rauch, S. G. Kravchenko, and O. G. Kravchenko, "Effect of resin bleed out on compaction behavior of the fiber tow gap region during automated fiber placement manufacturing," *Polymers*, vol. 16, no. 1, 2024. [Online]. Available: https://www.mdpi.com/2073-4360/16/1/31 (Page 11)

[42] E. Kobler, J. Birtha, C. Marschik, K. Straka, G. Steinbichler, and S. Schlecht, "Modeling the anisotropic squeeze flow during hot press consolidation of thermoplastic unidirectional fiber-reinforced tapes," *Journal of Thermoplastic Composite Materials*, vol. 0, no. 0, p. 08927057231214458, 0. [Online]. Available: https://doi.org/10.1177/08927057231214458 (Page 11)

[43] D. Roach, K. Rackow, and R. Duvall, Eds., *Innovative Use of Adhesive Interface Characteristics to Nondestructively Quantify the Strength of Bonded Joints*, 01 2010. (Page 11)

[44] M. Biron, "Glossary," in *Thermoplastics and Thermoplastic Composites (Second Edition)*, 2nd ed., ser. Plastics Design Library. William Andrew Publishing, 2013, pp. 1027–1034. [Online]. Available: https://www.sciencedirect.com/science/article/pii/B9781455778980170015 (Page 12)

[45] P. Patel, T. R. Hull, R. W. McCabe, D. Flath, J. Grasmeder, and M. Percy, "Mechanism of thermal decomposition of poly(ether ether ketone) (peek) from a review of decomposition studies," *Polymer Degradation and Stability*, vol. 95, no. 5, pp. 709–718, 2010. [Online]. Available: https://www.sciencedirect.com/science/article/pii/S0141391010000340 (Page 12)

[46] Toray Advanced Composites, "Toray Cetex® TC1225," 2020. [Online]. Available: https://www.toraytac.com/product-explorer/products/gXuK/Toray-Cetex-TC1225 (Page 19, 22, 30, 45)

[47] T. M. Inc., "Matlab version: 9.13.0 (r2022b)," Natick, Massachusetts, United States, 2022. [Online]. Available: https://www.mathworks.com (Page 21, 24)

[48] M. Hagenbeek, J. Bramon, and I. Villegas, "Controlling the edge effect using a bypass conductor for induction welding of carbon fibre thermoplastic composites," 06 2018. (Page 57)

Appendix A

Temperatures

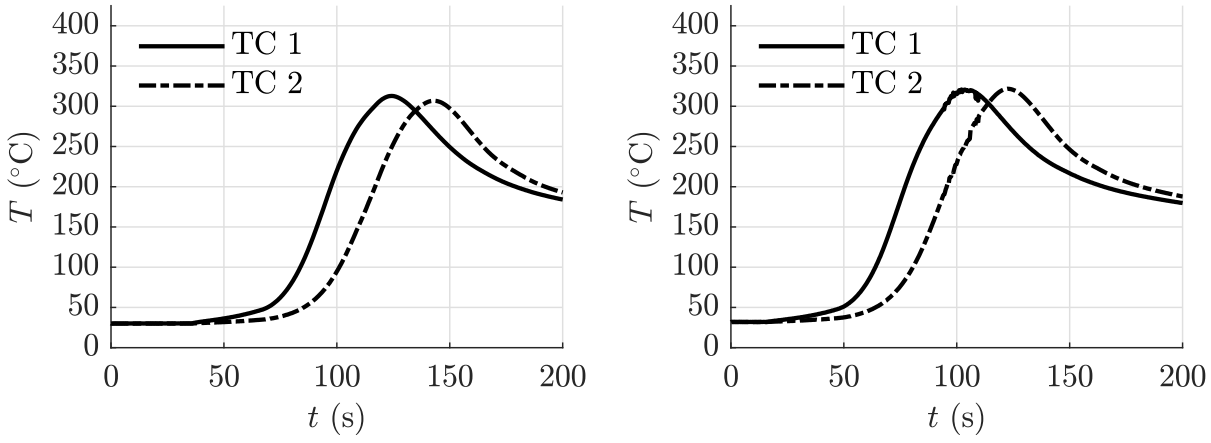

(a) *Low-temperature, low-pressure assembly, B1L2.*

(b) *Low-temperature, high-pressure assembly, B1L3.*

(c) *High-temperature, high-pressure assembly, B1L4.*

(d) *High-temperature, low-pressure assembly, B1L5.*

Figure A.1: *Measured assembly temperatures of the first batch (B1) excluding the reference assembly (B1L1), in-plane and through-the-thickness temperature distributions (B2) (see chapter 5).*

Appendix B

Visual inspection

B.1 Photographs

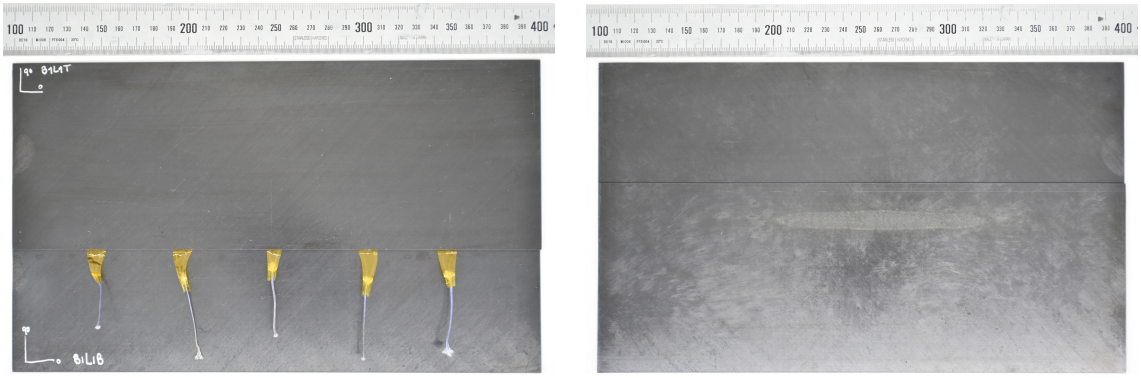

(a) *Front of reference assembly.* **(b)** *Back of reference assembly.*

Figure B.1: *Photographs of the reference assembly.*

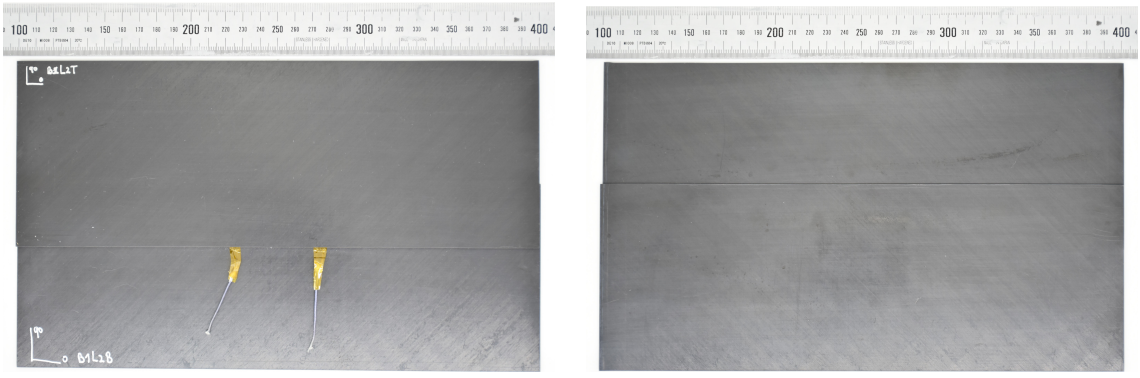

(a) *Front of B1L2 assembly.* **(b)** *Back of B1L2 assembly.*

Figure B.2: *Photographs of the B1L2 assembly, having a low power and pressure.*

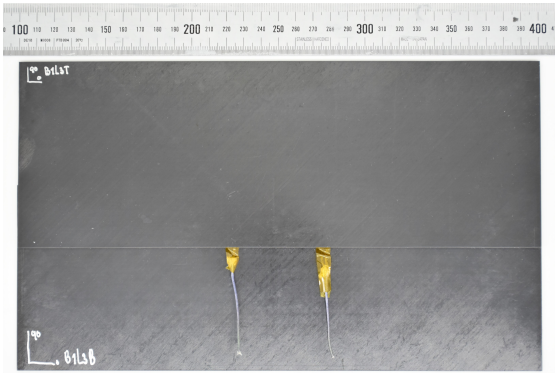

(a) *Front of B1L3 assembly.*

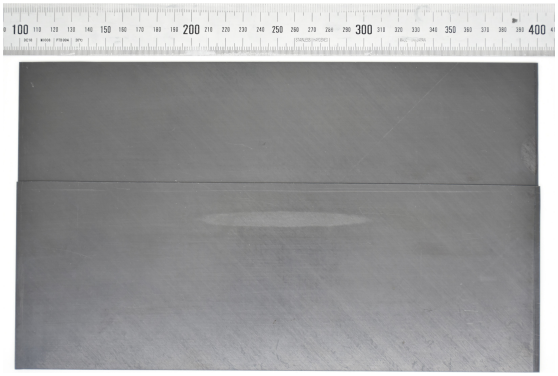

(b) *Back of B1L3 assembly.*

Figure B.3: *Photographs of the B1L3 assembly, having a low power and a high pressure.*

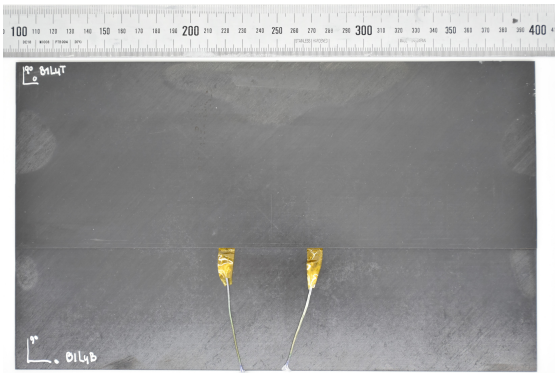

(a) *Front of B1L4 assembly.*

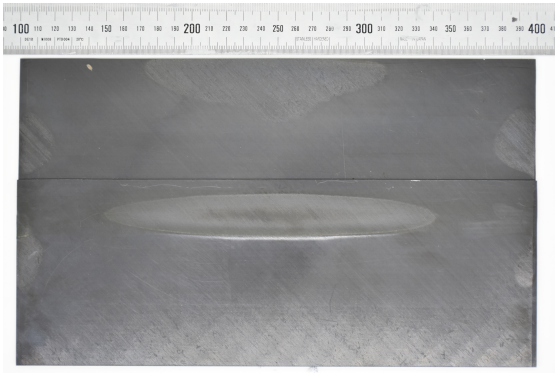

(b) *Back of B1L4 assembly.*

Figure B.4: *Photographs of the B1L4 assembly, having a high power and a pressure.*

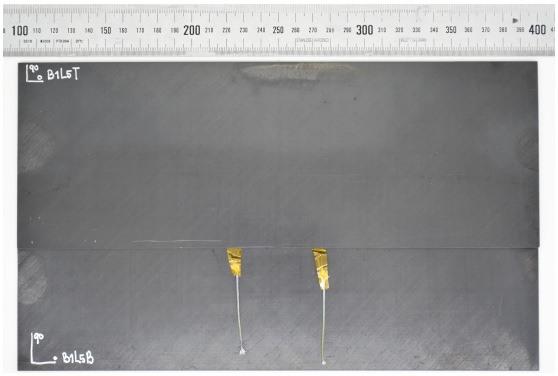

(a) *Front of B1L5 assembly.*

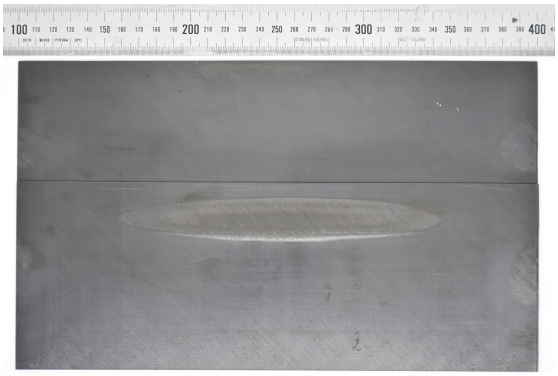

(b) *Back of B1L5 assembly.*

Figure B.5: *Photographs of the B1L5 assembly, having a high power and a low pressure.*

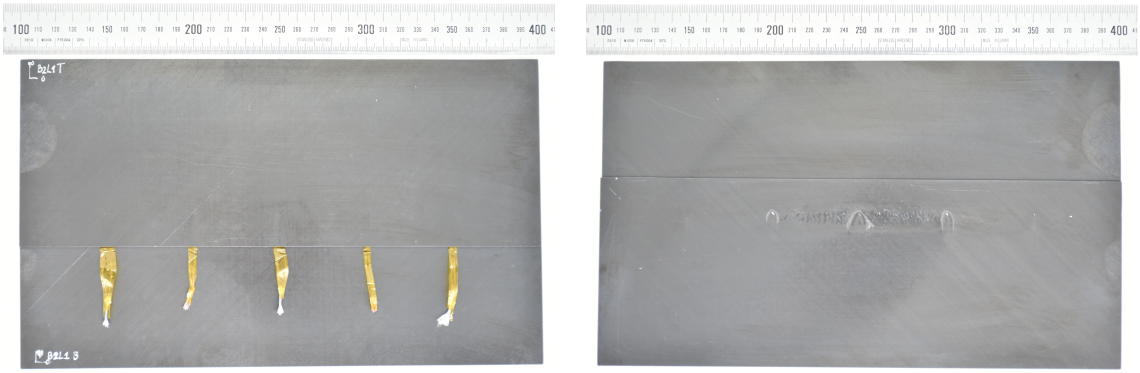

(a) *Front of B2L1 assembly.* **(b)** *Back of B2L1 assembly.*

Figure B.6: *Photographs of the B2L1 assembly, used for the through-thickness distribution at recommended temperatures.*

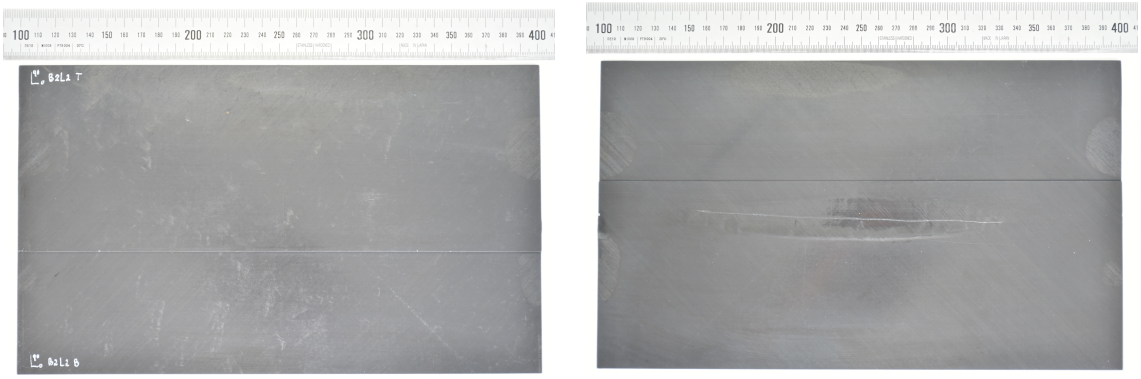

(a) *Front of B2L2 assembly.* **(b)** *Back of B2L1 assembly.*

Figure B.7: *Photographs of the B2L2 assembly, used for the bottom in-plane temperature distribution at high power and high pressure.*

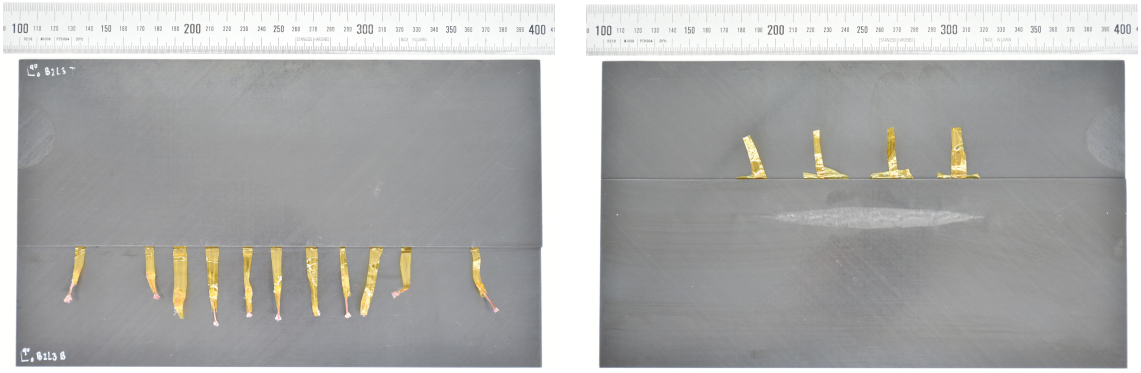

(a) *Front of B2L3 assembly.* **(b)** *Back of B2L3 assembly.*

Figure B.8: *Photographs of the B2L3 assembly, used for the assembly interface in-plane temperature distribution at recommended temperatures.*

B.2 Bottom surface defects

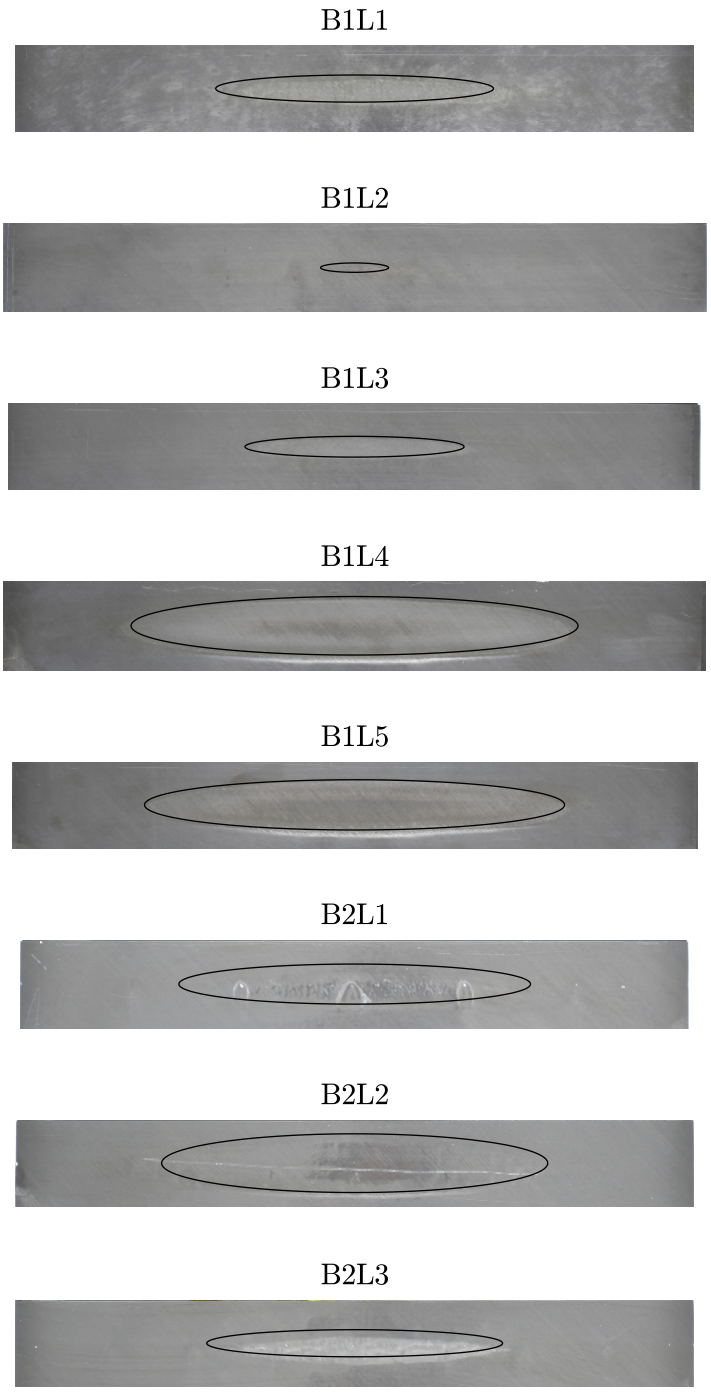

Figure B.9: *The elliptical surface defect at the back of the assembly overlap.*

Appendix C

Ply thickness

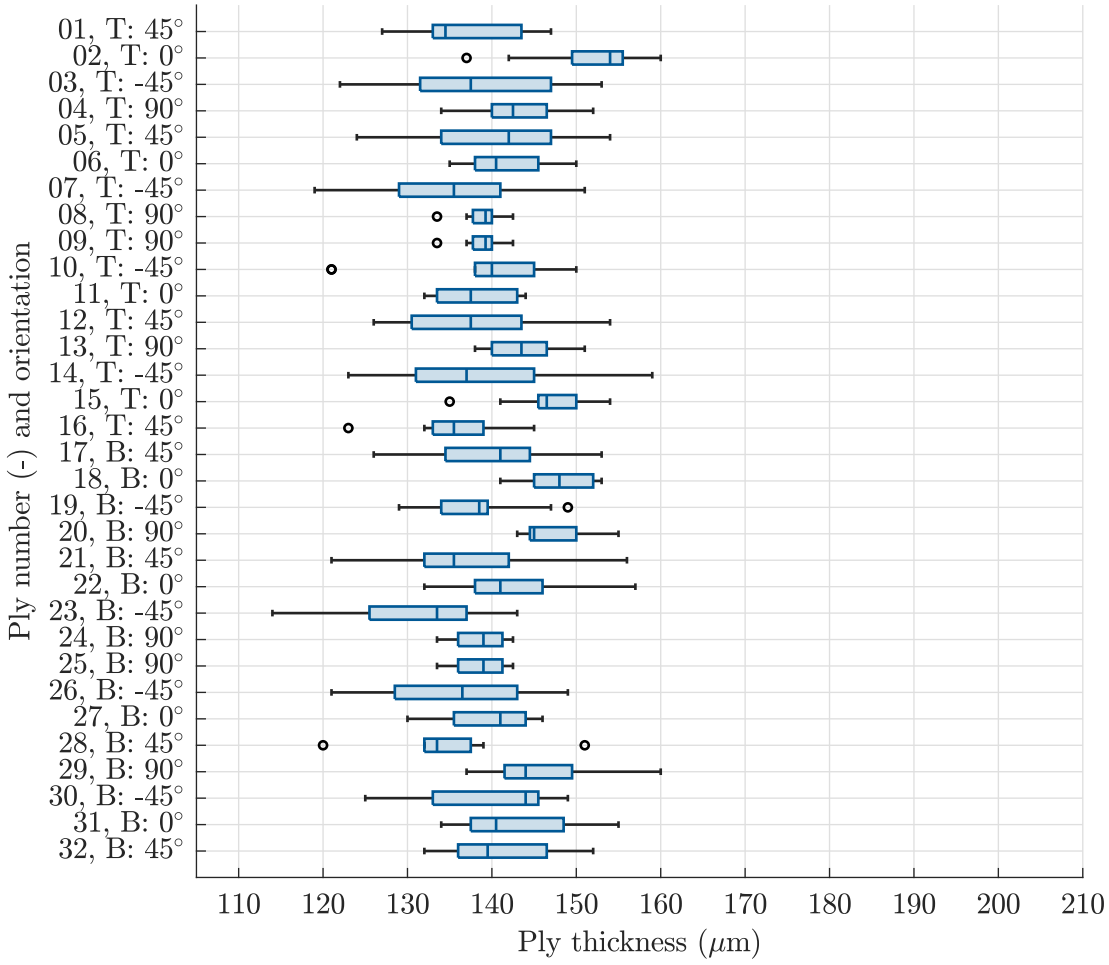

Figure C.1: *Boxchart of the reference assembly (B1L1).*

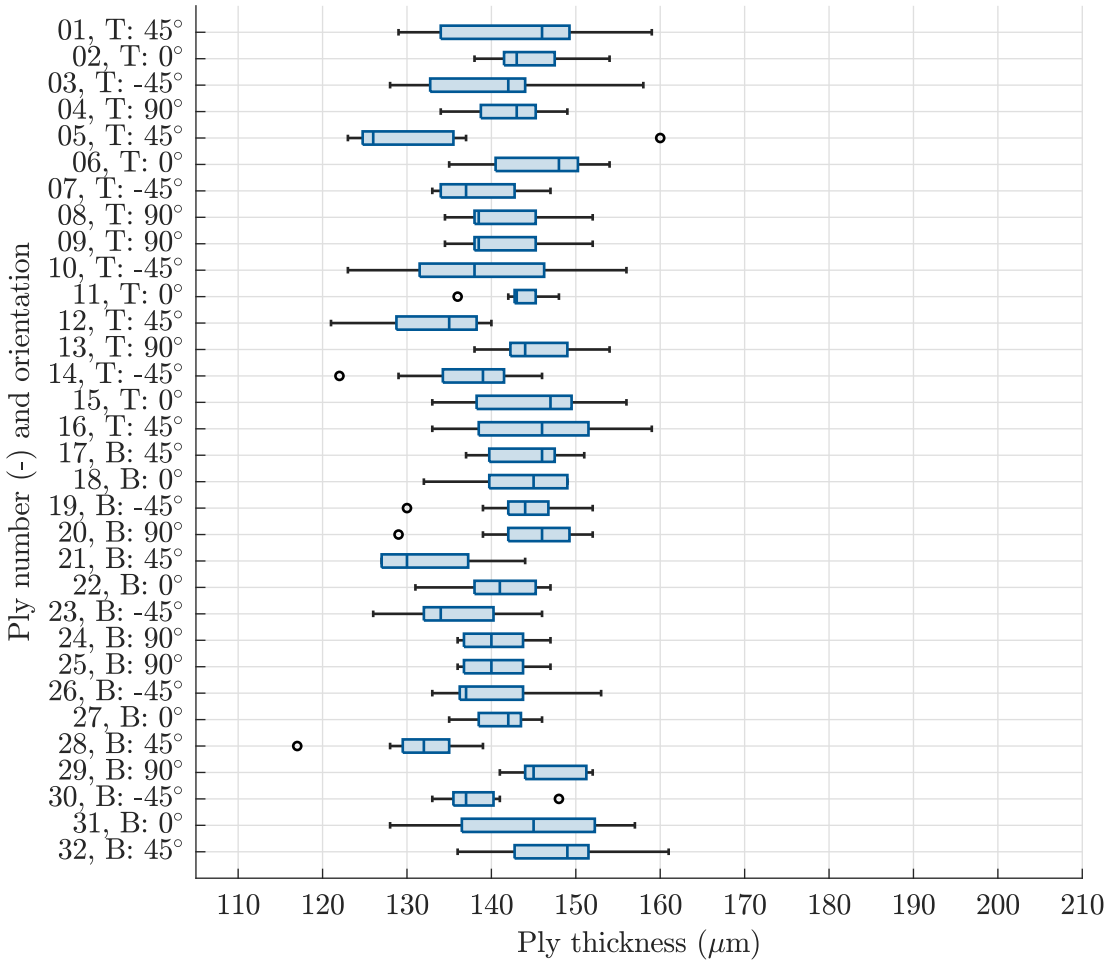

Figure C.2: *A boxchart of the ply thicknesses in of the low-power, low-pressure assembly (B1L2).*

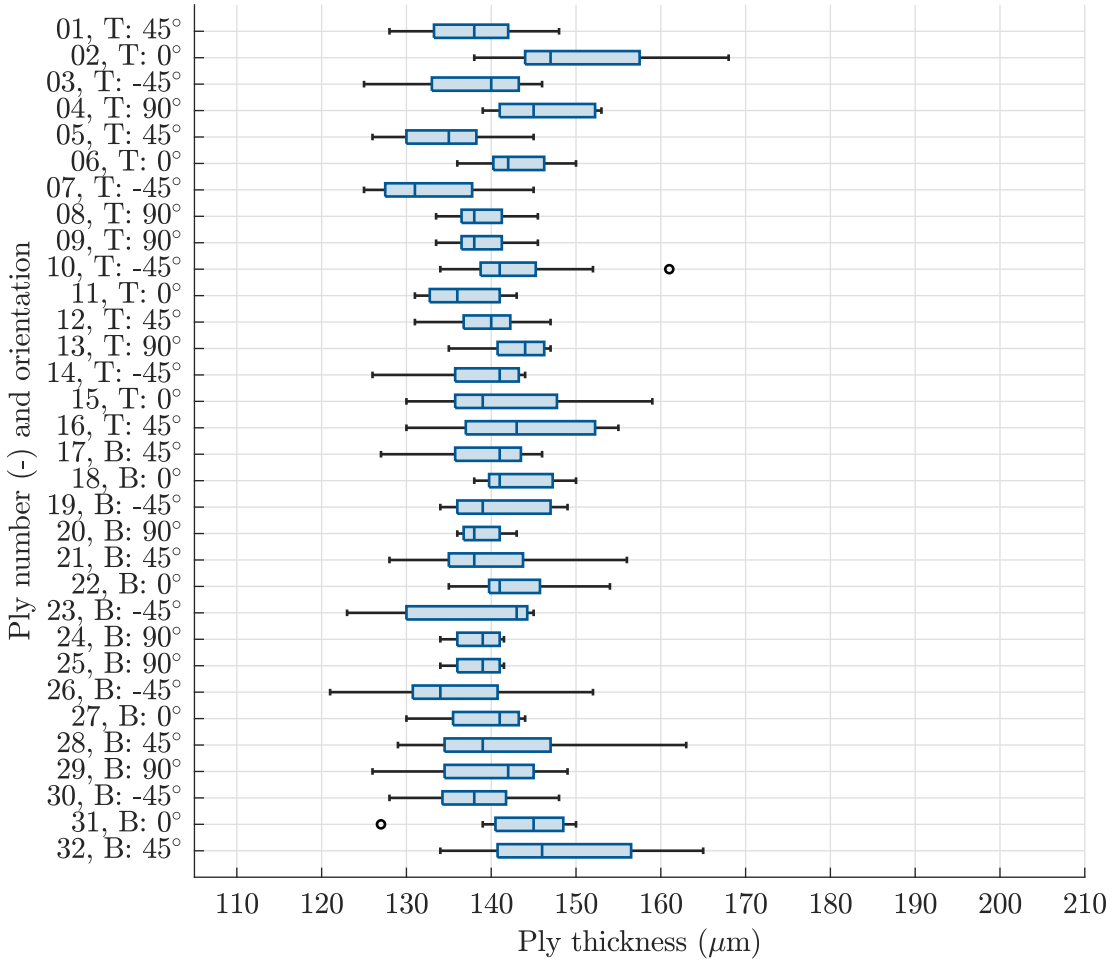

Figure C.3: *A boxchart of the ply thicknesses in the low-power, high-pressure assembly (B1L3).*

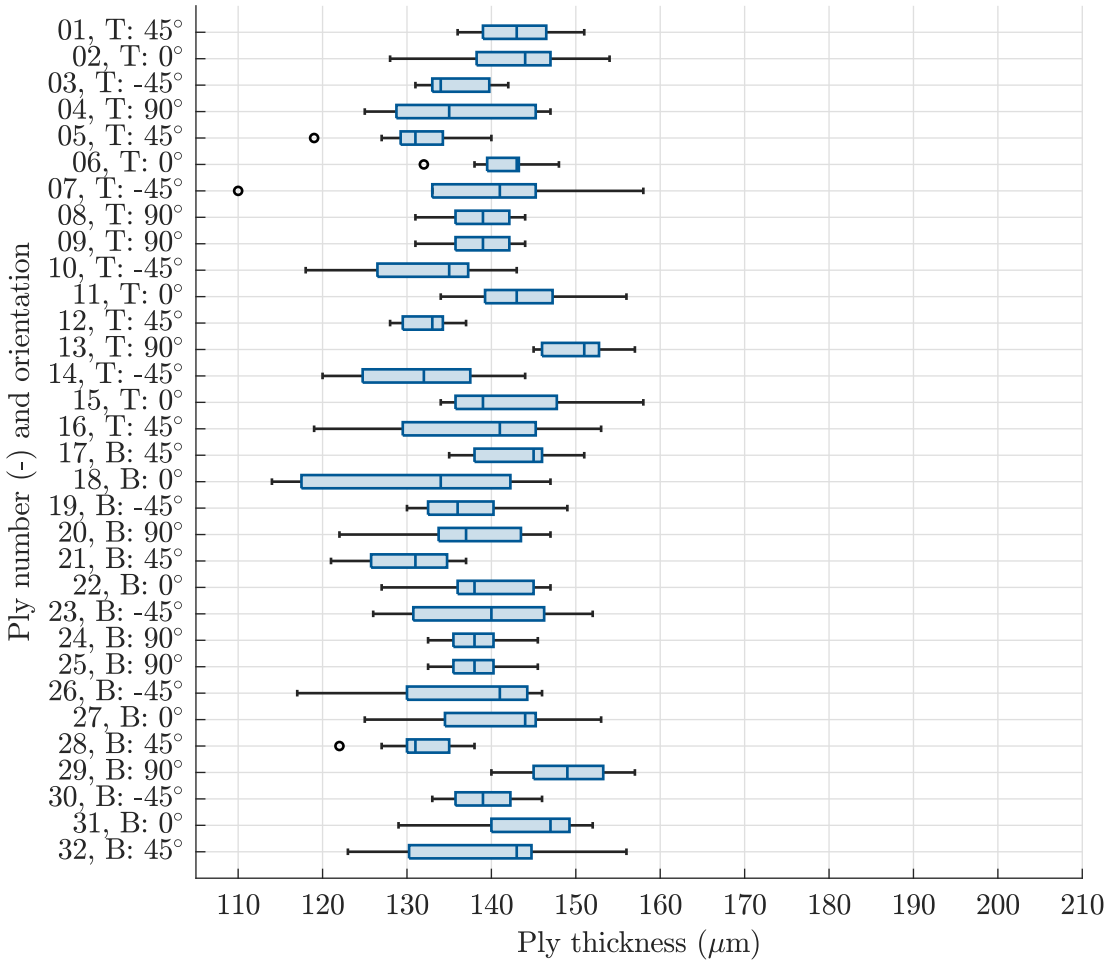

Figure C.4: *A boxchart of the ply thicknesses in the high-power, high-pressure assembly excluding defects (B1L4).*

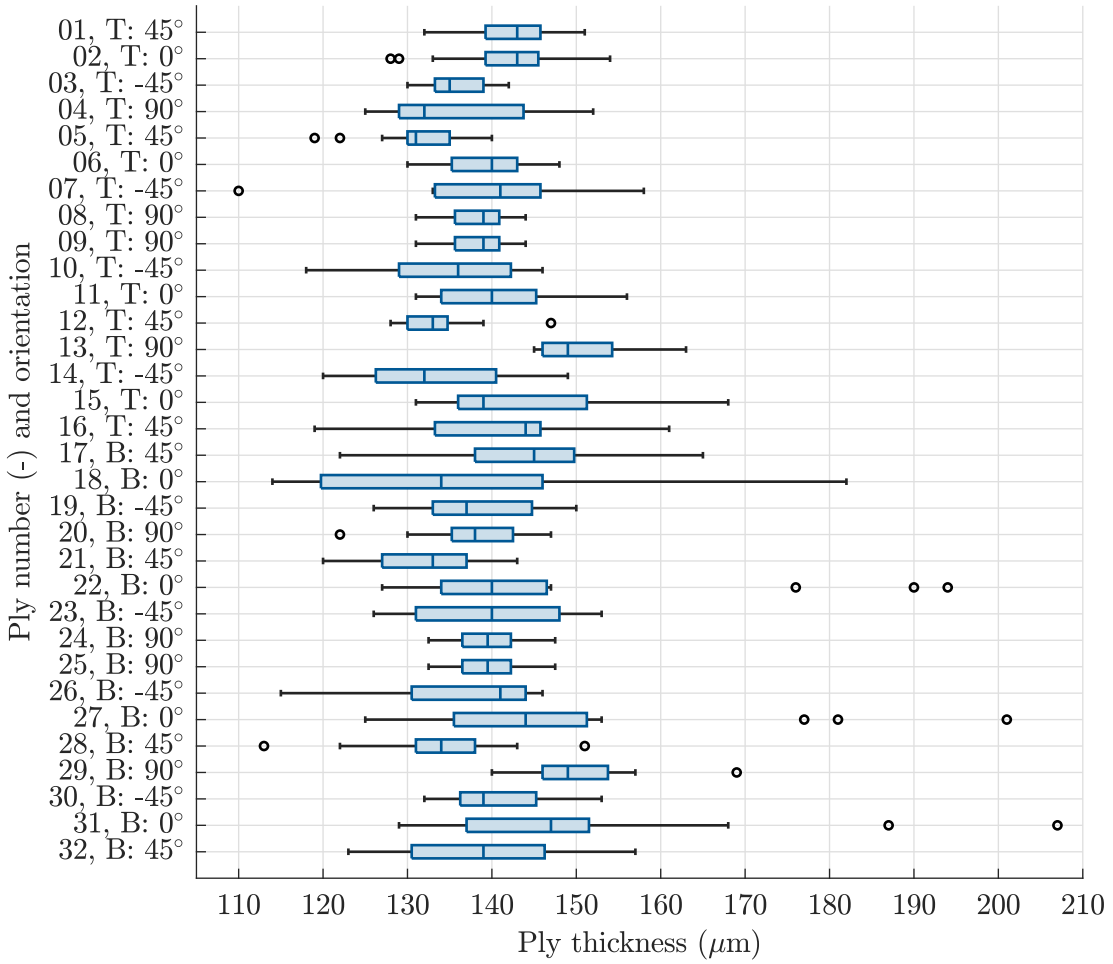

Figure C.5: *A boxchart of the ply thicknesses in the high-power, high-pressure assembly including defects (B1L4).*

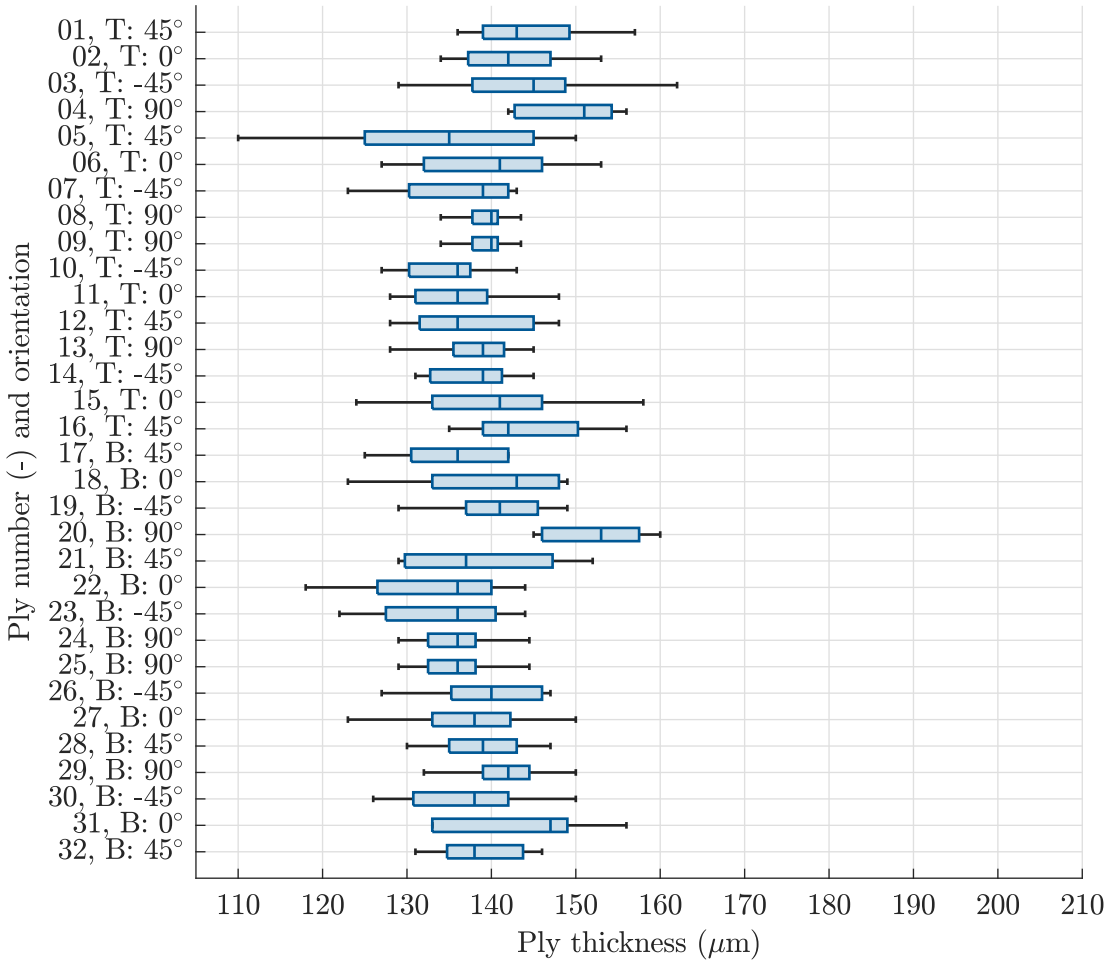

Figure C.6: *A boxchart of the ply thicknesses in the high-power, low-pressure assembly excluding defects (B1L4).*

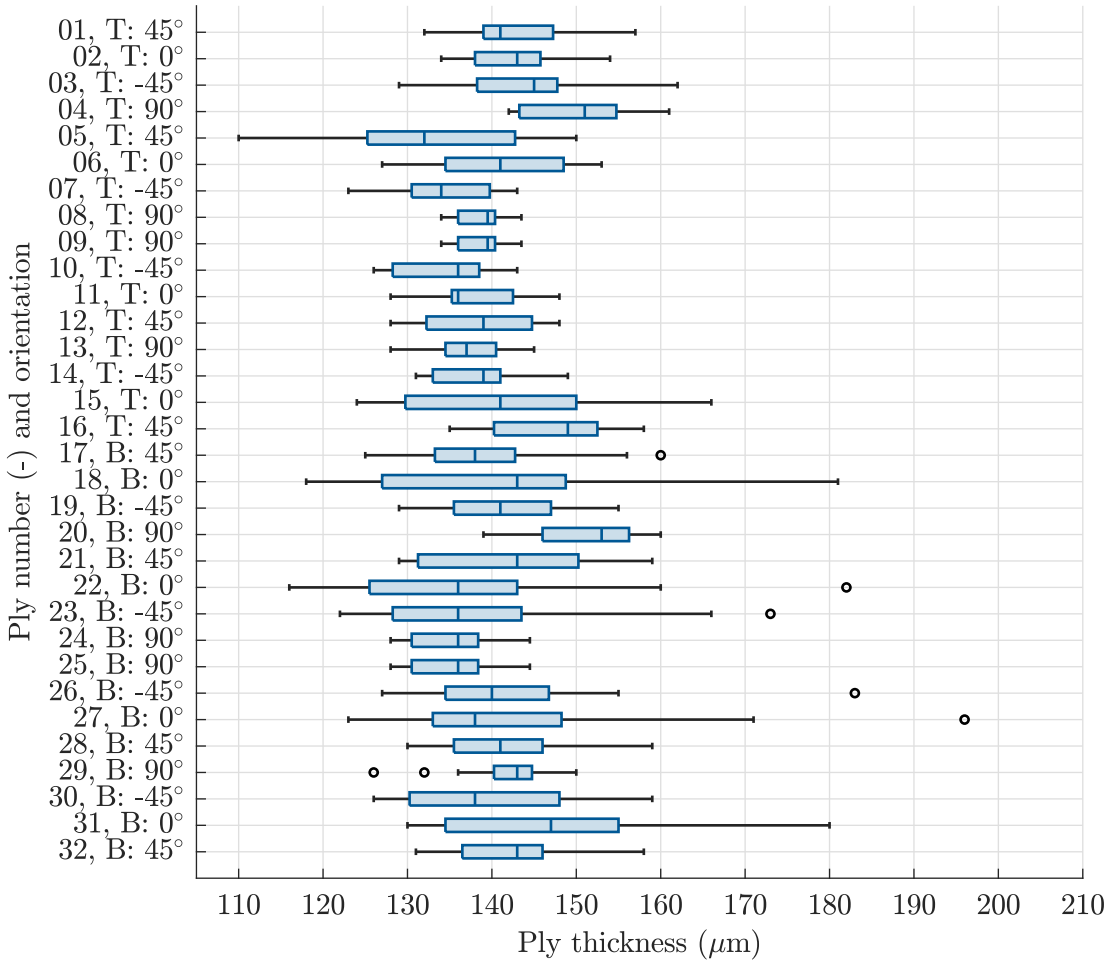

Figure C.7: *A boxchart of the ply thicknesses in the high-power, low-pressure assembly including defects (B1L5).*

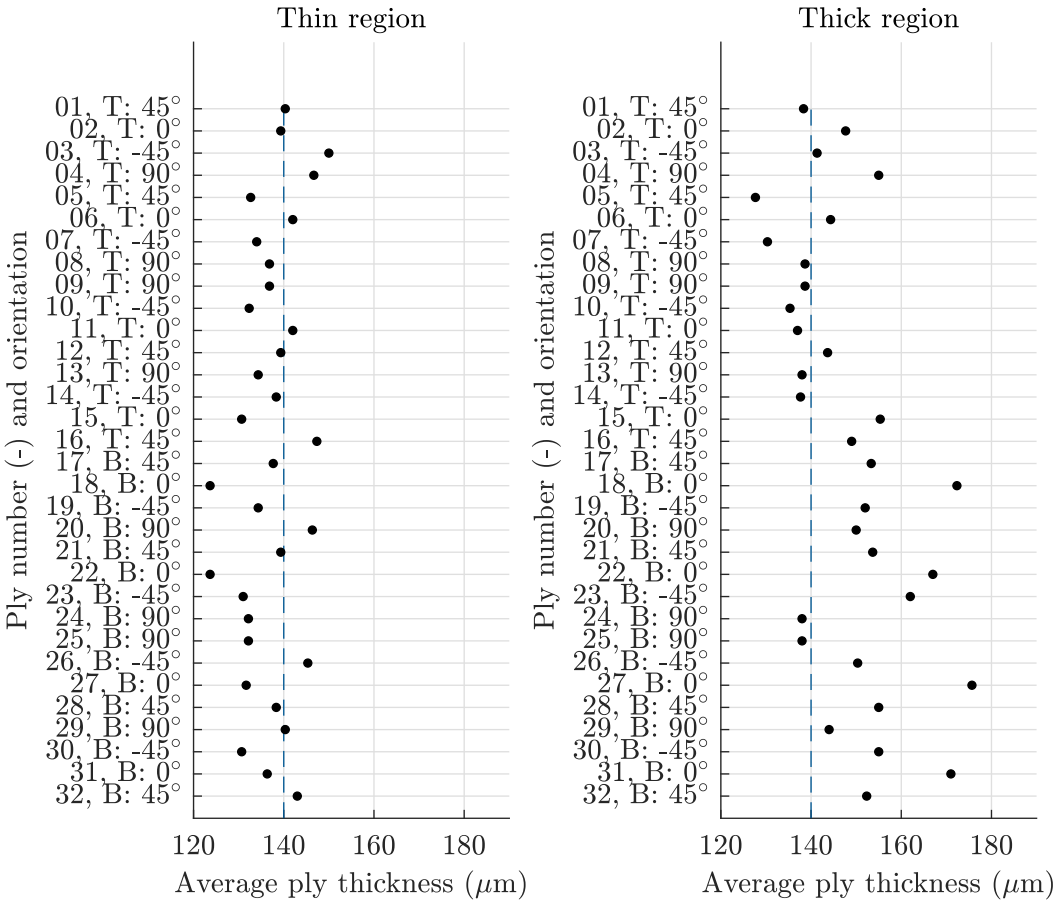

Figure C.8: *Average ply thickness of the thin and thick regions in the high-power, low-pressure assembly (B1L5).*

Appendix D

Pressure distribution

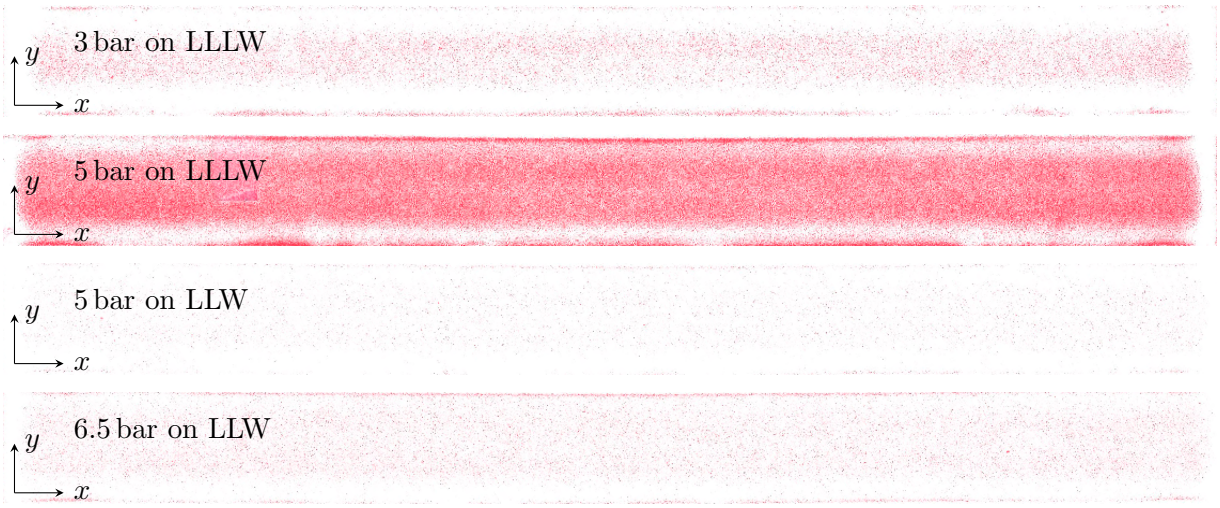

Figure D.1: *Pressure distributions of* 3 bar, 5 bar *and* 6.5 bar *on pressure sensitive foils.*

Appendix E

Microscopic inspection

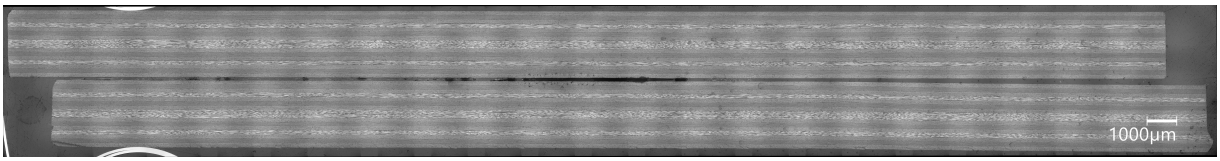

(a) *B1L1, sample L.*

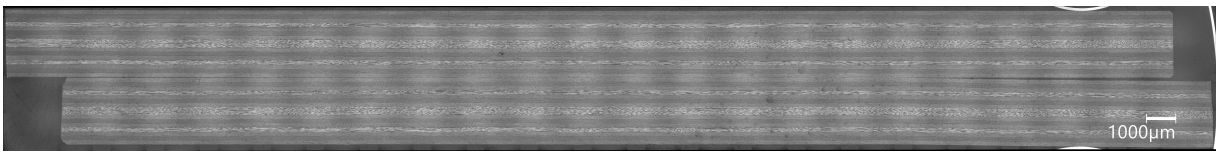

(b) *B1L1, sample LM.*

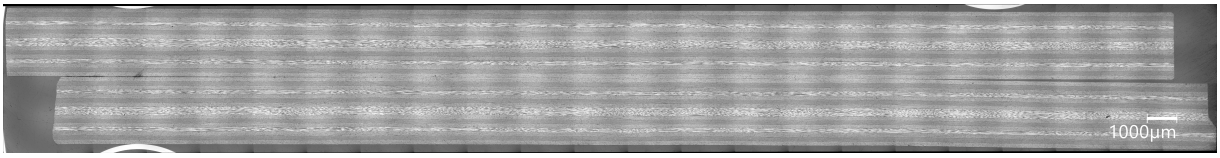

(c) *B1L1, sample RM.*

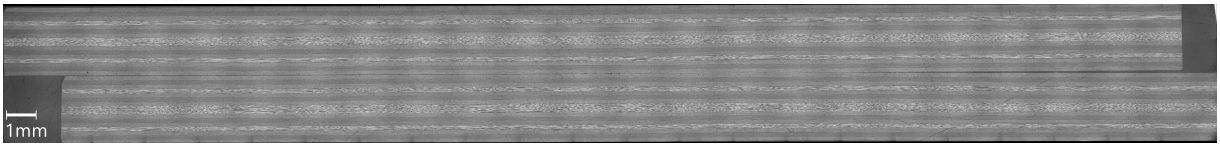

(d) *B1L1, sample R.*

Figure E.1: *Micrographs of the reference assembly at recommended conditions (B1L1).*

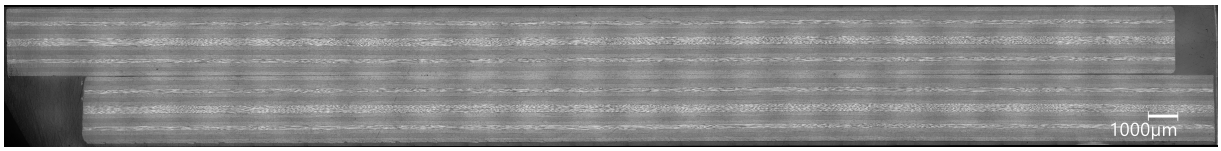

(a) *B1L2, sample L.*

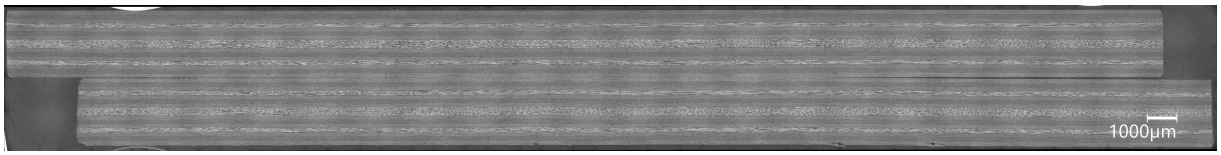

(b) *B1L2, sample M.*

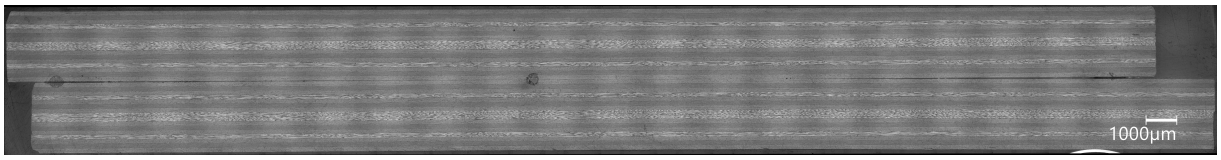

(c) *B1L2, sample R.*

Figure E.2: *Micrographs of the low-power, low-pressure assembly (B1L2).*

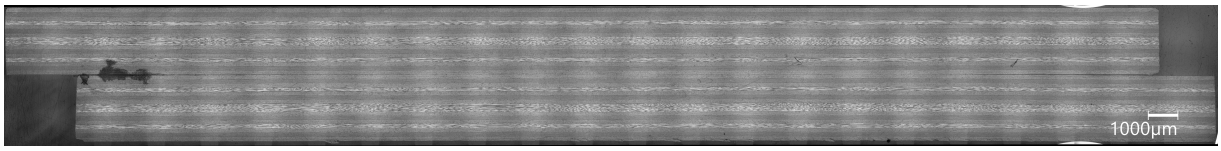

(a) *B1L3, sample L.*

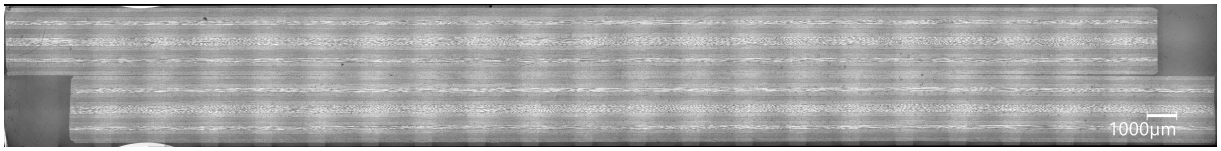

(b) *B1L3, sample M.*

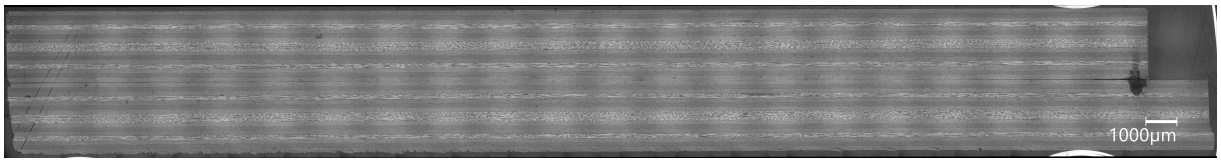

(c) *B1L3, sample R.*

Figure E.3: *Micrographs of the low-power, high-pressure assembly (B1L3).*

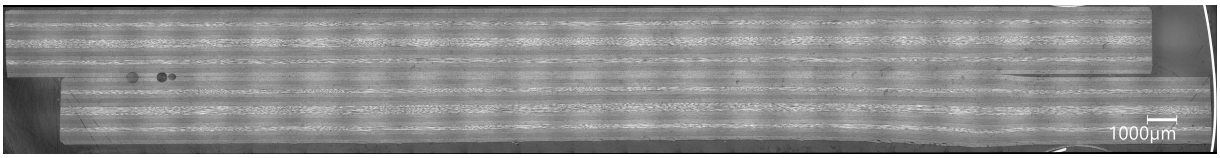

(a) *B1L4, sample L.*

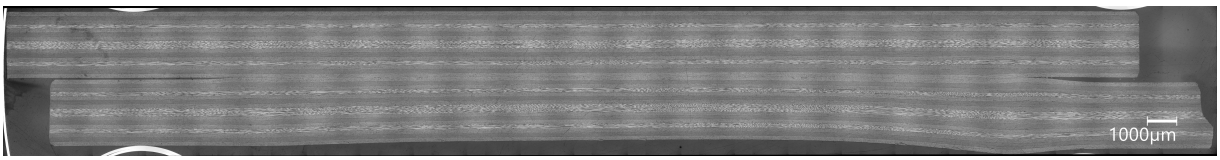

(b) *B1L4, sample M.*

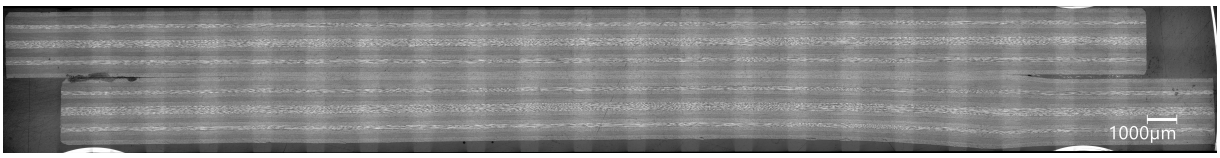

(c) *B1L4, sample R.*

Figure E.4: *Micrographs of the high-power, high-pressure assembly (B1L4).*

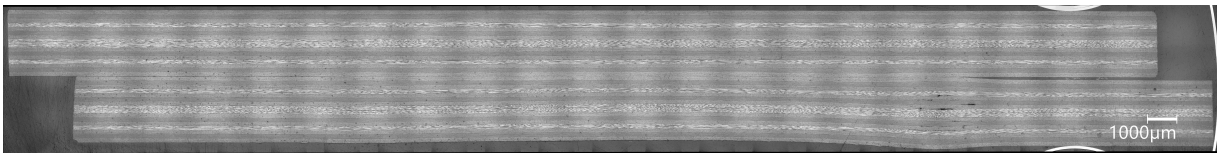

(a) *B1L5, sample L.*

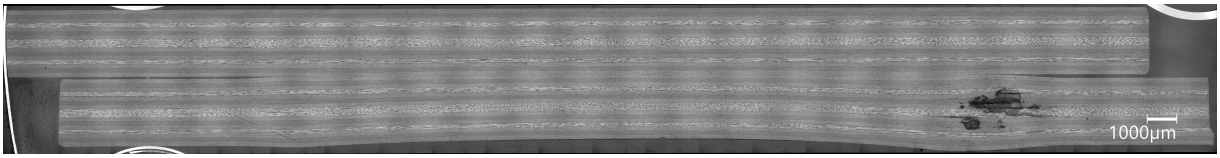

(b) *B1L5, sample M.*

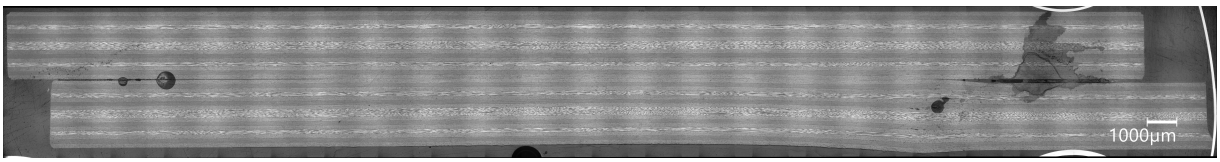

(c) *B1L5, sample R.*

Figure E.5: *Micrographs of the high-power, low-pressure assembly (B1L5).*

PAPER NAME

Lamers_2024_MSc.pdf

AUTHOR

Monique Lamers

WORD COUNT

20614 Words

CHARACTER COUNT

106942 Characters

PAGE COUNT

90 Pages

FILE SIZE

3.4MB

SUBMISSION DATE

Jun 28, 2024 8:18 PM GMT+2

REPORT DATE

Jun 28, 2024 8:20 PM GMT+2

3% Overall Similarity

The combined total of all matches, including overlapping sources, for each database.

- 2% Internet database
- 2% Publications database
- Crossref database
- Crossref Posted Content database
- 1% Submitted Works database

Excluded from Similarity Report

- Bibliographic material
- Quoted material
- Cited material